NASA/CR–2014-218264

Evaluation of the Trade Space Between UAS Maneuver Performance and SAA System Performance Requirements

Devin P. Jack, Keith D. Hoffler, and Sally C. Johnson
Adaptive Aerospace Group, Inc., Hampton, Virginia

May 2014

NASA STI Program . . . in Profile

Since its founding, NASA has been dedicated to the advancement of aeronautics and space science. The NASA scientific and technical information (STI) program plays a key part in helping NASA maintain this important role.

The NASA STI program operates under the auspices of the Agency Chief Information Officer. It collects, organizes, provides for archiving, and disseminates NASA's STI. The NASA STI program provides access to the NASA Aeronautics and Space Database and its public interface, the NASA Technical Report Server, thus providing one of the largest collections of aeronautical and space science STI in the world. Results are published in both non-NASA channels and by NASA in the NASA STI Report Series, which includes the following report types:

- TECHNICAL PUBLICATION. Reports of completed research or a major significant phase of research that present the results of NASA Programs and include extensive data or theoretical analysis. Includes compilations of significant scientific and technical data and information deemed to be of continuing reference value. NASA counterpart of peer-reviewed formal professional papers, but having less stringent limitations on manuscript length and extent of graphic presentations.

- TECHNICAL MEMORANDUM. Scientific and technical findings that are preliminary or of specialized interest, e.g., quick release reports, working papers, and bibliographies that contain minimal annotation. Does not contain extensive analysis.

- CONTRACTOR REPORT. Scientific and technical findings by NASA-sponsored contractors and grantees.

- CONFERENCE PUBLICATION. Collected papers from scientific and technical conferences, symposia, seminars, or other meetings sponsored or co-sponsored by NASA.

- SPECIAL PUBLICATION. Scientific, technical, or historical information from NASA programs, projects, and missions, often concerned with subjects having substantial public interest.

- TECHNICAL TRANSLATION. English-language translations of foreign scientific and technical material pertinent to NASA's mission.

Specialized services also include organizing and publishing research results, distributing specialized research announcements and feeds, providing information desk and personal search support, and enabling data exchange services.

For more information about the NASA STI program, see the following:

- Access the NASA STI program home page at *http://www.sti.nasa.gov*

- E-mail your question to help@sti.nasa.gov

- Fax your question to the NASA STI Information Desk at 443-757-5803

- Phone the NASA STI Information Desk at 443-757-5802

- Write to:
  STI Information Desk
  NASA Center for AeroSpace Information
  7115 Standard Drive
  Hanover, MD 21076-1320

Evaluation of the Trade Space Between UAS Maneuver Performance and SAA System Performance Requirements

Devin P. Jack, Keith D. Hoffler, and Sally C. Johnson
Adaptive Aerospace Group, Inc., Hampton, Virginia

Acknowledgments

Available from:

NASA Center for AeroSpace Information
7115 Standard Drive
Hanover, MD 21076-1320
443-757-5802

Table of Contents

Nomenclature

Abbreviations and Acronyms

2PAIRS	2 degree-of-freedom Prototyping Airplane Interaction Research Simulation
ATC	Air Traffic Control
CAT	Collision Avoidance Threshold
CFR 14	Title 14 of Code of Federal Regulations (FAA Regulations)
CPA	Closest Point of Approach
DOD	United States Department of Defense
FAA	Federal Aviation Administration
GA	General Aviation
GUI	Graphical User Interface
IFR	Instrument Flight Rules
KCAS	Knots Calibrated Air Speed
KTAS	Knots True Air Speed
MSL	Mean Sea Level
NAS	United States National Airspace System
NASA	National Aeronautics and Space Administration
NMAC	Near Mid-Air Collision
SC-228	RTCA Special Committee 228 – Minimum Operational Performance Standards for Unmanned Aircraft Systems
SAA	Sense and Avoid
SST	Self-Separation Threshold
TCAS	Traffic Alert and Collision Avoidance System
UAS	Unmanned Aircraft System
VFR	Visual Flight Rules
WCV	Well Clear Volume

Variable Definitions

AR	Aspect Ratio of the wing, wing span divided by chord
CPA	Closest Point of Approach (ft)
C_D	Drag Coefficient
C_{d_0}	Zero-lift drag coefficient also called parasite drag
C_L	Coefficient of lift
$C_{L_{max}}$	Lift coefficient at stall, i.e., maximum lift coefficient
D	Drag (lbs)
e	Oswald's Efficiency Factor
g	Load factor or acceleration due to gravity (32.17 ft/sec^2)
g_{limit}	Load factor limit (g)
h	Altitude (ft MSL)
$\dot{h}$	Rate of change of altitude (ft/min) or (ft/sec)
L	Lift (lbs)
$\frac{L}{D}_{max}$	Maximum lift-to-drag ratio
m	Mass
n_z	Normal load factor (g)
P_S	Specific excess energy (ft/sec)
$\bar{q}$	Dynamic pressure (lbs/ft^2)
R	Radius of turn (ft)
S	Wing area (ft^2)

T	Thrust (lbs)
$\frac{T}{W}$	Thrust-to-Weight ratio
V	Velocity (knots)
V_{NE}	Velocity Never to Exceed (KCAS)
W	Aircraft weight (lbs)
$\frac{W}{S}$	Wing loading (lbs/ft^2)
α	Angle of attack (deg)
Δ	Change in value
γ	Vertical flight-path angle (deg)
ϕ	Bank angle in Euler axis (deg)
$\dot{\phi}$	Rate of change of bank angle or roll rate (deg/sec)
ψ	Track angle (deg)
$\dot{\psi}$	Rate of change of track angle or turn rate (deg/sec)
ρ	Density of air (slugs/ft^3)
τ	Estimated or actual time-to-go to closest point of approach (seconds)
$\%C_{L_{max}}$	Initial percent of maximum coefficient of lift

Subscripts

$actual$	The actual experienced value vs. initial predicted value
$command$	Commanded value
BA	Best Angle of climb
BR	Best Rate of climb
i	Initial
$intr$	Intruder
min	Minimum
max	Maximum
$SLUF$	Straight Level Unaccelerated Flight
$Sustainable$	Sustainable flight condition given thrust available and aerodynamic parameters

Abstract

A need exists to safely integrate Unmanned Aircraft Systems (UAS) into the National Airspace System. Replacing manned aircraft's see-and-avoid capability in the absence of an onboard pilot is one of the key challenges associated with safe integration. Sense-and-avoid (SAA) systems will have to achieve yet-to-be-determined required separation distances for a wide range of encounters. They will also need to account for the maneuver performance of the UAS they are paired with. The work described in this paper is aimed at developing an understanding of the trade space between UAS maneuver performance and SAA system performance requirements. An assessment of current manned and unmanned aircraft performance was used to establish potential UAS performance test matrix bounds. Then, near-term UAS integration work was used to narrow down the scope. A simulator was developed with sufficient fidelity to assess SAA system performance requirements for a wide range of encounters. The simulator generates closest-point-of-approach (CPA) data from the wide range of UAS performance models maneuvering against a single intruder with various encounter geometries. The simulator is described herein and has both a graphical user interface and batch interface to support detailed analysis of individual UAS encounters and macro analysis of a very large set of UAS and encounter models, respectively. Results from the simulator using approximate performance data from a well-known manned aircraft is presented to provide insight into the problem and as verification and validation of the simulator. Analysis of climb, descent, and level turn maneuvers to avoid a collision is presented. Noting the diversity of backgrounds in the UAS community, a description of the UAS aerodynamic and propulsive design and performance parameters is included. Initial attempts to model the results made it clear that developing maneuver performance groups is required. Discussion of the performance groups developed and how to know in which group an aircraft belongs for a given flight condition and encounter is included. The groups are specific to airplane, flight condition, and encounter, rather than airplane-only specific. Results and methodology for developing UAS maneuver performance requirements are presented for each maneuver as well. Results for the vertical maneuver indicate that a minimum specific excess power value can assure a minimum CPA for a given time-to-go prediction. However, smaller values of specific excess power may achieve or exceed the same CPA if the UAS has sufficient speed to trade for altitude. Level turn results are less impacted by specific excess power and are presented as a function of turn rate. The effect of altitude is also discussed for the turns. Next steps and future work are discussed. Future studies will lead to better quantification of the preliminary results and cover the remainder of the proposed test matrix. It is anticipated that this will be done in conjunction with RTCA SC-228 over the next few months.

1   Introduction

The United States National Airspace System (NAS) has evolved to both support and rely on the capabilities of manned aircraft. Currently, the Department of Defense (DOD), other public entities, and private industry are showing increasing interest in gaining regular access to fly unmanned aircraft systems (UAS) in the NAS. One of the major barriers to integrating UAS in the NAS is the requirement to see and avoid other aircraft, a task currently performed by the onboard pilot. Title 14 of the Code of Federal Regulations (14 CFR) Part 91.113 [1] states, "vigilance shall be maintained by each person operating an aircraft so as to see and avoid other aircraft." Thus, pilots are expected to see and avoid other aircraft and to maneuver in predictable ways to preserve the safety, orderliness, and efficiency of the NAS environment. UAS will be expected to operate in a similar manner, but with sense and avoid (SAA) systems replacing the see-and-avoid capability of manned aircraft. However, the acceptable design space and required capabilities for SAA in this environment remains largely undefined. According to the Second Caucus Report from the Federal Aviation Administration (FAA) sponsored Sense and Avoid workshop, "for a technical system to perform the function of a pilot to remain well clear, it is necessary to have an unambiguous, implementable definition of the separation minima" [2]. Without a quantitative definition of "well clear," it is difficult to develop a UAS that is able to conform to current airspace rules. In addition to quantification of well-clear separation minima, understanding the trade space between UAS maneuver performance capabilities and SAA system requirements necessary to maintain the minimum separation standards is needed. Some separation boundaries are currently defined as the last time to maneuver to avoid penetration of the next boundary. This type of definition has UAS performance inherent in the definition and incorporates encounter parameters as well. Under these definitions, UAS performance and the well-clear or near mid-air collision (NMAC) boundaries must be combined to determine when the SAA system must initiate an avoidance maneuver. Therefore, as the FAA works to define new rules that will lay out the requirements for all UAS SAA systems, it is essential to understand and quantify the trade space between aircraft maneuver performance and the capabilities of the SAA system. UAS designers will also benefit from a deeper understanding of this trade space.

A large body of work related to collision avoidance was generated during the development of the Traffic Alert and Collision Avoidance System (TCAS) [3]. TCAS is now required equipment on large manned aircraft acting as a last line of defense against collisions with other aircraft. TCAS analyzes the projected flight path of ownship and intruders and issues advisories to pilots based on a complex algorithm, thereby providing a layer of protection against collisions other than air traffic control (ATC) and the pilot's vision and discernment. However, TCAS was designed and intended for use on aircraft having a large number of passenger seats and meeting standards defined in CFR 14 Part 25. This generally defines a class of aircraft that flies at high altitudes and at relatively fast speeds (transport category airplanes) when compared to many general aviation (GA) aircraft and UAS. TCAS relies on timely pilot responses and aircraft performance parameters to achieve collision-avoidance minimums based on "Resolution Advisory" times prior to a predicted collision. Transponders provide limited relative state information of intruder aircraft used by the threat detection and maneuver advisory algorithms. Technological limitations of transponders at the time TCAS was developed further restricted TCAS design options. Additionally, TCAS is intended for collision avoidance only and, therefore, does not address other separation requirements, such as remaining well clear as described earlier. As a result of these limitations, TCAS requirements do not take advantage of currently available sensor capabilities and require higher climb and descent performance than the broad

array of current *manned* aircraft exhibit. The widely diverse UAS fleet often exhibits even less maneuver performance currently, sometimes because of airframe and power-plant limitations and sometimes because of the flight-control system.

These observations led to the development of a simplified simulation tool and design of a simulation experiment to analyze the interaction of UAS and SAA system performance requirements. The simulation tool allows broad and rapid variation of UAS design parameters that impact maneuver performance. For each simulation run, a UAS and a non-maneuvering intruder are set on a collision course, and the UAS immediately initiates a maneuver to avoid the intruder, with resulting Closest Point of Approach (CPA) and other airplane states recorded. The avoidance maneuvers evaluated were commanded climbs, descents, and level turns across a range of rates with airplane performance limitations impacting the resulting maneuver. Intruder azimuths in the UAS' forward hemisphere were evaluated as well as climbing and descending intruders. The encounter scenarios resulted in CPAs spanning from NMAC ranges to well beyond those that could be considered well clear. Three simulation models were developed to account for UAS maneuver performance limitations associated with climb, descent, and level turn maneuvers independently. This approach significantly reduces model complexity and, therefore, the amount of time required for each simulation run.

A wide range of diverse existing fixed-wing airplane types were used to define parameter ranges representing the broad spectrum of UAS with present and future aerodynamic and propulsive performance and maneuverability. The UAS parameter ranges were then narrowed to focus the simulation on performance ranges that could potentially limit conduct of avoidance maneuvers and to align with near-term UAS integration concepts as defined in the RTCA Special Committee – Minimum Operational Performance Standards for Unmanned Aircraft Systems (SC-228) Terms of Reference [4] and work plan [5]. Even with the parameter range reductions, millions of combinations of airplane performance and encounter parameters were analyzed in an effort to describe the trade space between SAA system and UAS maneuver performance requirements.

Design parameters that have first-order effects on airplane performance were used to develop the simulation test matrix resulting in a broad set of airplane maneuver performance capabilities. The parameter matrix was also used to determine likely initial UAS speeds. Rather than simulating specific airplanes, the approach was used to cover a broad range of maneuver performance. Before data gathering began, a verification and validation study was performed to ensure that the simulation accurately modeled maneuver performance across the parameter ranges of interest. Example results from one manned aircraft that was modeled are included.

Using results from the simulation, a number of candidate performance parameters were evaluated to determine the best universal predictors of CPA. The objective was to identify a set of performance parameters that could be used to predict the avoidance maneuver result given current or future UAS. The performance parameters could also be used to identify when a maneuver must be initiated to generate a desired CPA from a series of encounters. To be useful, the performance parameters must be known or easily estimated for a given UAS or future UAS design. Extensive analysis was done of the vertical climb maneuver and a proposed approach for evaluating performance parameters was developed for aircraft that can sustain a commanded climb and those that cannot. A more limited analysis of the vertical descent and level turn maneuvers was conducted with lessons learned and methodology developed included in the paper. The descent maneuver is evaluated in detail in a companion document [6]. Airplanes that can sustain the commanded maneuver were analyzed for all three maneuvers. Approaches for analyzing the aircraft that cannot sustain a commanded maneuver are also discussed. Conclusions from analysis of performance-limited groups are for more specific sets of parameters with the focus on methodology.

This paper shows results and trends in CPA associated with the best performance predictors. As indicated by the able to sustain, and unable to sustain, commanded maneuvers

references above, maneuver performance groups that are analyzed separately to make the problem more manageable became necessary and are discussed. The performance groups are specific to the UAS airframe/power-plant, commanded maneuver, and the encounter. A means to identify into which group an airplane, flight condition, and encounter falls is defined. Analysis of results shows how specific performance parameters can be used to identify when a maneuver must be initiated to generate a certain CPA from a series of encounters. In some cases the results are broad and in other cases analyzed against a particular CPA. In the latter case, the existing data and approach described can be analyzed against other CPAs in the likely event that values defined by regulators differ from those used in the examples herein.

The results and methodology presented in this paper will help regulators determine minimum maneuver performance requirements for UAS operating in the NAS with a SAA system. Results will also help determine the point in the SAA system timeline at which the maneuver must be initiated, whether the desired maneuver is maximum performance or something less. The resulting trade space is expected to support development of flexible SAA system design requirements, thus accommodating as many UAS types in the NAS as possible.

2   Performance Model and Simulation

This section describes the simulation in detail and includes: the range of UAS modeled; the simplified simulation tool developed to enable rapid evaluation of millions of combinations of aircraft and encounter parameters; and the commanded avoidance maneuvers modeled. A description of validation and verification of the simulation conducted to ensure the simulation accurately captured flight performance is included. The section starts with a derivation of parameter ranges to be used and description of the modeling technique to provide the reader an understanding of the simulation fidelity.

2.1   Derivation of UAS Parameter Ranges

Since the goal of the simulation was to evaluate UAS performance in conducting avoidance maneuvers across a wide range of UAS, the UAS maneuver performance was modeled by varying key airplane design parameters across applicable ranges. A survey of existing airplanes was done to identify applicable parameter ranges of UAS and manned fixed-wing airplanes. Most current UAS fly slowly and have limited maneuverability, while others have performance approaching that of airliners and corporate jets. UAS with higher performance and maneuverability are expected in the future, but these aircraft do not represent a limiting case; thus, along with fighter aircraft, they are absent from the sample.

A broad sample of existing manned and unmanned airplanes is shown in Table 1 to represent the spanning set of airplane performance of interest. Key design parameters for these airplanes, which coarsely define the performance of each, were obtained from publically available sources. Some of these airplanes have cruise speeds on the order of 60 knots true airspeed (KTAS) while others cruise at 500 KTAS or more. Some can barely climb at 500 ft/min and others can sustain thousands of ft/min. Some in the table have stall speeds that are higher than the velocity not to exceed (V_{NE}) of others in the sampling. Finally, some of these airplanes cannot reach 18,000 ft Mean Sea Level (MSL) (bottom of Class A airspace) and others cruise above 30,000 ft MSL.

Table 1: Selected aircraft and publicly available design parameters. Some values were estimated from publically available data.

#	Aircraft	T/W min	T/W max	W/S (lb/ft^2) min	W/S (lb/ft^2) max	AR	e	$\left(\frac{L}{D}\right)_{max}$	C_{Lmax}	Aircraft type
1	Aerosonde	0.07	0.10	4	6	10	0.90	20	1.85	Small UAS
2	Boeing 757-200	0.31	0.63	65	131	8.0	0.85	18	2.75	Transport
3	C-17	0.28	0.57	74	154	7.2	?	?	3.54	Cargo Transport
4	Cessna 172	0.22	0.38	9.7	15	7.5	0.80	9	2.38	General Aviation
5	Cessna R182	0.25	0.35	13	18	7.4	0.80	11	2.27	General Aviation
6	Embraer EMB-145	0.16	0.33	46	77	7.8	0.80	15	2.35	Regional Jet
7	Fokker Dr. 1	0.30	0.44	4.4	6.4	4.0	0.65	8	1.24	Triplane
8	Global Hawk	0.26	0.77	16	48	24	0.98	30	1.21	Large UAS
9	Ikhana	0.19	0.40	19	41	17	0.90	30	1.88	Large UAS
10	Nimbus 4M	0.10	0.13	6.2	8.6	39	0.98	60	?	Motor Glider
11	Piper PA-28-180	0.15	0.26	7.7	15	5.6	0.76	10	1.99	General Aviation
12	Shadow B	0.32	0.35	12	13	11	0.90	13	1.60	Small UAS
13	Stemme S10	0.10	0.13	7.0	9.3	28	0.98	50	1.54	Motor Glider

Using the broad sample of airplanes shown in Table 1 as a baseline, and applying related subject matter expertise, a test range for each UAS design parameter was selected for the current study, as shown by the blue lines in Figure 1. Note that these test ranges fall inside the parameter range for the airplanes in Table 1. In order to reduce the number of combinatorial runs to a more manageable size, a decision was made to focus the simulation on UAS performance characteristics that would cause more difficulty in conducting effective avoidance maneuvers and more closely align with near-term needs. A key reason for doing this study is to assess airplanes that do not have the performance capability of those for which TCAS was originally designed. A high-performance UAS can easily conduct an avoidance maneuver, while a UAS that can marginally maintain its desired straight, level, unaccelerated flight condition is a limiting case of interest. Note that marginally able to maintain straight and level unaccelerated flight is a fairly normal flight condition for GA airplanes and for some types of UAS. This condition can be mission related; for example, a slow flight speed can be used for maximum endurance. "Marginally able" can also mean straight and level at maximum throttle and speed with no excess energy, meaning any climb or turn maneuver would result in a loss of speed.

Figure 1:   Test matrix of aircraft design parameters. Red dots are the values from the sample aircraft in Table 1 with the number corresponding to the aircraft number in the table. The blue bars show where the test matrix boundaries were set.

The reduced matrix allowed results to be published earlier and they cover UAS performance in the near term as well as the focus area associated with RTCA SC-228 Terms of Reference [4].

Each design parameter is briefly described in the subsection below and rationale for the selected range is discussed. The simulation input is made in terms of these key design parameters, and they are related to key performance parameters within the simulator. Both the design and performance parameters used are readily available to airplane designers. Thus, the results can be readily applied to existing and new UAS designs. The parameters chosen are essentially for a "unit" airplane, which is to say that given the same set of parameters, the performance of the resulting airplane can be estimated without knowing the size of the airplane, i.e., a wing span of 6 ft or a wing span of 200 ft with the same set of parameters used here would have the same performance. This allows for comparison of airplane performance regardless of the physical size of the vehicle. Thus, an airplane designed to carry a 10-lb camera or a 100-lb camera at the same speed and altitude ranges could have very similar sets of design parameters because they could be essentially scale models of each other. In reality it is not quite this simple, as specific structural mechanics, aerodynamics, and engine performance may differ, but it is illustrative of the value of using these parameters.

2.2 Parameter Values for Simulated UAS

This section gives a brief description of each of the UAS design parameters used in the study and describes the test range used in the simulation and the rationale for choosing that range.

2.2.1 Thrust-to-Weight Ratio ($\frac{T}{W}$)

Range: 0.1 to 0.4 (non-dimensional)

The ratio of thrust to weight is a measure of the propulsion system's thrust per unit weight of the airplane. The range of 0.1 to 0.4 was chosen because the vast majority of existing airplanes have $\frac{T}{W} \leq 0.4$ for at least part of their flight regime and, as can be seen from Table 1 most do not exceed it. Low $\frac{T}{W}$ values are experienced when most airplanes reach their service ceiling and are near their maximum gross weight. UAS with higher $\frac{T}{W}$ values are not the focus of this study as they will be able to outperform the airplanes of interest and do not represent a limiting case. Many of the configurations tested had sufficient thrust for the commanded climb maneuvers as will be seen in the results section.

2.2.2 Wing Loading ($\frac{W}{S}$)

Range: 1 to 25 (lb/ft^2)

Wing loading is the airplane's weight divided by the wing area, measured in pounds per square foot. A $\frac{W}{S}$ range of 1 to 25 lb/ft^2 was chosen as the range of interest for this work because it is generally associated with single-engine CFR 14 Part 23 airplanes[1]. It does not nominally cover airplanes that fly fast or at very high altitudes which are left for later studies.

2.2.3 Aspect Ratio (AR)

Range: 5 to 40 (non-dimensional)

Aspect ratio is a fineness ratio of the wing computed as wing span divided by mean aerodynamic cord. High AR airplanes are characterized as having lower induced drag resulting in higher lift-to-drag ratios and higher aerodynamic efficiency. Conversely, low AR airplanes generally are capable of greater roll accelerations and rates but have lower aerodynamic efficiency. The range of interest for this study spans a wide range from unusually low aspect ratio airplanes to high aspect ratio motor gliders. It does not include the extreme AR values of some high-performance manned gliders. Note that the highest aspect ratios (AR) and maximum lift-to-drag ratios $\left(\left(\frac{L}{D} \right)_{max} \right)$ in Table 1 are from high-performance sailplanes.

2.2.4 Maximum Lift/Drag ($\frac{L}{D}_{max}$)

Range: 5 to 50 (non-dimensional)

---

[1] Part 23 single engine land aircraft will generally have $\frac{W}{S}$ less than 25 lb/ft^2 because their stall speed cannot exceed 61 KCAS per 14 CFR Part 23 [7]

This is the maximum lift-to-drag ratio for the airplane configuration. This value is used in the simulation to define the parasite drag of the airplane, a value that is difficult to obtain otherwise. The selected range of interest includes all airplanes in Table 1 but excludes a limited set of very-high-performance sailplanes.

2.2.5   Maximum Coefficient of Lift ($C_{L_{max}}$)

Range: 0.6 to 2 (non-dimensional)

The maximum coefficient of lift coupled with $\frac{W}{S}$ is used to define the minimum velocity (stall speed) of the airplane configuration. The 2-D airfoil theory (potential flow) used in the simulation does not predict stall. Thus, $C_{L_{max}}$ is an independent variable in the study, effectively imposing a stall constraint. It is also used in conjunction with initial percent of $C_{L_{max}}$ to specify the airplane's initial speed. This study evaluated airplanes at initial speeds ranging from nominal cruise to loiter.

2.2.6   Initial Percent of Maximum Coefficient of Lift ($\%C_{L_{max}}$)

Range: 0.08 to 0.80 (non-dimensional)

This variable is used in conjunction with $C_{L_{max}}$ and $\frac{W}{S}$ to define the initial velocity of the airplane. The approach sets up conditions associated with different phases of flight and parts of the flight envelope. It avoids direct association with angle of attack, which has different zero reference lines associated with specific configurations. As mentioned in the previous section, the range chosen spans from a nominal cruise condition to a loiter condition. Loiter is considered to be a best endurance condition, typical of many current UAS missions, and is therefore close to the $\frac{L}{D}_{max}$ condition and at a relatively low speed and energy state. The approach is represented as:

$$\%C_{L_{max}} = \frac{C_{L_i}}{C_{L_{max}}} * 100. \hspace{3cm} \text{Equation 1}$$

2.2.7   Maximum Load Factor (g_{limit})

Range for Climb: 1.25 to 3 (g)
Range for Descent: 0 to 0.75 (g)
Range for Level Turn: 1.5 (g)

These climb and descent ranges represent current normal category airplanes [7] for the climb maneuvers, but go to zero for descent maneuvers. Zero g is not sustainable by most airplanes primarily because of fuel and oil systems. For the vertical maneuvers, the 0.25 increment on either side of 1-g straight and level flight is what TCAS expects a pilot to use for transition from one 1-g condition to another. Thus, it was selected as a minimum.
The g_{limit} effectively limits rate of change of the flight-path angle vertically (climb and descent) and track horizontally (level turn). This can be represented mathematically as:

for the vertical maneuver:

$$\dot{\gamma}_{max} = \frac{g}{V} * (g_{limit} - 1), \hspace{3cm} \text{Equation 2}$$

for the horizontal maneuver:

$$\dot{\psi}_{max} = \frac{g}{V} * \sqrt{g_{limit}^2 - 1} \,,$$

Equation 3

where g is the constant acceleration due to gravity.

Maximum load factor available may be aerodynamically limited to less than the command limits at low speeds due to the amount of aerodynamic lift available at the current flight condition, i.e., if the airplane is below its "corner speed" or "maneuver speed" it cannot generate enough aerodynamic lift to reach the structural g_{limit} (see [8,9]). In that case, the simulation models the aerodynamic g_{limit}. A single level turn g_{limit} was used in this study.

The load factor is expressed as:

$$n_z = \frac{L}{W} = \frac{\frac{1}{2}*\rho*V^2*C_L}{\frac{W}{S}}.$$

Equation 4

The aerodynamic limitation results from a limited amount of lift an airplane can produce.

$$n_{z_{max}} = \frac{L_{max}}{W} \leq g_{limit}.$$

Equation 5

For this study, all airplanes are initially trimmed to steady level flight. At this flight condition, the lift the airplane generates is equal to the weight. Thus, Equation 5 becomes:

$$n_{z_{max}} = \frac{L_{max}}{L_i} = \frac{C_{L_{max}}}{C_{L_i}} = \frac{1}{\%C_{L_{max}}} \leq g_{limit}.$$

Equation 6

Using Equation 6, in order for an airplane to generate 3 g's, the maximum value within the range of interest, it must be flying at an initial C_L less than or equal to 33.3% of $C_{L_{max}}$.

2.3   Simplified Airplane Performance Model

A simulation tool was developed to evaluate SAA maneuver time requirements for a spanning set of airplane performance models over a broad range of encounters. The tool is referred to as the 2-degree-of-freedom Prototyping Airplane Interaction Research Simulation (2PAIRS). While the 2PAIRS tool technically models more than two degrees-of-freedom of the airplane, the tool is limited to two-axis motion for any given maneuver, i.e., vertical climb, vertical descent, or level turn individually. The 2PAIRS tool was developed in the MATLAB® programming environment.

The 2PAIRS simulation tool was developed to analyze the interaction between two airplanes involved in a single encounter. The airplane performance model is based upon simplified two-dimensional airfoil theory with finite-wing approximations. These assumptions allow for a simple model that includes performance limitations while still running fast enough for a comprehensive study of the overall design space.

The simulation uses the basic design parameters from Table 1: $\frac{T}{W}$, $\frac{W}{S}$, AR, $C_{L_{max}}$, $\frac{L}{D_{max}}$, and Oswald's wing efficiency factor (e). Basic aerodynamic properties are estimated from these parameters using two-dimensional airfoil theory [8]. This simple approach was used to provide generally applicable results, versus understanding the performance capabilities of a specific airplane configuration. Moreover, this allows evaluation of a spanning set of performance capabilities by varying the design parameters across a range of values of interest in a matrix form. To estimate airplane performance, basic airplane performance principles were used, starting with the assumption that straight and level flight requires thrust to equal drag ($T = D$)

and lift to equal weight ($L = W$). The following discussion provides some background on the approach.

Aerodynamic performance metrics, i.e., lift and drag coefficients, can be estimated using 2-D airfoil theory applied to 3-D elliptical wings resulting in:

$$C_L = \frac{2*\pi*AR*\alpha}{AR+2} \qquad\qquad \text{Equation 7}$$

and

$$C_d = C_{d_o} + \frac{(C_L^2)}{\pi e AR} \qquad\qquad \text{Equation 8}$$

where α is the angle of attack in radians. The parasite drag coefficient (C_{d_0}) may be estimated using:

$$C_{d_o} = \frac{\pi*e*AR}{4\left(\frac{L}{D}\right)^2_{max}}. \qquad\qquad \text{Equation 9}$$

Then, for level flight

$$L = \bar{q}SC_L = W, \qquad\qquad \text{Equation 10}$$

and consequently

$$C_L = \frac{W}{\bar{q}S} \qquad\qquad \text{Equation 11}$$

where

$$\bar{q} = \frac{1}{2}\rho V^2. \qquad\qquad \text{Equation 12}$$

The 2PAIRS simulation tool was developed using the aerodynamic performance approximations above and simplified equations of motion for the vertical and horizontal planes separately. This resulted in kinematic equations that drove the simulation as follows:

Forces acting parallel to the flight path for a vertical maneuver:

$$T\cos(\alpha) - D - W\sin(\gamma) = m\frac{dV}{dt}. \qquad\qquad \text{Equation 13}$$

Forces acting normal to the flight path for a vertical manevuer:

$$L - W\cos(\gamma) + T\sin(\alpha) = mV\frac{d\gamma}{dt} = \frac{mV^2}{R} \qquad\qquad \text{Equation 14}$$

where γ is the flight-path angle in degrees. Similarly for the horizontal maneuver:

$$T\cos(\alpha) - D = m\frac{dV}{dt} \qquad\qquad \text{Equation 15}$$

$$L\sin(\phi) = mV\frac{d\psi}{dt} = m\frac{V^2}{R} \qquad\qquad \text{Equation 16}$$

$$L\cos(\phi) = W \qquad\qquad \text{Equation 17}$$

where ϕ is the bank angle in degrees and ψ is the track angle in degrees.

The high-level descriptions above are here to provide the reader insight to the modeling approach used and therefore fidelity of the simulation. For more information please refer to [8].

2.4   Simulation Description

The simulation initializes each run with two airplanes on a collision course, the UAS and a non-maneuvering intruder. The intruder may be flying level or given a constant rate of climb or descent. It may approach the UAS's initial trajectory through 360° of azimuth, although a more limited azimuth range that accounts for right-of-way rules was used in the current study. At time zero, the UAS initiates the commanded maneuver and attempts the maneuver, but may be limited by its maneuver performance envelope. The UAS will transition to the commanded climb, descent, or turn rate based on g_{limit} or roll-rate limit. It will reach and sustain the rate as long as performance allows. If it has insufficient performance for the commanded maneuver, it will transition to its best sustainable performance over time based on its unique capabilities. For example, an airplane that cannot sustain a commanded climb rate will attempt to reach the rate, and if it reaches the commanded climb rate, it will sustain the rate as long as possible while losing speed. When the selected minimum speed, best-angle-of-climb speed (V_{BA}) herein, is reached, the airplane will reduce climb rate to sustain that speed. The simulation measures the CPA between the UAS and intruder (Figure 2) and stops the run just after CPA is passed. The simulator's graphical user interface (GUI) version provides time histories of the UAS and intruder states, while a batch interface compiles initial states, states at CPA, and selected other mid-point states of interest. The simulation uses discrete time interval integration of the related equations of motion at 20 Hz.
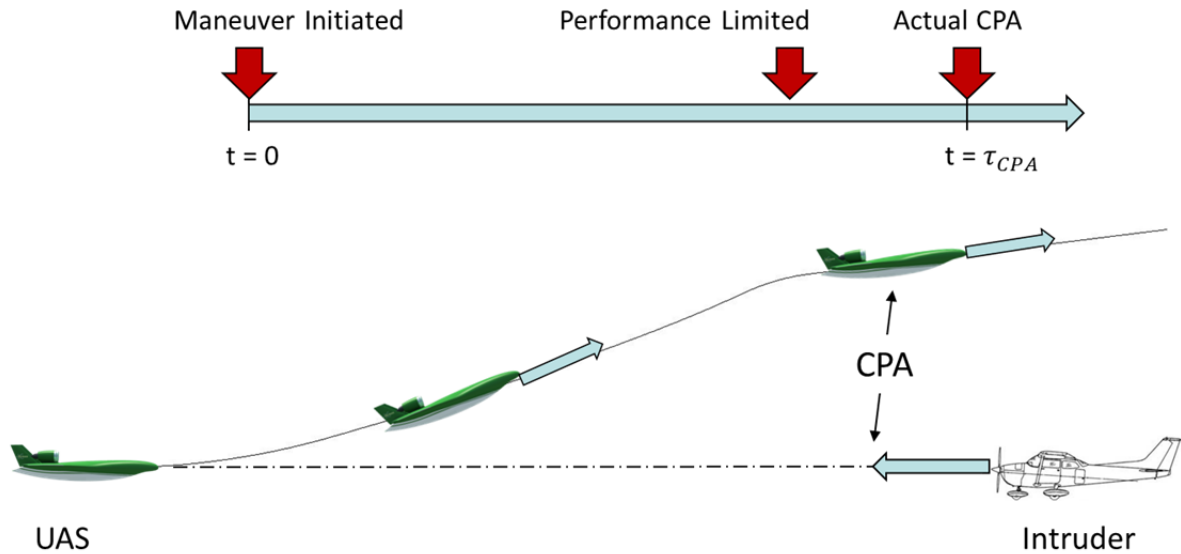

Figure 2:   2PAIRS encounter time line.

The encounters are set up based on initial τ to the predicted CPA. Thus, the initial range is greater for faster-moving UAS and intruders, but the time available to avoid a collision is consistent between runs with the same τ. The approach of having the UAS initiate its maneuver at time = 0 seconds makes the results independent of sensors and trackers. With this approach the predicted time-to-go at which a maneuver must be initiated to result in the desired CPA can be discerned. Regulators can use the data to help determine when a SAA system needs to act, define an acceptable design space, and develop required capabilities for SAA systems taking UAS performance into account. UAS designers can back out times for Detect, Track, Evaluate, Prioritize, Declare, Determine, Command and Execute (Figure 3) based on their SAA system design to determine when initial detection must occur.

Three separate 2PAIRS implementations were developed to assess basic maneuver elements: vertical climb, vertical descent, and level turn. The simulations account for airplane performance limitations associated with the particular maneuver, e.g., climb performance limitations in the vertical climb version or V_{NE} in the vertical descent version. The UAS performance in 2PAIRS is limited by either aerodynamic/propulsive limitations, maneuver command limits, or a combination of both. Note that current UAS inner-loop controllers generally limit maneuvers far below airframe capability. The variation in commanded rates models those limitations in 2PAIRS as well as cases with commands greater than the UAS can sustain.

The 2PAIRS batch capability was set up to allow for a multitude of parameter combinations to be run and analyzed in a time-efficient manner. This requires marching through each parameter variation while holding the others constant with no consideration of whether each particular parameter combination results in an airplane that can fly at a given initial condition, or even at all. Additionally, it does not make any assessment of whether an airplane would be a 'good' design or not. This was deemed to be the most efficient way to set up the test matrix and assure that the set of results would be a spanning set of likely UAS performance within the region selected. This approach required some pre-run constraints to be implemented in the batch simulation to limit analyses to the airplanes that could fly (meeting physics-based constraints) and that were at an initial condition suitable for the maneuver to be executed. If these checks were met, the simulation would proceed with the particular parameter combination; otherwise, the combination would be skipped.
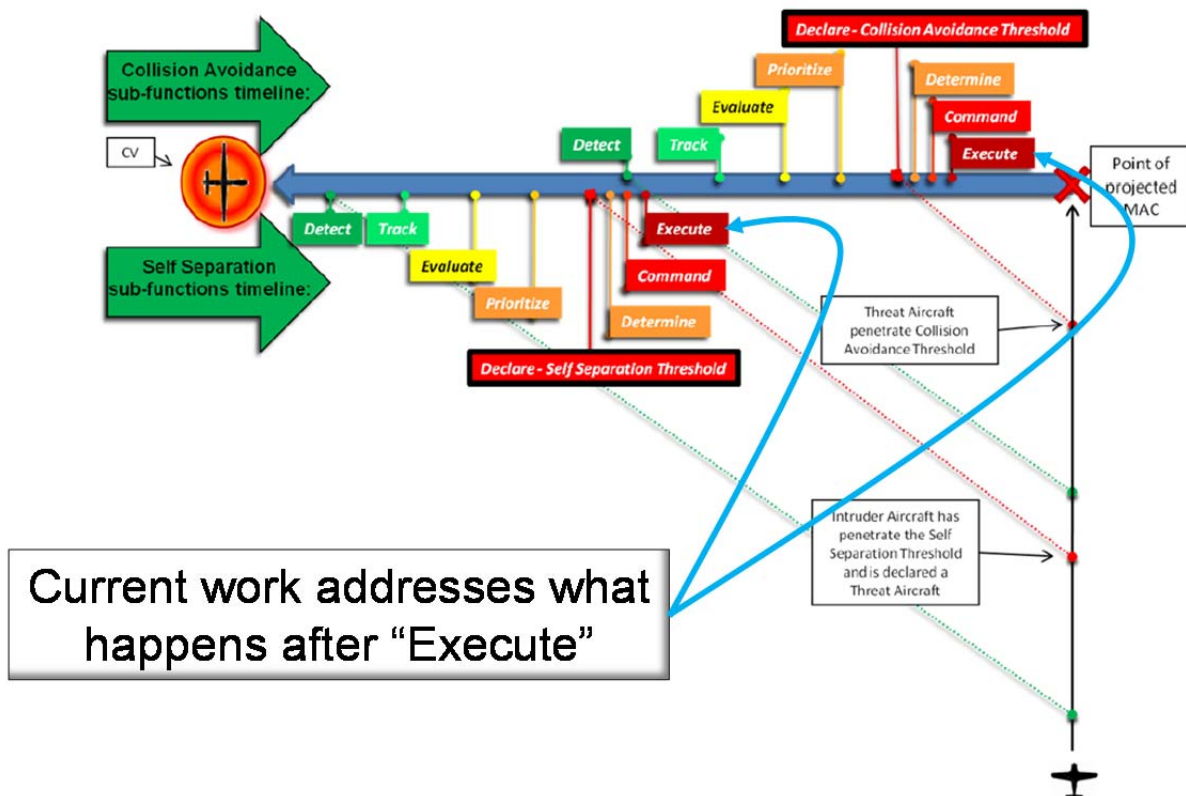

Figure 3: Diagram from 2nd FAA SAA workshop report showing SAA self-separation and collision avoidance functions on a timeline. The work herein starts at "Execute." [2]

The first constraint requires that the thrust available to the airplane is greater than or equal to that required to maintain steady, level flight at the initial knots calibrated airspeed (KCAS) (i.e., the initial condition of each airplane within the simulation). This constraint is represented mathematically by:

$$\frac{T}{W_{max}} \geq \frac{T}{W_i} = \frac{T}{W_{SLUF}}.$$ Equation 18

If the thrust available is only equal to the thrust required to maintain steady, level flight, the airplane is able to maintain the initial flight condition, but will not have excess power to enable a climb without sacrificing speed. More thrust available can provide at least some climb rate without sacrificing speed. Conversely, if the thrust available is not at least equal to the thrust required, the airplane cannot maintain the straight, level, unaccelerated initial trim condition and will not be analyzed.

The next physical constraint of the airplane is associated with the simulation minimum allowable velocity of an airplane for the desired maneuver. The constraint requires the vehicle's 1-g stall speed to be below V_{BA}. Since speed is dictated by C_L, this constraint may be represented by:

$$C_{L_{max}} \geq C_{L_{BA}}.$$ Equation 19

If this constraint is violated, the airplane will attempt to fly below its stall speed, which would result in a loss of control for the airplane.

2.5   CPA Ranges of Interest

Some consideration of CPA ranges of interest is required both for analyzing results and for scoping the test matrix. Given the test matrix approach used, many post-maneuver CPAs in the results would seem to far exceed the critical CPAs of interest. However, which CPA ranges are of interest has not yet been determined by the community. This section discusses an attempt to determine a reasonable range for CPAs of interest, noting that results need to include any possible CPA range that may be determined to be of interest in the future. The FAA 2nd SAA Workshop Report [2] describes notional boundaries (Figure 4) but only associates numbers with the NMAC volume. The report provides descriptions but no values for the Collision Avoidance Threshold (CAT), Well Clear Volume (WCV), or Self-Separation Threshold (SST). Note that the definitions of CAT and SST include "last chance to maneuver to avoid" the next boundary. Thus, these two bounds are encounter and airplane-performance dependent.

In order to draw conclusions from the results, there is a need to determine what CPA values would mean success. The measures of success must include both successfully avoiding a collision and maintaining well clear or self-separation. Thus, both small and large CPAs are of interest. The NMAC volume has been accepted by the aerospace community to be a cylinder defined as ±100 ft of the intruder vertically with a horizontal radius of 500 ft.
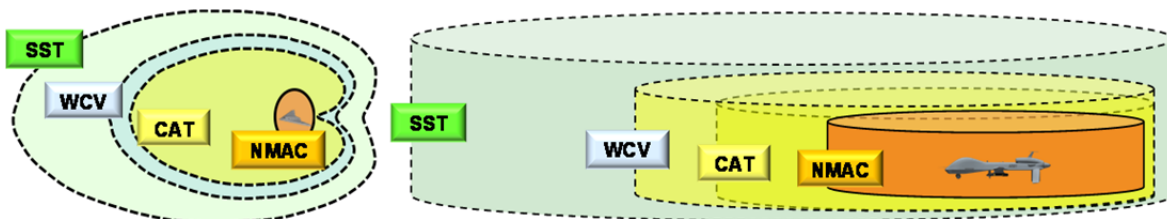

Figure 4:   Figure from FAA 2nd SAA Workshop showing collision avoidance and self-separation boundaries. [2]

The WCV is much more difficult to define. Results from this study may help define it and are expected to contribute directly to the definition of the CAT and SST. In order to put an upper bound on the goal of obtaining a spanning set of CPA results, some assumptions are required. The intent of these assumptions is to assure that results from this study are a superset of ranges ultimately determined for the WCV. That means our encounter set must include CPAs that exceed the currently undefined WCV. The current regulations of CFR 14 were used to gain some insight on what an upper limit is likely to be. CFR 14 Part 91.159 and 91.179 [1] state that aircraft operating under Instrument Flight Rules (IFR) on easterly headings are to fly at odd thousands of ft MSL, while ones on westerly headings fly at even thousands of ft MSL. Visual Flight Rules (VFR) aircraft are required to use the same even/odd thousands of ft altitudes, but add 500 ft (ee Figure 5). The current airspace allows these aircraft to pass with these vertical separation distances and no horizontal separation. Thus, it seems reasonable to assume that either 500 or 1000 ft vertical separation is the current definition of vertical well clear. As a result, this study presents results in relation to three values of vertical separation: 1) ≤ 100 ft for NMAC; 2) ≤ 500 ft referred to as IFR-VFR; and 3) ≤ 1000 ft referred to as IFR-IFR or VFR-VFR. CPAs greater than 1000 ft are considered to have exceeded the WCV requirements likely definition.
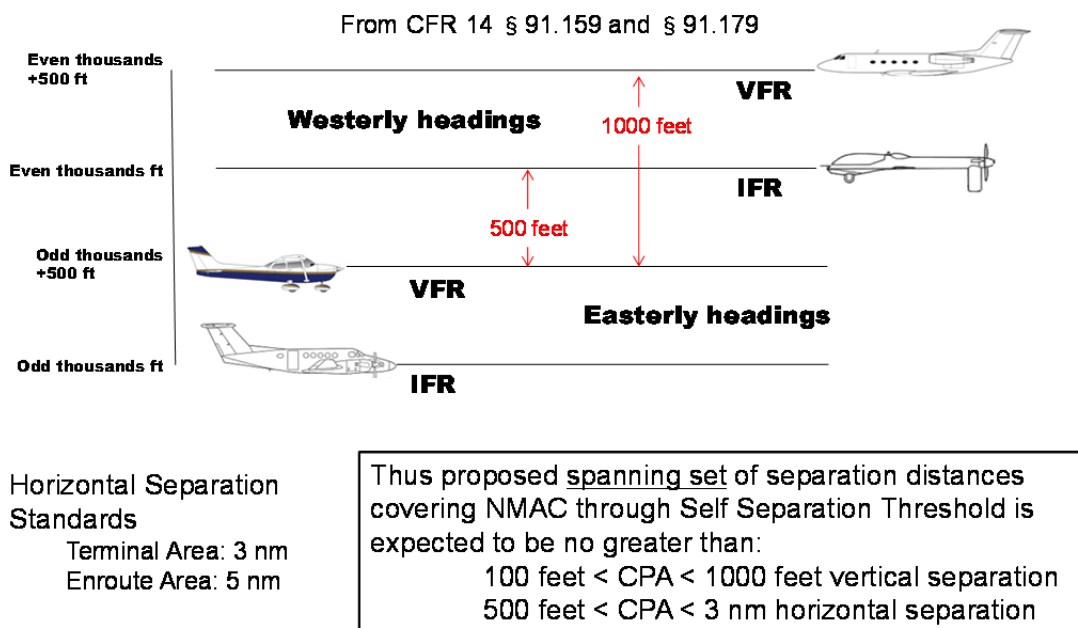

Figure 5:   Information used to Select Maximum CPAs of Interest.

A maximum horizontal CPA is more difficult to discern. Controllers are required to separate IFR traffic by 3 nautical miles in terminal areas. However, VFR traffic self separates visually and even two aircraft operating under IFR may be allowed to self separate after the pilots acknowledge to controllers that they have visually acquired the other aircraft. The result is that self separation is maintaining well clear as defined by the onboard pilot's discretion. Thus, well clear could mean anything inside 3 nm. As a result, this study will assess horizontal separations encompassing 500 ft (NMAC) out to 3 nm (terminal area IFR separation).

2.6   Avoidance Maneuvers and Encounter Parameters

This section describes the avoidance maneuvers and the intruder behavior modeled. Parameter ranges are given for the commanded vertical climb and descent and horizontal turn avoidance maneuvers, and for the encounter scenario and intruder behavior. Descriptions of the GUI simulator tools are also given.

2.6.1   Climb Maneuver

When a simulation run starts, the UAS is trimmed in straight and level flight and immediately initiates a maneuver to the commanded climb rate. The UAS transitions from level flight to the commanded climb rate at the maximum load factor (referred to as max nz in Figure 6) set for the maneuver or the aerodynamic limit, whichever is lower. If the UAS has sufficient performance to sustain the climb without decelerating, it will do so. If it does not, it will lose speed while maintaining the climb rate (if possible) until the minimum allowable speed, or V_{BA}, is reached. At that point it will push over to the corresponding sustainable climb angle using the same g-increment used in the pull up. It will then continue the climb at the sustainable climb speed and angle.

The GUI for the vertical climb maneuvers is shown in Figure 6. The user can enter numbers in each box to visually see the results of changes. By clicking the button next to each parameter name, the slider can be used to see the resulting trajectory and CPA change as the value of the selected parameter changes incrementally. Results can be sent to the workspace to allow analysis of time histories of a wide number of states for the run. Additionally, the colored squares allow the plot to be exported. Selecting another color after changing parameters will cause the result to be plotted with the result from the last time a colored button was selected. Up to six results can be added to a plot in this manner. The batch tool allows sweeps of all parameters shown on the GUI and outputs initial, final, and some interim states of interest for the UAS and intruder.
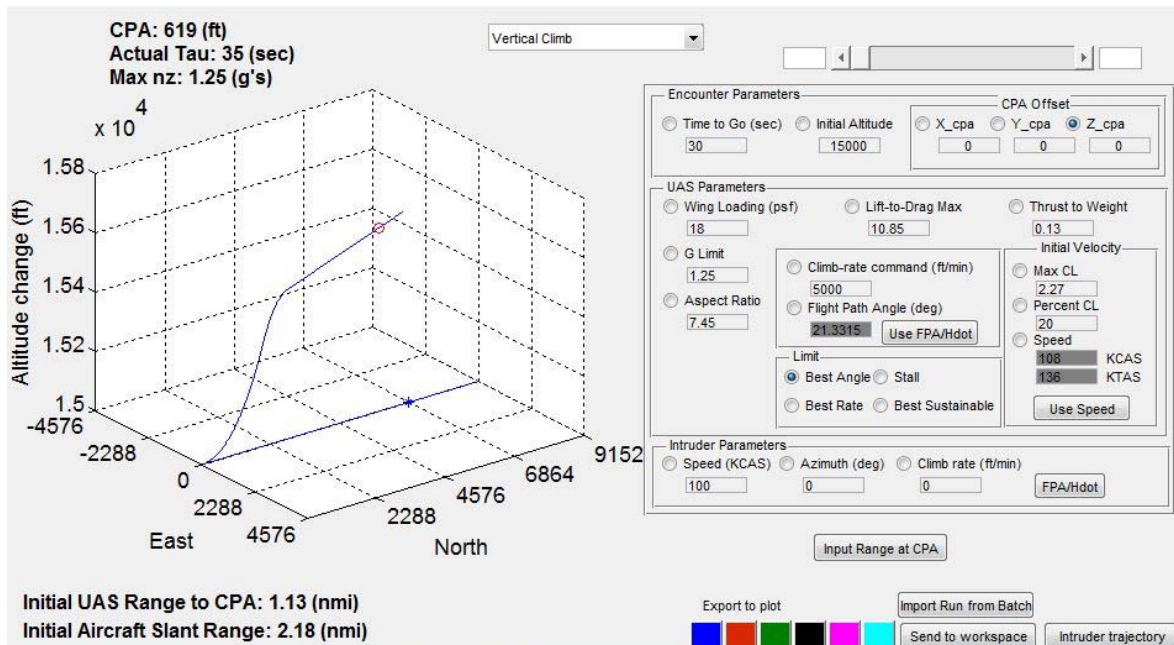

Figure 6:   2PAIRS GUI tool – Vertical Climb.

2.6.2 Descent Maneuver

Similar to the climb maneuver, the UAS is initially trimmed in straight and level flight. When a simulation run starts, the airplane immediately initiates the commanded descent rate. It rotates at the commanded or minimum aerodynamic load factor for the configuration to reach the commanded descent rate. The airplane attempts to maintain the initial speed by reducing the throttle position until minimum power is reached. In 2PAIRS, that means $\frac{T}{W}$ = throttle = 0. Depending on the magnitude of the commanded descent rate, the airplane may gain speed while continually adjusting flight-path angle to maintain the steady rate of descent until V_{NE} is reached. If V_{NE} is reached, the airplane will pull up at the commanded or available g_{limit} to the glide path that will maintain V_{NE}. The airplane will maintain this speed and descent rate until CPA is reached and the run ends. The GUI for the vertical descent maneuver is shown in Figure 7. A batch tool front end was also developed.
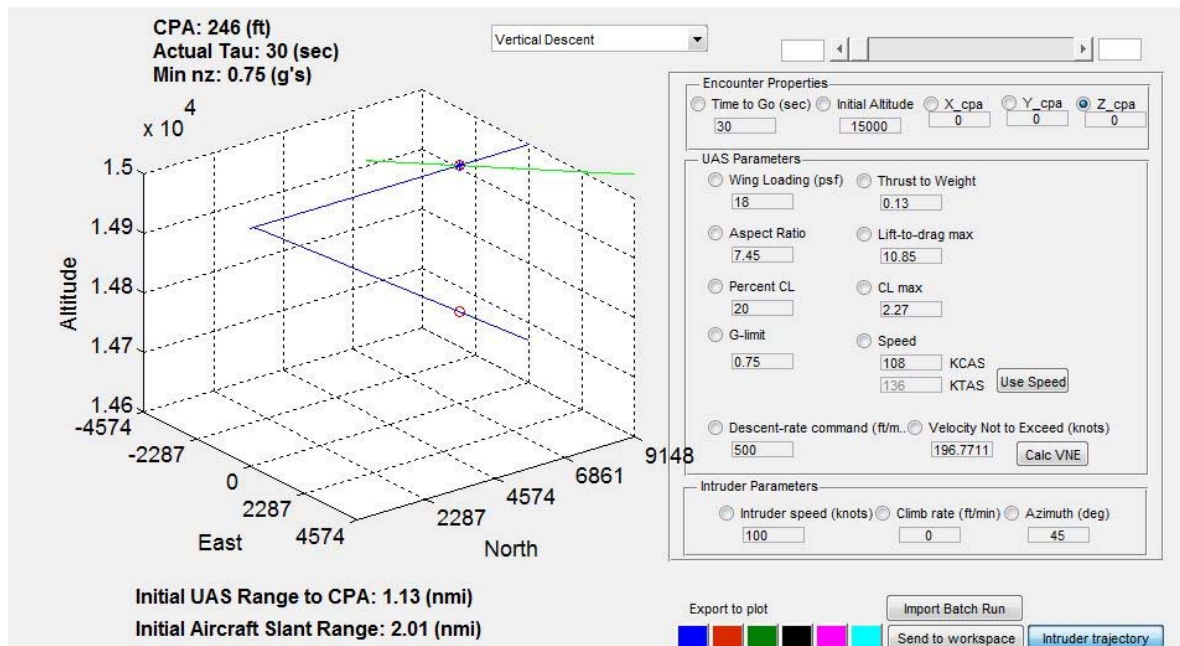

Figure 7:   2PAIRS GUI tool – Vertical Descent.

2.6.3 Vertical Maneuver Parameters

This section gives ranges and descriptions of parameters associated with the vertical climb and descent maneuvers.

2.6.3.1 Commanded Vertical Rate ($\dot{h}_{command}$)

Range: 500 to 5000 (ft/min)

This is the commanded rate of climb or descent, for the respective maneuvers, that the airplane receives at time = 0 seconds in the simulation. The airplane will attempt the commanded rate while trying to maintain forward speed. If forward speed cannot be maintained, the airplane will adjust its flight path to maintain the limiting speed, as described earlier.

2.6.3.2 Best-Angle-of-Climb Speed (V_{BA})

Range: Varies based on other parameter values

Unique to the vertical climb maneuver, this parameter is used to restrict the minimum speed for the maneuvering airplane to the speed associated with $\frac{L}{D_{max}}$. This restriction keeps the airplane at a best sustained climb condition and prevents stall. If the airplane must sacrifice forward speed to achieve or maintain vertical speed, it will do so until V_{BA} is reached. The airplane will then adjust the climb rate to the sustainable best-angle-of-climb rate associated with the airplane configuration.

V_{BA} is calculated from airplane design parameters at the start of each run:

$$V_{BA} = \sqrt{\left(\frac{2*\frac{W}{S}*\frac{L}{D}_{max}}{\rho*\pi*e*AR}\right) * \sin^{-1}\left(\frac{T}{W} - \frac{1}{\frac{L}{D}_{max}}\right)}. \qquad \text{Equation 20}$$

In real world practice, pilots rarely fly below V_{BA}, often referred to as loiter speed, unless practicing slow flight procedures and stall recovery.

2.6.3.3 Velocity Not to Exceed (V_{NE})

Range: 1.15 * V_{cruise} (KCAS)

Unique to the vertical descent maneuver, this parameter is used to define a maximum velocity the airplane can reach. This can be a structural limit, a control law limit, or a velocity restriction imposed by rules of the NAS (i.e., airplane speed limit). This value is not directly related to aerodynamic and propulsive performance, so some gross assumptions were made about margins above cruise speed. The results presented herein are from one increment above cruise. For this study, cruise speed is defined as the 1-g speed associated with 8% of the $C_{L_{max}}$, expressed as:

$$V_{cruise} = \sqrt{\frac{2*\frac{W}{S}}{\rho*.08*C_{L_{max}}}}. \qquad \text{Equation 21}$$

2.6.4 Level Turn Maneuver

Similar to the vertical maneuvers, the airplane is initially trimmed to straight and level flight. At the start of the simulation run, the airplane begins to roll at the specified rate to the bank angle that will yield the commanded turn rate. If the commanded rate is greater than the rate of turn achievable within the structural limit or bank-angle limit, the airplane will be limited to the maximum achievable turn rate. The UAS will continue the turn until CPA is reached or the point at which it rolls to wings-level at the specified roll rate to achieve the commanded track change of 90º. It will then continue to fly level at a steady speed until CPA is reached and the simulation ends. The GUI for the level turn maneuver is shown in Figure 8. A batch front end was also developed for this maneuver.
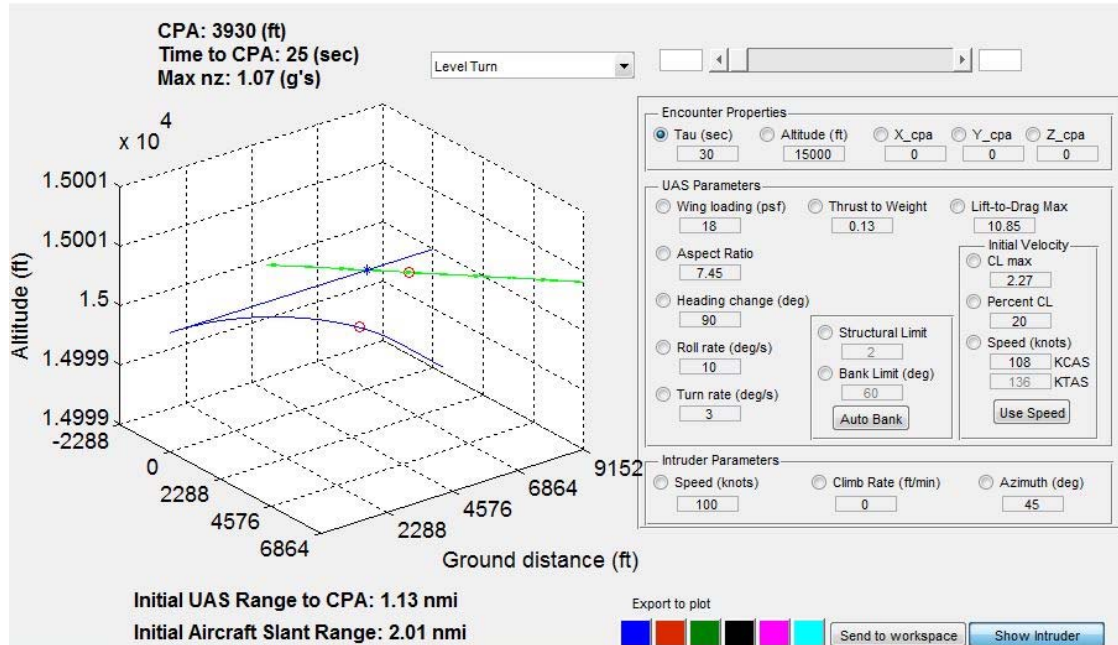
Figure 8: 2PAIRS GUI tool – Level Turn.

2.6.5 Level Turn Parameters

This section gives ranges and descriptions of parameters associated with the level turn maneuver.

2.6.5.1 Bank Angle Limit (ϕ_{limit})

Range: 10º to 60º

This parameter limits the bank angle an airplane can achieve. This parameter has a direct effect on an airplane's achievable turn rate. There is a direct relationship between the bank limit and imposed g_{limit} that is not related to airplane speed. However, the bank angle or g_{limit} determine the turn rate and radius for a given airplane speed. For this study, g_{limit} is used to set the bank angle limit. The equation relating these two parameters can be expressed as:

$$g_{limit} = \frac{1}{\cos(\phi)}.$$

Equation 22

2.6.5.2 Heading Change Command ($\Delta\psi$)

Range: 90º

This parameter is the commanded heading change the airplane will make before returning to straight and level flight. The implementation makes this heading capture within ±2° for all runs.

2.6.5.3 Roll Rate Limit ($\dot{\phi}_{limit}$)

Range: 30 (deg/sec)

This parameter sets the roll rate for transition between straight and level flight and the level turn and back to straight and level flight. This value is not expected to be a major player given the required time associated with horizontal turns, i.e., the time required to roll in and roll out of the turns is small compared to the time to turn to the specified heading. Thus, only one value was run in the dataset. Additionally, the airplane reaches and stops the roll rate in one time step, i.e., roll acceleration is not modeled.

2.6.5.4 Turn Rate Command ($\dot{\psi}_{command}$)

Range: 1 to 10 (deg/sec)

This parameter is the commanded turn rate the airplane will attempt to maintain. The airplane may not reach the commanded rate if there are turn rate limits imposed by a bank limit or g_{limit}, as outlined in Equation 3.

2.6.6 Encounter Parameters

This section gives ranges and descriptions of the encounter parameters used with all three maneuvers. The encounter geometry definitions, azimuth in particular, align with a white paper presented and discussed in RTCA SC-203 and that will be discussed in SC-228. It has not yet been formally published. However, the definitions are described in [10].

2.6.6.1 Time-to-go (τ)

Range: 10 to 120 (seconds)

Time-to-go is the predicted time until CPA between two airplanes involved in an encounter. For the encounters simulated, the predicted CPA was always 0 ft, i.e., a collision. If no maneuver is performed, the two airplanes will collide or reach CPA τ seconds after the run starts. This parameter is also used to define the initial range between the two airplanes given the initial velocity of both airplanes and the encounter geometry. It should be noted that the initial time-to-go (predicted τ) is not necessarily the time at which the actual CPA occurs due to changes in the closure rate and encounter geometry as a result of the UAS's maneuver. Since the initial τ range must encompass Collision Avoidance and Self-Separation thresholds, τ was varied from 10 – 120 seconds in the simulation.

2.6.6.2 Intruder Velocity (V_{intr})

Range: 50 to 250 (KCAS)

The intruder flies at a constant velocity throughout the simulation, input as KCAS. The speed of intruders ranges from 50 to 250 KCAS for the full range of altitudes tested. This is the speed limit in the NAS below 10,000 ft MSL. Thus, faster intruders could be encountered above that altitude. Aircraft above 10,000 ft MSL are required to have transponders so they are very likely to be dealt with by ATC. Still, faster intruders should be assessed at a later date.

2.6.6.3 Intruder Azimuth (β)

Range for Vertical Maneuvers: 0º to 90º
Range for Horizontal Maneuvers: -90º to 90º with UAS always turning right.

The angle of the encounter was limited to the forward quadrants of the UAS in order to avoid scenarios with the UAS being overtaken. These scenarios were omitted because, in the current airspace, it is always the duty of the overtaking aircraft to avoid the slower-moving aircraft, and this rule is currently expected to carry over to UAS. The intruder was always heading toward the UAS as well, thus overtaking scenarios by either the intruder or the UAS were not included in the results to date. They would require lower maneuver performance than the scenarios evaluated.

From Figure 9 and reference [10], β is the angle measured between the ownship's and the intruder's initial horizontal flight paths. For vertical maneuvers (i.e., vertical climb or descent), this value will range from 0° (head-on) to 90° (crossing) because results will be symmetrical for approaches from the other side. The horizontal maneuver ranges from -90° (crossing from left) through head-on to 90° with the UAS always turning right. Symmetry can be used for assessing left turns.

For this study, the range at CPA (R_{CPA} in Figure 9) is always 0 ft, meaning the two airplanes always begin on a direct collision course. Thus, there are no asymmetries associated with encounter offsets.

2.6.6.4 Intruder Vertical Rate ($\dot{h}_{intr}$)

Range: -5000 to 5000 (ft/min)

Intruder vertical rate is input as a positive or negative rate in ft/min. The value is held constant throughout a simulation run. It is assumed that the intruder can maintain the specified vertical rate, and therefore, no performance limitations are considered for the intruder. The vertical rates simulated for the intruder range from a constant climb at 5000 ft/min to a constant descent at 5000 ft/min. While the full range of intruder climb and descent rates were run, a post-analysis exclusion was placed on the maximum flight-path angle from which the intruder could approach. For the data presented herein, the intruder did not approach at a vertical flight-path angle with magnitude greater than ±12°. For instance, this limitation excludes 50 KCAS intruders climbing or descending at 5000 ft/min, which results in an extreme and unreasonable flight-path angle of 80°.
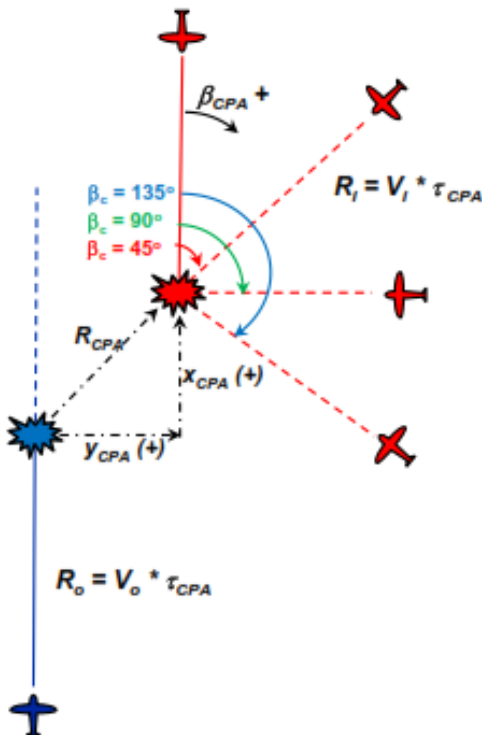

Figure 9:   Encounter Geometry and
encounter parameter
definitions. Diagram from
SC-203 document. [9]

2.6.6.5 Altitude (h)

Range: 1000 to 18,000 (ft MSL)

Measured in ft MSL, altitude is used primarily to specify the air density for the encounter. During the run, avoidance maneuver vertical deviations of interest are small. Thus, atmospheric density is held constant through each simulation run to save computational complexity. Test runs were conducted to show this assumption made no significant difference in the resulting trajectory or CPA. Altitude has a direct effect on the difference between the calibrated airspeed, which drives aero-propulsive performance, and true airspeed, which dictates the inertial reference frame. The test range chosen for the encounters ranges from 1,000 to 18,000 ft MSL, which is generally landing pattern altitude to the bottom of Class A airspace. This range follows the RTCA SC-228 Terms of Reference which outlines that the focus of initial work will be on UAS transitioning to and from Class A airspace [4] or special purpose areas.

2.7   Verification and Validation of Simulation

Before moving into the large volume of data available from the 2PAIRS batch tool, data from individual airplanes found in Table 1 were used for verification and validation of results from the simulator and to illustrate trends. Figure 10 shows climb performance results for a representation of a Cessna 172, which is a single-engine general-aviation airplane that has four seats and is capable of cruising at approximately 110 KTAS and achieving a best rate of climb of approximately 750 ft/min at maximum gross weight and MSL. Results shown are from runs conducted at 1000 ft MSL with τ = 30 seconds using the GUI tool which provides time history data. The simulation data for the Cessna 172 matched the behaviors that were anticipated, showing that the simulation accurately modeled how the Cessna airplane could react in the scenarios. At time zero, the airplane was commanded to climb at 5000 ft/min, which is well beyond its capability. The four runs represent the airplane at near maximum gross weight (high $\frac{W}{S}$ and low $\frac{T}{W}$) and near a minimum likely flying weight (low $\frac{W}{S}$ and high $\frac{T}{W}$). The low-speed initial conditions are at V_{BA} speed and the higher-speed conditions represent cruise speed. The results show that the airplane immediately went to V_{BA} climb condition from the two slower initial conditions. For the faster initial conditions, the airplane tried to achieve 5000 ft/min but was performance limited as expected. As it lost speed, the climb became steeper until V_{BA} was reached. Then climb rate was reduced to the rate of the sustainable condition. Note the CPA differences. The worst-case, heavy and slow configuration, took approximately 9 seconds to clear an NMAC and did not achieve the IFR-VFR separation of 500 ft in 30 seconds. The other three configurations resulted in clearing the 500-ft separation threshold. Only the faster and lighter initial condition exceeded the 1000-ft CPA threshold.
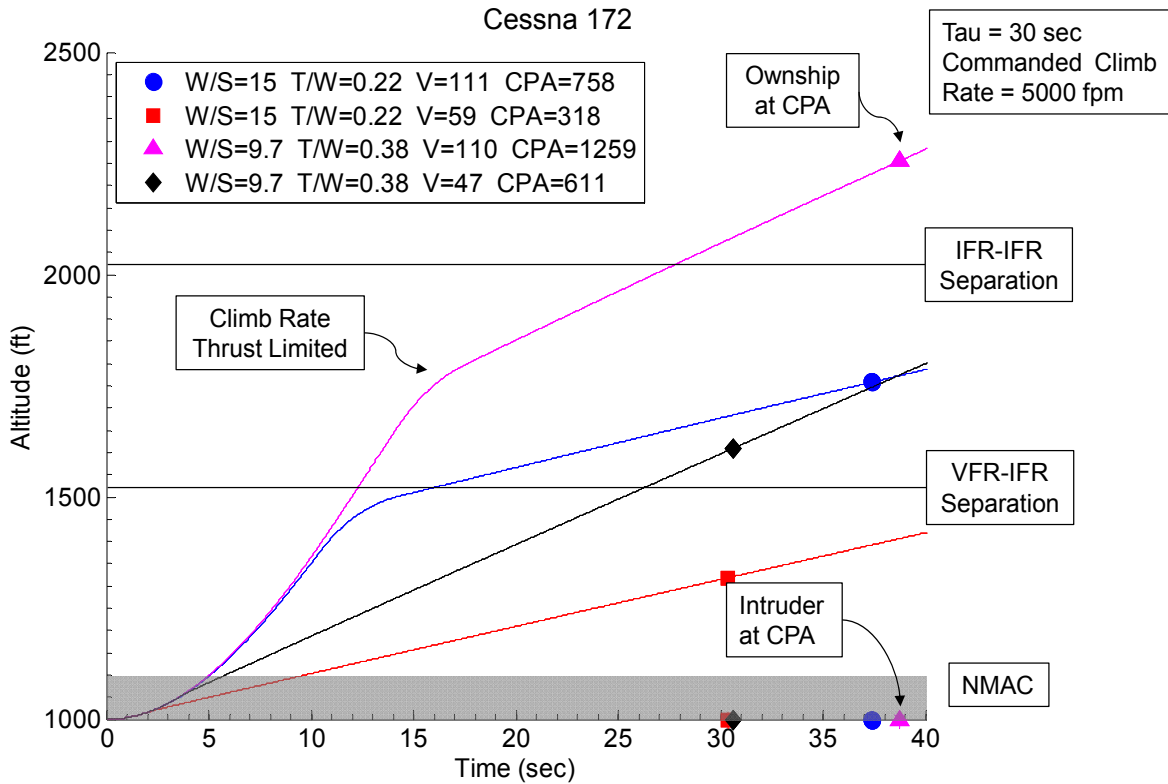
Figure 10: Data from Cessna 172 using 2PAIRS climb tool.

Figure 11 shows CPA results from all of the configurations in Table 1 as a function of $\frac{T}{W}$, $\frac{W}{S}$, V_i, and specific excess power (P_S). Results from each configuration with both a heavier and lighter weight condition are shown. Time histories of these scenarios were inspected as part of verification and validation but are not presented in this paper. Note that no attempt was made to model the flight controls of any of the aircraft in this work, only the aerodynamic/propulsive potential to maneuver was modeled. Additionally, neither sensor noise nor navigation error were modeled; thus, the results are for idealized navigation.

The largest CPA values in Figure 11 create a fairly flat line across all subplots. This is a result of the same commanded climb rate being used for all runs and is representative of the configurations that could achieve and nearly sustain the rate. With insufficient performance to achieve or sustain the commanded climb rate, the results varied. The resulting CPAs for this insufficient performance group show no definite trend against parameters other than P_S, which is a key performance parameter related to vertical maneuvers. The scales are not shown on the plots because the reader should not assume the results represent the actual aircraft, especially the UAS. In the simulations presented, a high commanded climb rate was input and the modeled aircraft tried to follow it. Most current UAS control laws would not allow such a high rate to be attempted. Also, while the trends look very reasonable, the simulation is not intended to match a specific airplane but rather provide a broad span of performance results.
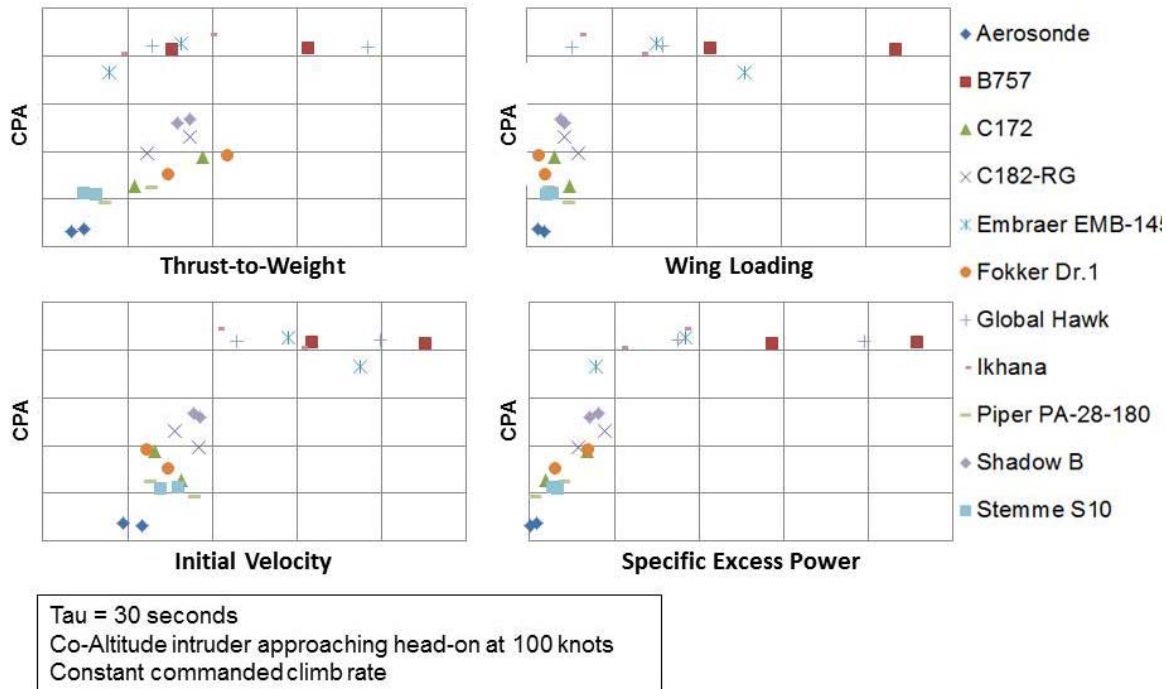
Figure 11: CPA Results For Heavy and Lightweight Conditions for All Configurations in Table 1 as a Function of $\frac{T}{W}$, $\frac{W}{S}$, V_i, and P_{S_i}. Scales are not shown on the plots because the results should not be assumed to represent the actual aircraft, especially the UAS.

3   Results and Analysis of Climb Maneuver

This section presents the data from the vertical climb maneuvers along with analysis of the results. Descriptions of key influential performance parameters are included as they are presented. Data from the vertical descent maneuvers is presented in Section 4, and level turn maneuver results are shown in Section 0.

3.1   Climb Maneuver Performance Parameters

Analysis of this multi-dimensional design space is an iterative process with a goal of characterizing the relationship between design and performance parameters to CPA values across the range of airplanes and encounters. In order to deliver the most usable information for both UAS designers and the regulators developing certification requirements to allow UAS regular access to the NAS, performance parameters that are readily available, practical, and meaningful were sought. Maneuver performance for a given encounter is a function of the airplane's design parameters and initial condition. Thus, performance parameters which are derived from the design parameters and initial flight condition were anticipated to be more useful than design parameters alone because they relate more directly to the airplane's maneuverability and, therefore, its ability to increase CPA for a given encounter.

For reference during the following discussions, the design and encounter parameters relevant to the climb maneuver simulations are listed in Table 2 showing the discrete values simulated. These parameters were described above in Sections 0 and 0.

Table 2: Simulation Parameters Relevant to Climb Maneuver

Parameter Name	Parameter Symbol	Discrete Values Simulated
Wing loading (lbs/ft^2)	$\frac{W}{S}$	1, 9, 17, 25
Thrust-to-weight ratio	$\frac{T}{W}$	0.1, 0.2, 0.3, 0.4
Aspect ratio	AR	5, 16.67, 28.3, 40
Maximum coefficient of lift	$C_{L\,max}$	0.6, 1.3, 2
Initial percent of maximum coefficient of lift	$\%C_{L\,max}$	8, 44, 80
Maximum lift-to-drag ratio	$\frac{L}{D}_{max}$	5, 20, 35, 50
Load factor Limit	g_{limit}	1.25, 3
Altitude (ft MSL)	h	1000, 6666.7, 12333, 18000
Commanded climb rate (ft/min)	$\dot{h}_{command}$	500, 2000, 3500, 5000
Intruder velocity (KCAS)	V_{intr}	50, 150, 250
Intruder vertical rate	$\dot{h}_{intr}$	-5000, -2750, -500, 0, 500 5000
Intruder azimuth (deg)	β	0, 45, 90
Time-to-go (seconds)	τ	10, 20, 30, … 120

3.1.1 Specific Excess Power (P_S)

The first step was to consider the total set of climb maneuver data to look for overall trends and start to drill down to useful results. Based on previous experience and the verification and validation study data shown in Figure 11 it was anticipated that P_S, or some related parameter, would be a good predictor of climb maneuver performance. The energy state of an airplane is described by the combination of speed and altitude: kinetic and potential energy, respectively. Specific excess power is a measure of the ability to change energy state [9], i.e., increase or decrease velocity, altitude, or a combination of both. Thus, the performance parameter P_S reflects the maneuverability margin of a given airplane from a given flight condition. Specific excess power can be represented mathematically in many forms. A relatively simple one was suitable for this work:

$$P_S = \frac{T-D}{W} * V = V \sin(\gamma) = \dot{h}. \qquad \text{Equation 23}$$

This equation can be expanded to directly use the design parameters outlined in Section 0:

$$P_S = \left(\frac{T}{W} - \frac{\pi e AR}{4\frac{L^2}{D}C_L} - \frac{C_L}{\pi e\, AR} \right) * \sqrt{\frac{2\frac{W}{S}}{\rho\, C_L}}. \qquad \text{Equation 24}$$

From Equation 23, it is clear that if P_S is a positive quantity, that is to say thrust is greater than drag, the airplane is able to increase energy, i.e., climb at some rate without losing speed (change in potential energy) and/or accelerate in level flight (change in kinetic energy). Note that an airplane that is at or near maximum throttle and speed can only climb by sacrificing kinetic
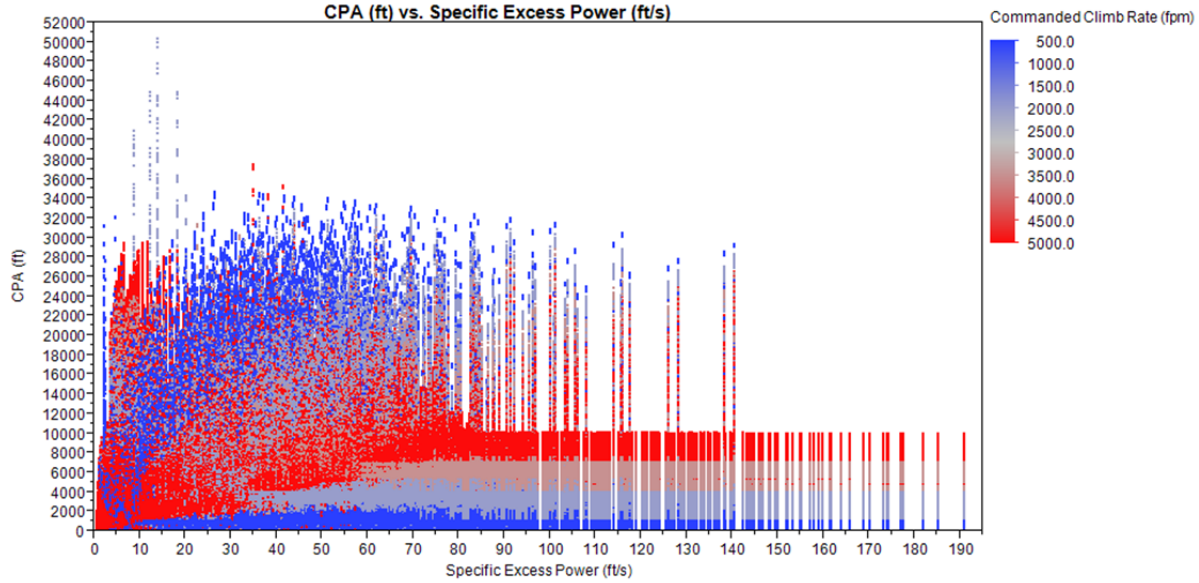
Figure 12: Design Space Overview; Commanded Climb Rate Shown by Color.

energy for potential energy and would have a P_s value near zero. Also, for an airplane trimmed to straight, level, unaccelerated flight, the excess power available to change from the initial energy state is zero if the throttle is not changed. The airplane must adjust throttle position to either accelerate or climb without losing speed, and thus, the initial P_s is not as useful as the potential of the airplane to change energy state. For this reason, P_s calculations are typically made using maximum $\frac{T}{W}$ available. Under this assumption, the equation for the initial P_s for the vertical climb becomes:

$$P_{S_{i\,max}} = \left(\frac{T}{W}_{max} - \frac{\pi e AR}{4\frac{L}{D}^2 C_L} - \frac{C_L}{\pi e\,AR} \right) * \sqrt{\frac{2\frac{W}{S}}{\rho\,C_L}} \qquad \text{Equation 25}$$

For the discussion of vertical climb performance, all references to P_{S_i} refer to the $P_{S_{i\,max}}$, as calculated in Equation 25.

Figure 12 shows the relationship between P_{S_i} and CPA for all 23.27 million climb maneuver runs resulting from the matrix of data in Table 2. A series of horizontal lines that represent a common CPA response regardless of the P_{S_i} value can be seen in the figure. These horizontal lines are from multiple UAS configurations that have sufficient P_{S_i} to maintain the commanded climb rate without sacrificing forward speed. As indicated by the color legend, lines correspond to a constant $\dot{h}_{command}$ and τ. This is discussed in more detail in the performance group discussion that follows.

Clear vertical lines are also apparent and become further separated as P_S increases. These vertical lines are grouped by close P_{S_i} values. For instance, there is a pair of vertical lines at constant P_{S_i} values of ~138 ft/s and ~140 ft/s. The UAS represented by these P_{S_i} values have common design parameter values except for $\frac{L}{D}_{max}$. The higher P_{S_i} value relates to a higher $\frac{L}{D}_{max}$ value because as $\frac{L}{D}_{max}$ increases, the UAS requires less of the available power to maintain straight, level, unaccelerated flight. It therefore has more excess power at the initial trimmed condition.

24

Figure 13 shows the experiment design space separated by τ. It is worth noting that there are bands of horizontal lines that share an $\dot{h}_{command}$ (i.e., the horizontal lines are the same color). The CPA difference between the top and bottom of the bands are due to variations in g_{limit}, and are more apparent than in the previous figure.
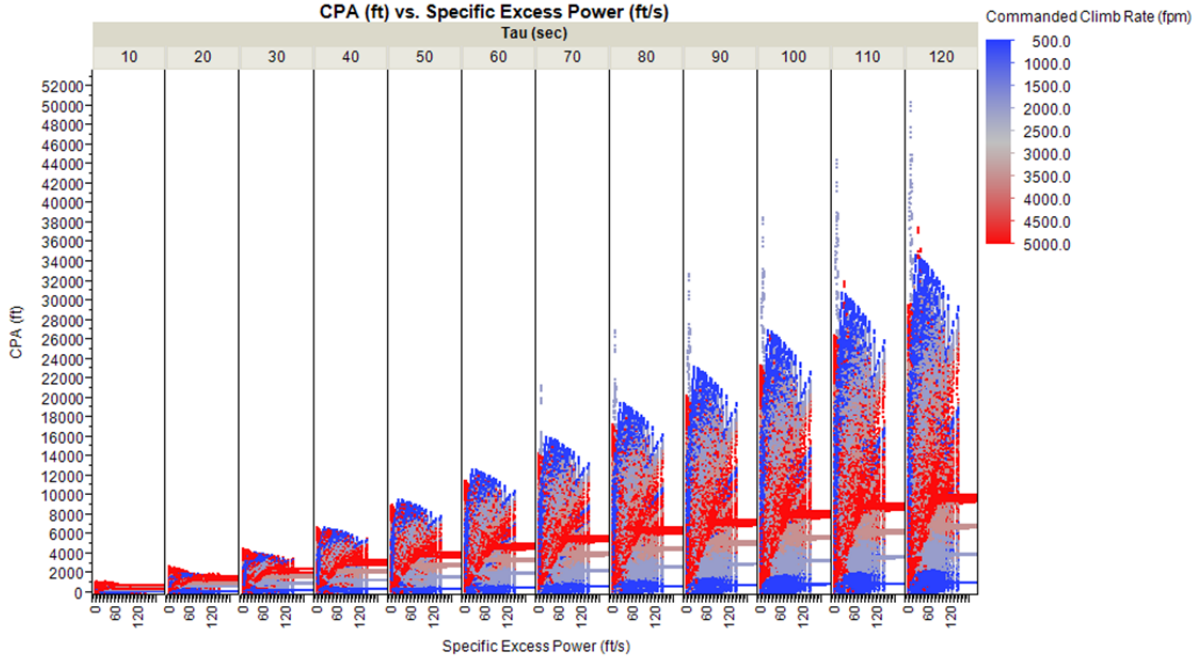

Figure 13: Design Space Overview; Segregated by Time-to-go; Commanded Climb Rate Shown by Color.

3.1.2 Analysis of Specific Excess Power's Effect at Various Flight Conditions

One relationship of interest is the difference between the airplane configuration's P_{S_i} and specific excess power at the Best Angle of Climb, $P_{S_{BA}}$. This relationship can be expressed mathematically as:

$$\Delta P_{S_{BA}} = P_{S_i} - P_{S_{BA}} = \dot{h}_{Sustainable} - \dot{h}_{BA}. \qquad \text{Equation 26}$$

where $\dot{h}_{Sustainable}$ is the maximum sustainable climb rate at the airplane's initial speed. The relationship can be conditionally simplified to:

$$If\ \Delta P_{S_{BA}} < 0, then\ \dot{h}_{Sustainable} < \dot{h}_{BA} \qquad \text{Equation 27}$$

$$If\ \Delta P_{S_{BA}} = 0, then\ \dot{h}_{Sustainable} = \dot{h}_{BA} \qquad \text{Equation 28}$$

$$If\ \Delta P_{S_{BA}} > 0, then\ \dot{h}_{Sustainable} > \dot{h}_{BA}. \qquad \text{Equation 29}$$

After studying these and the underlying relationships, it can be shown that it is not valid to exclude any range of $\Delta P_{S_{BA}}$ data from the study. Since the Best Angle of Climb is an optimization of the flight-path angle rather than the rate of climb, there is no constraint on $\dot{h}_{Sustainable}$ with respect to $\dot{h}_{BA}$. Therefore, $\Delta P_{S_{BA}}$ effectively represents the relationship between $\dot{h}_{Sustainable}$ and $\dot{h}_{BA}$. As a result, there is no constraint on $\Delta P_{S_{BA}}$.

3.1.3   Potential Change in Velocity (ΔV)

For the climb maneuver, this parameter is a direct measure of the speed (kinetic energy) a given airplane can lose from the initial condition before reaching the limiting velocity associated with the selected maneuver, i.e. V_{BA}. It is essentially a measure of the kinetic energy that can be traded for potential energy (altitude) before reaching the performance-limited state. It is calculated as:

$$\Delta V = V_i - V_{min}. \hspace{3cm} \text{Equation 30}$$

As the initial velocity of the airplane approaches the minimum velocity, the available speed margin decreases to zero. This affects the amount of time an airplane has to achieve, or that it can maintain, the commanded climb rate before adjusting to a sustainable climb condition. As the value of ΔV increases, the amount of time the aircraft can maintain the commanded rate before adjusting to a lesser rate increases for common deceleration rates. More time at the higher climb rate increases the achievable separation during an encounter.

3.1.4   Difference between Commanded Climb Rate and Sustainable Climb Rate ($\Delta \dot{h}_{Sustainable}$)

This parameter reflects the rate of speed lost by the airplane for the commanded climb rate. The sustainable climb rate at constant speed of a given airplane is directly measured by P_{S_i}. The equation that defines this parameter is:

$$\Delta \dot{h}_{Sustainable} = \dot{h}_{command} - P_{S_i}. \hspace{2cm} \text{Equation 31}$$

If the commanded climb rate is less than the sustainable rate, this value is negative, and the airplane is able to achieve and maintain the commanded rate without sacrificing forward speed, which results in geometrically predictable CPA values. As this value approaches zero (i.e., commanded climb rate approaches the sustainable climb rate), more throttle is required to maintain the commanded rate at the initial speed. If this value is positive, the commanded rate is greater than the airplane's sustainable climb rate. This means the airplane will be forced to sacrifice speed to maintain the commanded rate. As the simulation continues, the airplane's speed will approach V_{BA} and it may have to adjust to the associated sustainable climb rate. The higher the value of $\Delta \dot{h}_{Sustainable,}$ the faster the aircraft will decelerate to maintain the commanded rate. Combined with ΔV outlined in Section 3.1.3, the magnitude of this parameter has a large effect on achievable CPA.

3.2   Performance Grouping of Climb Maneuver Data

Numerous attempts to develop response surface models from the entire data set did not result in sufficiently accurate models. Thus, the data was divided into more homogeneous groups in a search for more useful alignment of analysis. Several different ways of grouping the climb maneuver data were considered. Initial response surface models were fit to preliminary data and residual analysis was done. Results contained several groups of responses independent of changes in airplane parameters. These groupings were revealed to be negatively affecting the accuracy of the model fit. Using JMP® [11] data exploration tools and 2PAIRS GUI functionality, individual airplane configurations within each grouping were analyzed.

Four major groups were developed, segregating airplanes by climb maneuver performance capabilities and resulting in more accurate model fitting for the airplane of interest. Notional climb maneuver performance representative of each of the four groups is shown in Figure 14.

The Sufficient Power Differential (SPD) group represents cases where airplanes have sufficient power to maintain the commanded climb rate throughout the given encounter without sacrificing forward speed. The Insufficient Power Differential (IPD) group is where airplanes do not have sufficient power to maintain the commanded climb rate without sacrificing forward speed. In these cases, the airplanes initiate the commanded climb, but as their speed slows, they must reduce their climb rate in order to not go below V_{BA}. In the Insufficient Initial Speed (IIS) group, the airplanes have insufficient initial speed to conduct the commanded climb, i.e. their initial forward velocity is below V_{BA}. These airplanes hold a level flight path and increase power output until V_{BA} is reached and then proceed to climb at the steady climb rate associated with V_{BA}. The Insufficient Time to Pitch (ITP) group represents cases where airplanes have insufficient time to pitch up to the commanded climb rate before the CPA is reached, thus they are still in the process of pitching up to the commanded climb rate throughout the entire encounter. Figure 15 shows CPA vs. P_{S_i} for each of the performance groups and highlights the differences between these groups. The climb maneuver performance for each of these groups is considered separately in Sections 3.2.1 through 3.2.4.
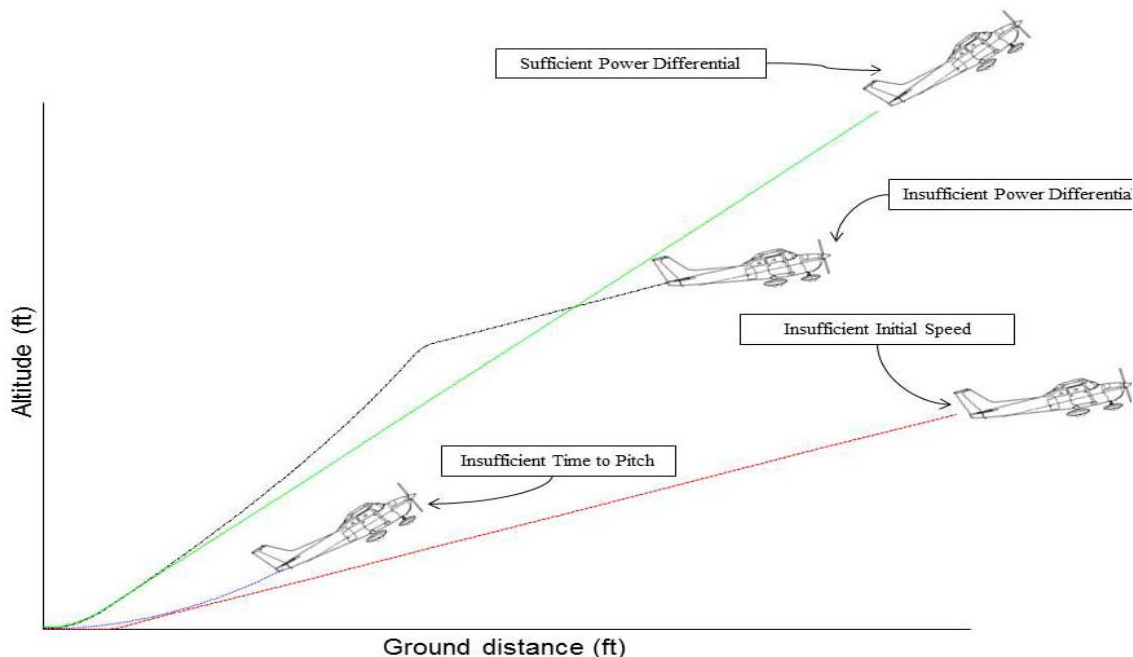

Figure 14: Notional chart depicting four climb maneuver performance groups

In order for the results of the study to be generally useful, it was important to select performance groups that support accurate prediction of the group to which a particular airplane configuration and flight condition belongs. 2PAIRS has the ability to predict the performance group of an airplane configuration before running the time history. An airplane configuration alone does not determine the performance group. The combination of airplane parameters, commanded maneuver rate, and initial flight condition are all required to determine performance group as it relates to the SAA system requirements. Additionally, small deviations within an airplane's design parameters or the commanded maneuver may result in that airplane changing performance groups. For instance, for a given airplane combination belonging to the SPD group (Section 3.2.3), an adjustment in commanded climb rate above the configuration's sustainable rate would result in that airplane shifting to the IPD group (Section 3.2.4). This can be addressed by studying an airplane configuration at different stages of its flight envelope performing a variety of maneuvers.

Each group is discussed separately in the following sections. Two of the groups are discussed in detail including analysis of results. One of these groups produces succinct CPA results as a function of a few parameters. The other proves much more difficult but some conclusions are drawn and a methodology is presented. The other two groups are explored in far less detail because it is unlikely either represents a real-world case. The two that are of less
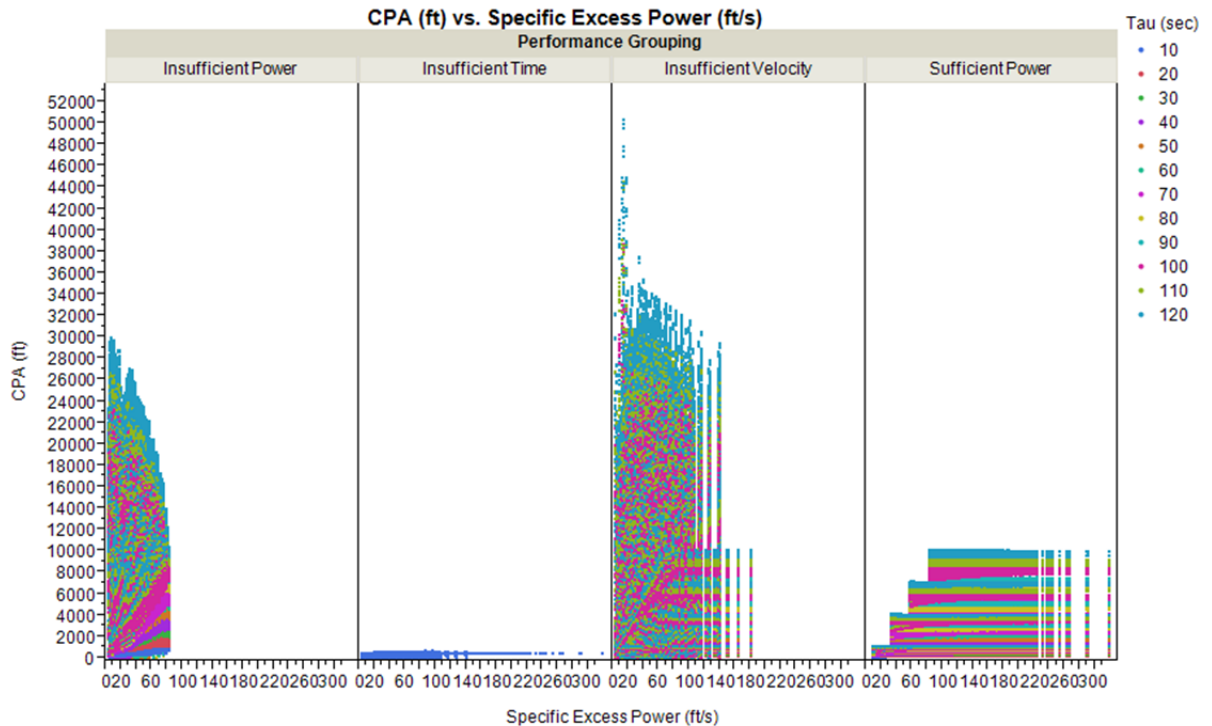

Figure 15: Design Space Overview; Segregated by Group; Time-to-go Shown by Color.

interest are explored briefly and first. It is worth reinforcing that the airplane design parameters and resulting performance parameters alone do not define the group. Thus, most design parameters that represent an airplane that can fly at all are represented in some part of the two groups that are explored in detail.

3.2.1   Insufficient Initial Speed Group

This airplane performance group is defined by airplanes whose initial velocity is below V_{BA} as described in Section 2.6.3.2. The simulation logic addresses this situation by forcing the airplane to hold a level flight path while accelerating to V_{BA}. The airplane then proceeds to climb at the steady climb rate associated with V_{BA}. These airplanes were not studied in detail because it is unlikely that an aircraft would fly in this condition under normal circumstances. Additionally, the same airplane configurations that occupy this performance group will also be given higher initial velocities as other test matrix points, which will place them into the performance categories of interest.

3.2.2   Insufficient Time to Pitch Group

This performance group is characterized by airplanes that are unable to reach the commanded climb rate due to very short simulation times and/or very high speeds. This group can be modeled using simple geometry and known performance limitations (i.e., limited pitch-up

rate). Note from Figure 15 that this performance group contains a very small number of simulation configurations. Specifically, it only includes encounters with τ of 10 seconds.

3.2.3   Sufficient Power Differential Group

Airplanes able to maintain the commanded climb rate throughout the encounter without sacrificing forward speed fall within this performance group. Considering the performance limitations of the pitch-up maneuver, it is easy to predict the trajectory of these airplanes using geometry. A parametric equation has been developed using response surface methodology that is able to accurately predict the achievable CPA for airplanes within this group.

The airplane's ability to maintain the commanded climb is dictated by the airplane's specific excess power. As shown in Section 3.1.1, the P_{S_i} of an airplane from a particular flight state indicates the airplane's ability to change energy state. Climbing at constant speed, acceleration or deceleration in level flight, and descent at constant speed are examples. If an airplane's P_{S_i} is greater than the commanded climb rate, the airplane will be able to sustain that rate without sacrificing forward velocity (i.e., kinetic energy). Therefore, this performance group is comprised of all airplane combinations with P_{S_i} greater than or equal to the commanded climb rate.

Since all airplanes in this group are able to maintain the commanded maneuver, there is no difference in achievable separation for airplanes with common design parameters but different thrust capabilities. For instance, an airplane that is able to sustain the commanded maneuver with a $\frac{T}{W}$ = 0.2 will have the same result as an airplane with the same design parameters but a $\frac{T}{W}$ = 0.4. The more powerful airplane will not require as much throttle to sustain the maneuver, however. The higher $\frac{T}{W}$ airplane will be capable of flying a more extreme maneuver than the low-power airplane so the $\dot{h}_{command}$ becomes the limiting factor and equalizer. As a result, commanded climb rate has a large impact on the distribution of airplanes within this group. More airplane configurations in the data set, as in the real world, are able to sustain the 500 ft/min climb than are able to sustain the 5000 ft/min climb. Conversely, all airplane configurations capable of flying at 5000 ft/min are able to sustain a 500 ft/min climb. This results in an increase in the number of airplane configurations in the SPD group as the commanded climb rate decreases.

Figure 16 shows the CPA response versus the initial range to the intruder for airplanes within this performance group. The colors represent the commanded climb rate. There are 4 commanded climb rates in the dataset as shown in Table 2 and evident in the figure. This figure shows that, as expected, an increase in commanded climb rate results in an increase in CPA for a given τ.
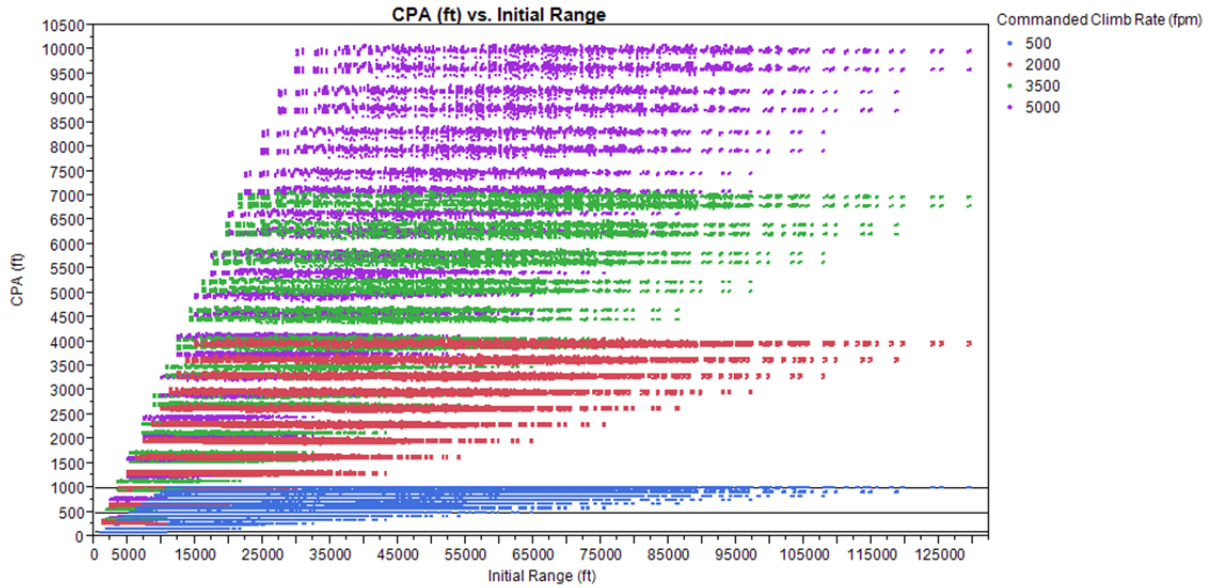
Figure 16: SPD Group; Commanded Climb Rate Shown by Color.

3.2.3.1 *Analysis of Parameter Effects on Climb Maneuver - SPD Group*

Although the performance of the UAS within this performance group is highly predictable, various components of the encounter have an effect on achievable separation or CPA. For instance, the speed and direction from which the intruder approaches have an effect as well as the altitude of the encounter. Analysis of a number of these parameters is presented in the following subsections to provide a better understanding of the effects of each parameter and their implications on the predictive equation.

3.2.3.1.1 *Effect of g_{limit}*

To show the impact an airplane configuration's g_{limit} has on achievable separation, Figure 17 shows airplanes within the SPD group involved in an encounter with τ = 60 seconds. For each commanded climb rate in the figure, two near-constant response values are seen due to the two discrete g_{limit} values in the data, as detailed in Section 2.2.7. The g_{limit} effect appears to increase as the commanded climb rate increases. For an airplane flying at a fixed speed, a higher commanded climb rate results in a higher commanded flight-path angle. As the commanded climb rate increases, the time required to pitch at a constant rate to the commanded rate or angle increases. With an increase in pitching time, the effect of g_{limit} becomes more influential on the achievable separation. Upon applying Equation 2, Table 3 shows the time spent pitching to 500 and 5000 ft/min at several g_{limit} values for an aircraft flying at 100 knots. More than 7 additional seconds are needed for the airplane with limited pitching capability (g_{limit} of 1.25) than are required by the more agile airplane to reach 5000 ft/min climb rate. Within those 7 seconds, the more agile airplane can gain over 550 ft.

Table 3: Time to pitch at various g_{limit} values for an aircraft at 100 knots.

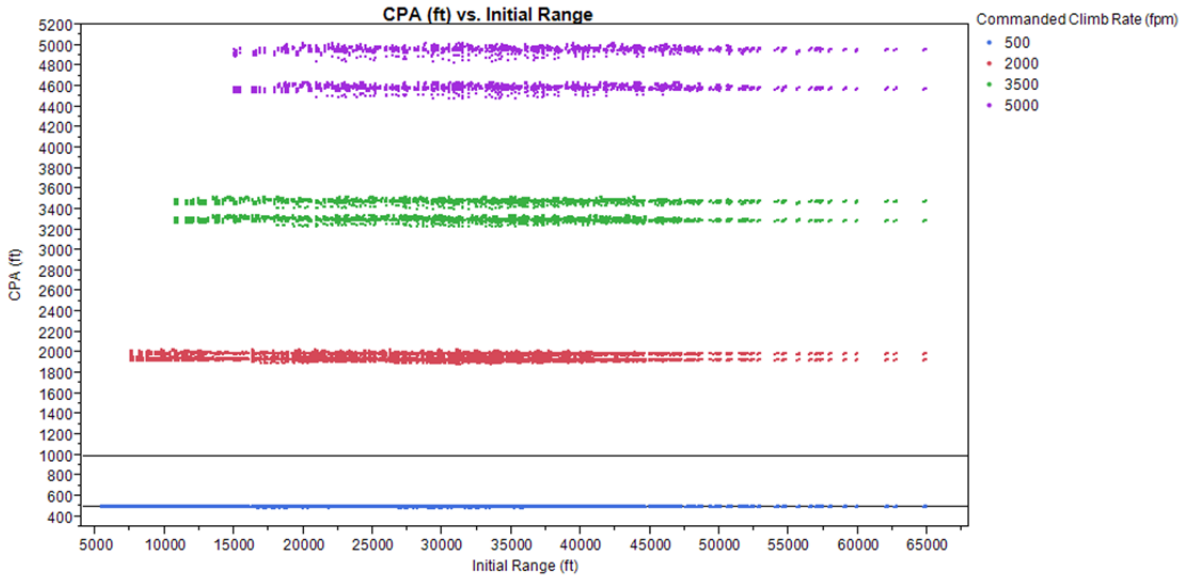| g_{limit}	Time to reach 500 fpm	Time to reach 5000 fpm
1.25	1.03 s	8.5 s
2	0.26 s	2.13 s
3	0.13 s	1.06 s

Figure 17: SPD Group; τ= 60 seconds; Commanded Climb Rate Shown by Color

Ignoring time to transition from level flight to the steady climb, an airplane climbing at 5000 ft/min for 60 seconds is able to gain 5000 ft of altitude. During the simulation, the UAS is initially trimmed to level flight and given a commanded climb rate. The faster the airplane is able to maneuver from level to the commanded climb rate, i.e., the higher the g_{limit}, the closer to the ideal change in altitude it can achieve. This is evident in Figure 18 as the higher g_{limit} value of each commanded climb rate is approaching the respective expected value.
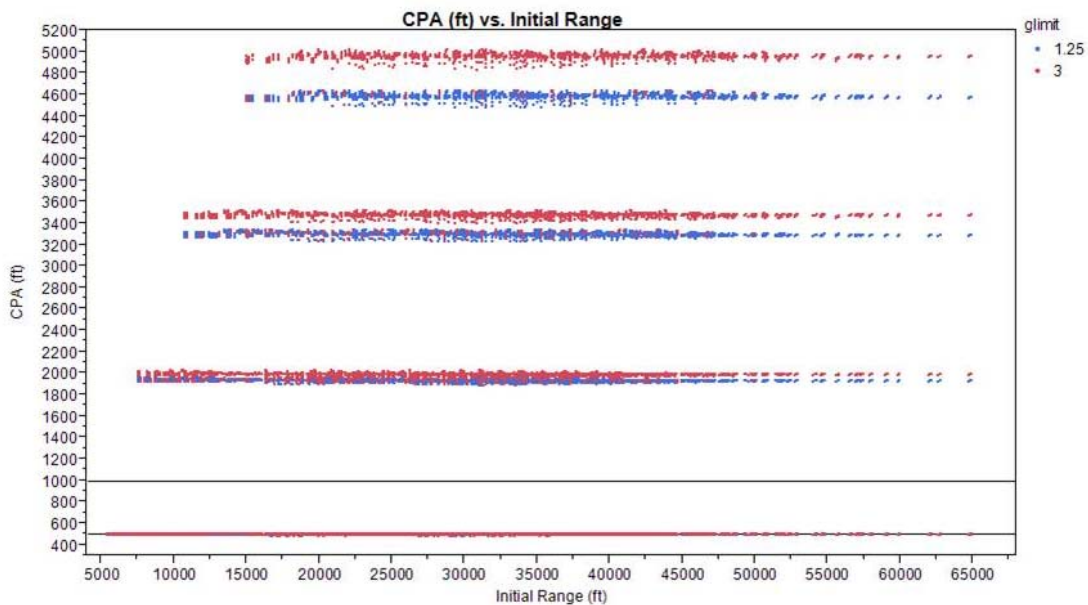

Figure 18: SPD Group; τ = 60 seconds; g_{limit} Shown by Color.

3.2.3.1.2 Effect of Intruder Velocity

For a given UAS configuration, the intruder velocity in combination with τ defines the initial range between the intruder and the point of collision. To identify the effect of the intruder's velocity, Figure 19 was developed. This figure shows airplanes in the SPD group that were commanded to climb at 500 ft/min. Each horizontal line represents a τ value from 10 to 120 seconds. The color in the figure represents the intruder's constant velocity. Trivially, as the intruder's velocity increases the initial range between the two airplanes increases, as shown in Figure 19. Conversely, the initial range has no impact on CPA. The CPA is a function of τ only in this figure. Thus, if the UAS initiates the same commanded climb rate to avoid either a fast or slow intruder at the same τ, the achievable separation is the same despite the larger range at maneuver initiation.
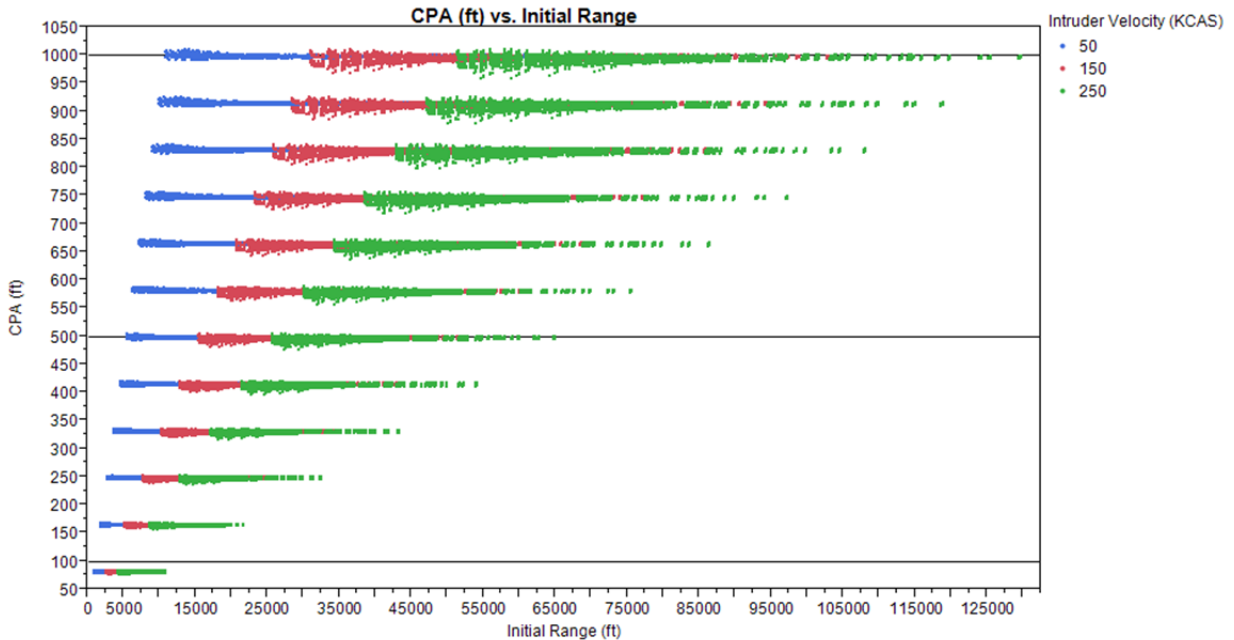

Figure 19: SPD Group; Commanded Climb Rate of 500 ft/min; Intruder Velocity Shown by Color.

From Figure 19, it can be seen that for a given CPA, there exists large variability in initial range for intruders of common velocity. Initial range is measured as a slant range between the two airplanes; the variability is due to the various approach azimuths, elevation angles, and closure rates between the two airplanes. There is also a bit of variability in CPA in the lower initial range values for each intruder velocity. The next subsection identifies the causes of this variability, focusing on a single τ value.

3.2.3.1.3 Effect of Intruder Climb Rate

Figure 20 focuses on a single commanded climb rate of 500 ft/min and τ of 60 seconds. The g_{limit} is constant at 1.25 g's for the UAS. The color in Figure 20 shows the vertical rate of the intruder. The lines defining ±5000 ft/min begin at a range of about 25,000 ft MSL due to the limitations in intruder climb angle described in Section 2.6.6.4. From the figure, it appears that the magnitude of the intruder's vertical rate is more significant than the sign. This is evidenced by the pairing of vertical rates with common magnitudes. It is important to note that the variability in response in Figure 20 is about 30 ft, 6% of the predicted separation. That difference can likely be deemed insignificant in practice.
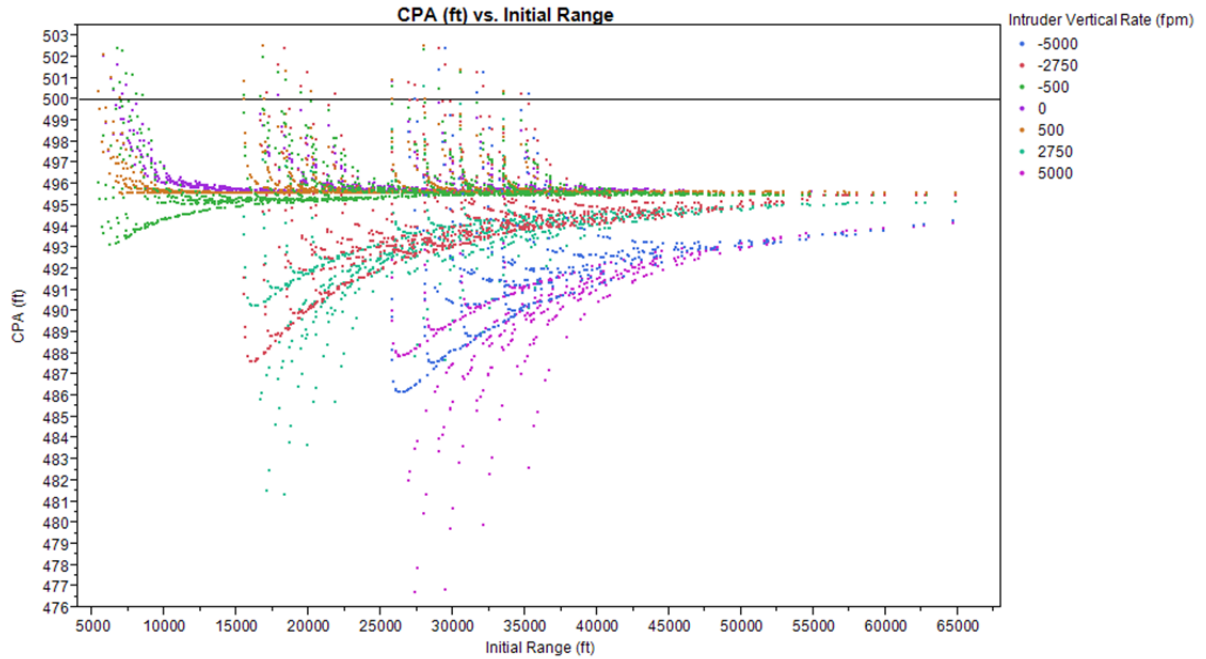
Figure 20: SPD Group; τ = 60 seconds; g_{limit} = 1.25, Commanded Climb Rate = 500 ft/min; Intruder Vertical Rate Shown by Color

To identify variance among encounters with common intruder vertical rates, Figure 21 shows only the ±2750 ft/min rates for the same configurations shown in Figure 20. From the figure, it appears that the descending intruder creates more separation than the climbing intruder. There are also clear groupings of performance trends for each vertical rate. Again the variation is small. Both of these were explored to understand fingers seen in the larger dataset.
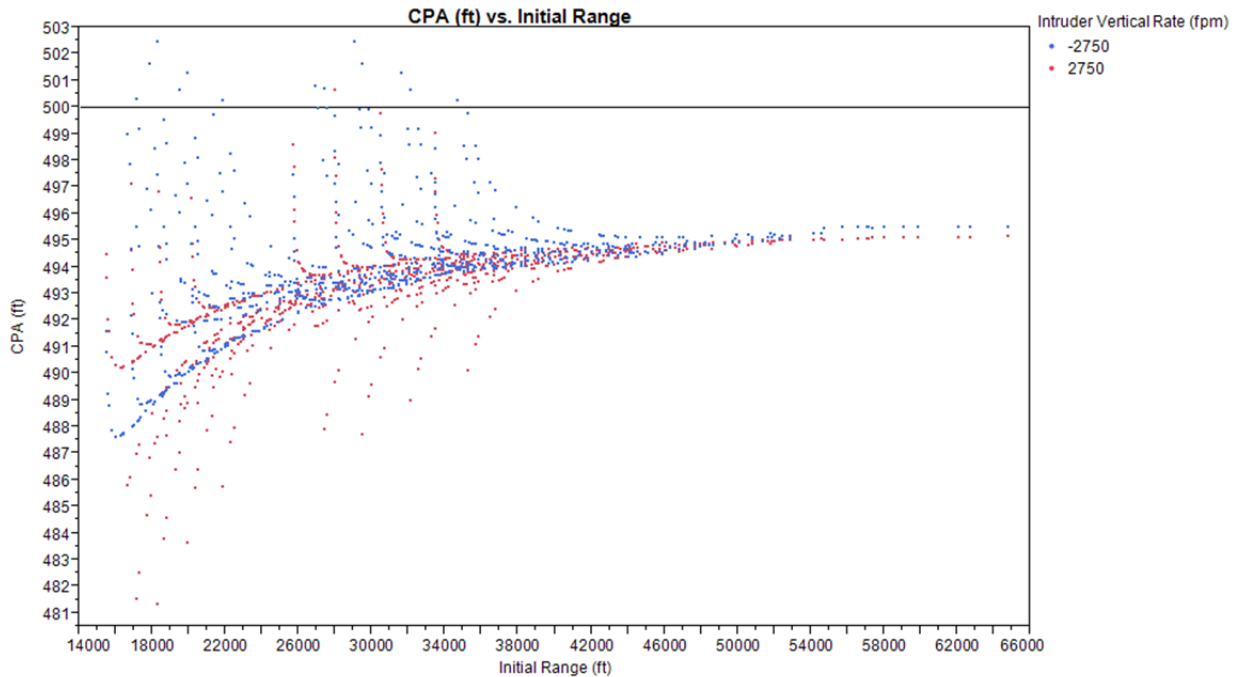

Figure 21: SPD Group; τ = 60 seconds; g_{limit} = 1.25 g's; Commanded Climb Rate = 500 ft/min; Intruder Vertical Rate = ±2750.

3.2.3.1.4 Effect of Intruder Azimuth

Figure 22 shows the CPA response versus initial range for airplanes within the SPD group given a commanded climb rate of 500 ft/min, a g_{limit} of 1.25 g's, and τ of 60 seconds. The intruder is flying at a vertical rate of either 2750 ft/min or -2750 ft/min. This plot clearly shows the impact of intruder velocity, azimuth, and vertical rate on CPA. Comparing the plots of the two
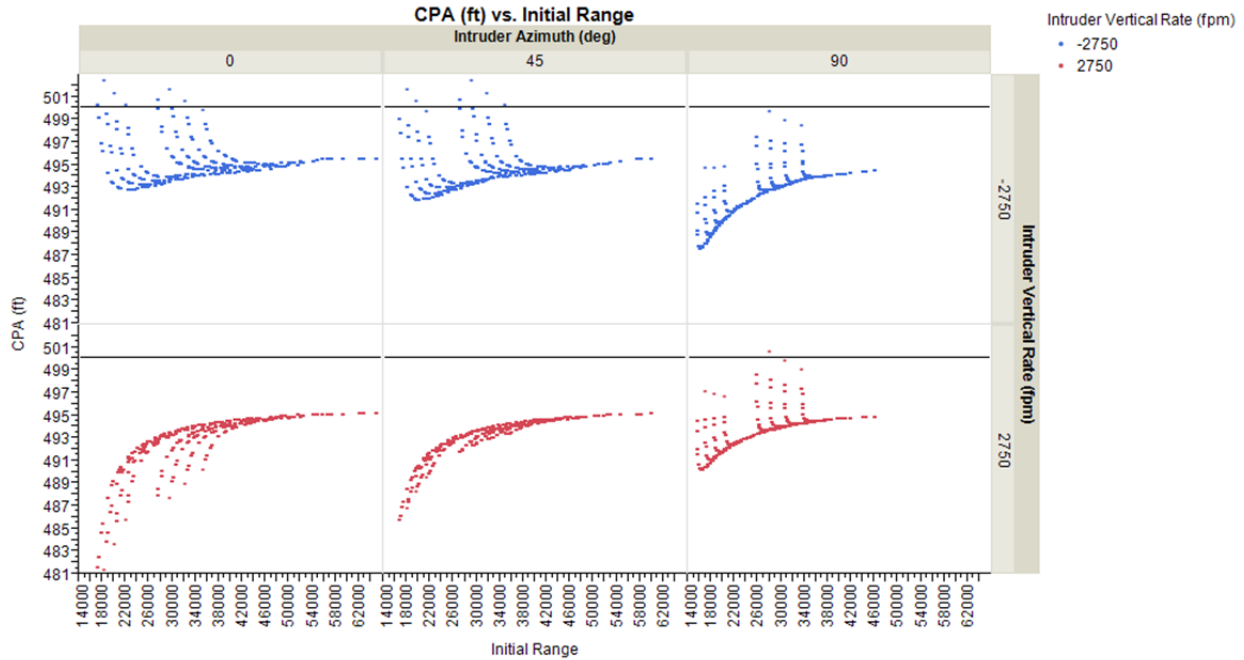

Figure 22: SPD Group; τ= 60 seconds; g_{limit} = 1.25 g's; Commanded Climb Rate = 500 ft/min; Intruder Vertical Rate = ±2750; Segregated by Intruder Azimuth and Intruder Velocity; Intruder Velocity Shown by Color.

intruder vertical rates containing head-on intruders (β = 0°) reveals the descending intruder enables more separation than the climbing intruder. This observation carries over to the encounters involving an intruder approaching from β = 45°. For an intruder approaching abeam to the UAS (β = 90°), the vertical rate of the intruder appears to have very little effect on CPA.

While these differences produced "fingers" in the data patterns of the full SPD group dataset, the differences in both intruder climb rate and β are small. Thus, after inspection they may be ignored in global analysis of the SPD group, and it is likely that a response surface model will be accurate enough to be useful.

3.2.3.2 Response Analysis

As shown in the previous section, the effects of multiple parameters used to define the encounter between the UAS and intruder resulted in small variations in the CPA response. It is therefore expected that the overall design space is readily predictable. Figure 23 shows the initial τ used to define the encounter versus the actual time to CPA. The change in encounter time increases as τ increases. This follows from the discussion in Section 3.2.3.1.1 which showed that the impact of g_{limit} on CPA increases with τ. In order to identify the cause of the change in encounter time, Figure 24 shows only the 120-second encounters. The color represents the commanded climb rate. From the figure, the larger commanded climb rates result

in further deviation from the predicted initial τ. Again this follows from discussion in Section 3.2.3.1.1.

Figure 25 shows the same design space of 120-second encounters as Figure 24, but separates and colors the plot by intruder vertical rate. The figure labels the initial τ value on the x-axis using a vertical dashed line. From the figure, intruders descending at -2750 and -5000 ft/min reduce the time to CPA. All other intruder vertical rates tend to increase the time to CPA and thus provide additional maneuvering time.
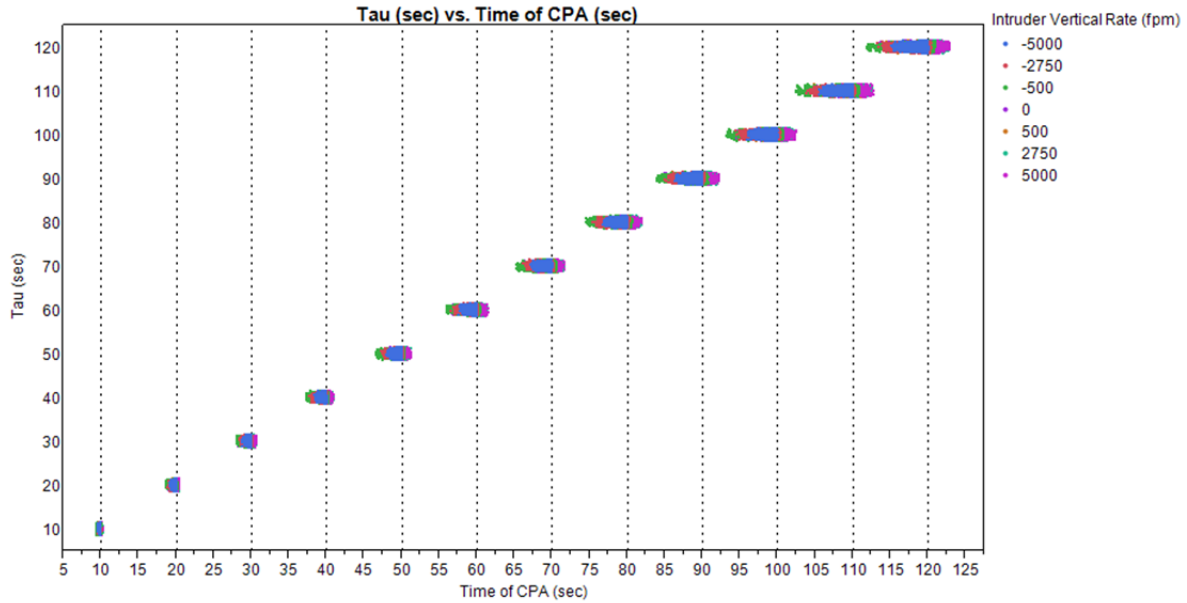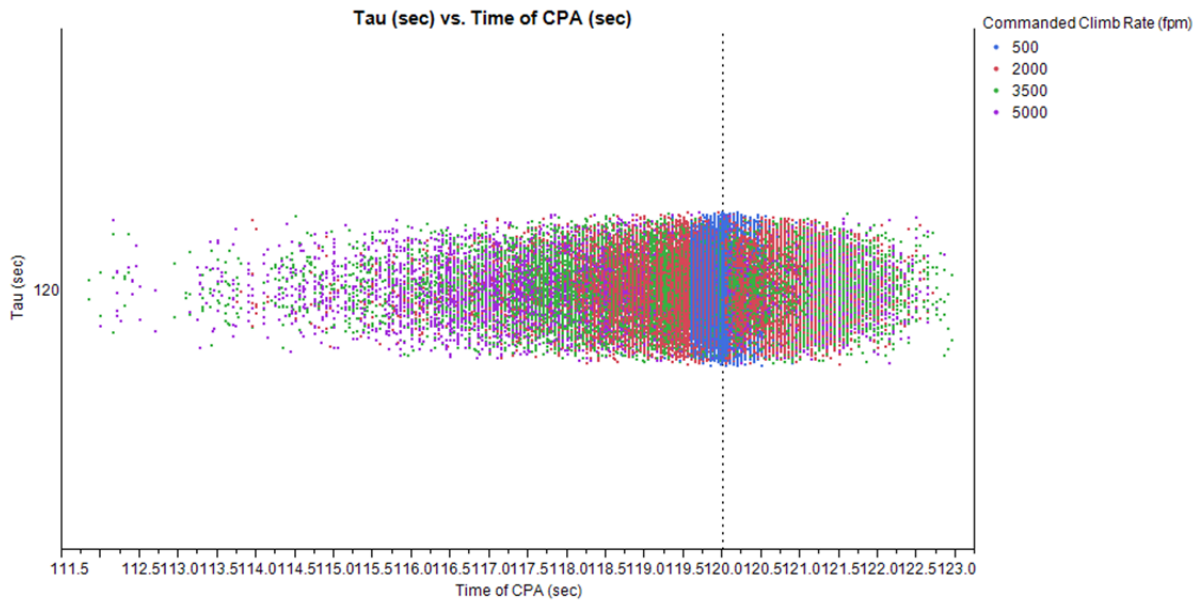

Figure 23: SPD Group; τ vs Time of CPA.

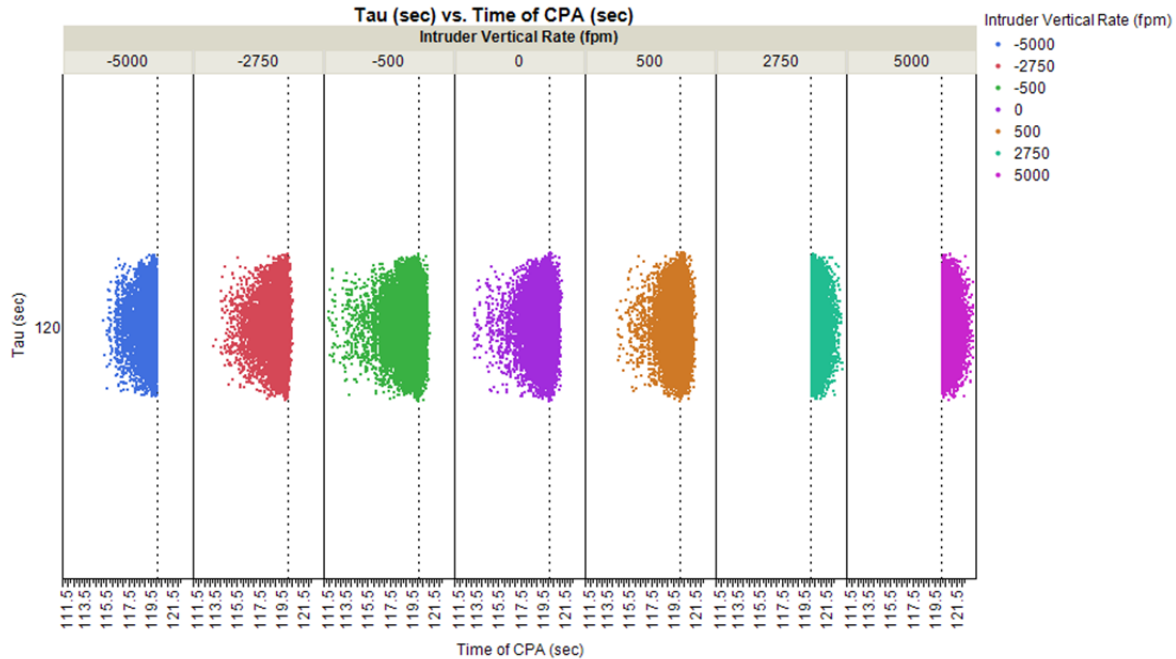Figure 24: SPD Group; τ vs Time of CPA; τ = 120 seconds.

35

Figure 25: SPD Group; Initial τ vs Time of CPA; τ = 120 seconds; Segregated by Intruder Vertical Rate.

3.2.3.3 Parametric Equation

The SPD group consists of cases where airplanes have enough energy to maintain the commanded climb rate without sacrificing forward speed. As shown in detail in the previous sub-sections, these airplanes have predictable climb performance defined by the airplane's g_{limit}, the τ, and the commanded climb rate. Applying response surface methodology using the JMP® software, the authors created an equation capable of predicting the achievable CPA for the configurations and encounters tested with sufficient accuracy to be useful. The result is Equation 32. The equation is of second order containing three primary independent variables and their associated interactions. Entering a matrix of the three independent parameters into the equations results in the data presented in Figure 26.

$$CPA = -818.76 + 14 * \tau + 0.93224 * \dot{h} + 12.4727 * g_{limit\,actual} + \left(\dot{h} - 837.45\right) * \{0.0171 * (\tau - 57.543) + 0.03456 * \left(g_{limit\,actual} - 1.8723\right)\}$$

Equation 32

Figure 26 shows the relationship between the commanded climb rate and achievable CPA for airplanes in the SPD Group. The CPA range is limited to 1500 ft to focus on the area of interest. The figure uses color to represent various τ values. As τ increases, an airplane's achievable separation increases for a constant climb rate. Each τ value is represented graphically by three lines with various g_{limit} restrictions: a lower line of 1.25 g's, a white dotted line of 2 g's, and an upper line of 3 g's. The 'coning' evident with constant τ represents the effect of g_{limit} on the response.

The same set of results is presented in a different relationship in Figure 27. This figure shows the CPA response as a function of τ. The effect of g_{limit} is represented as the constant thickness within a commanded climb rate and variations in thickness between climb rate values. For example, the 500-ft/min commanded climb rate shows that g_{limit} has very little effect on the achievable separation for such a benign maneuver. Table 3 shows that the time required to pitch to achieve the commanded maneuver is very small compared to the entire maneuver time

of the simulation. The fact that the effect of g_{limit} is constant for a given maneuver is also shown in Figure 26 as the constant height for each τ for a single x-axis value (commanded climb rate).
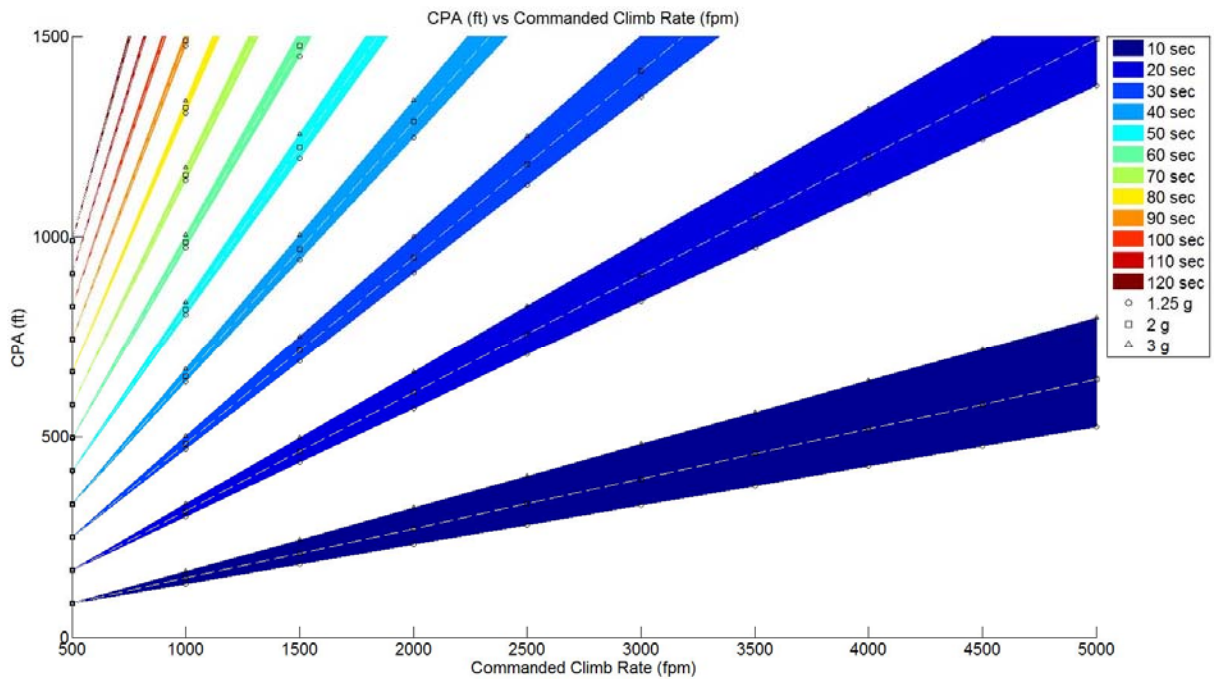

Figure 26: Application of SPD Group Parametric Equation; CPA vs Commanded Climb Rate; τ Shown by Color.
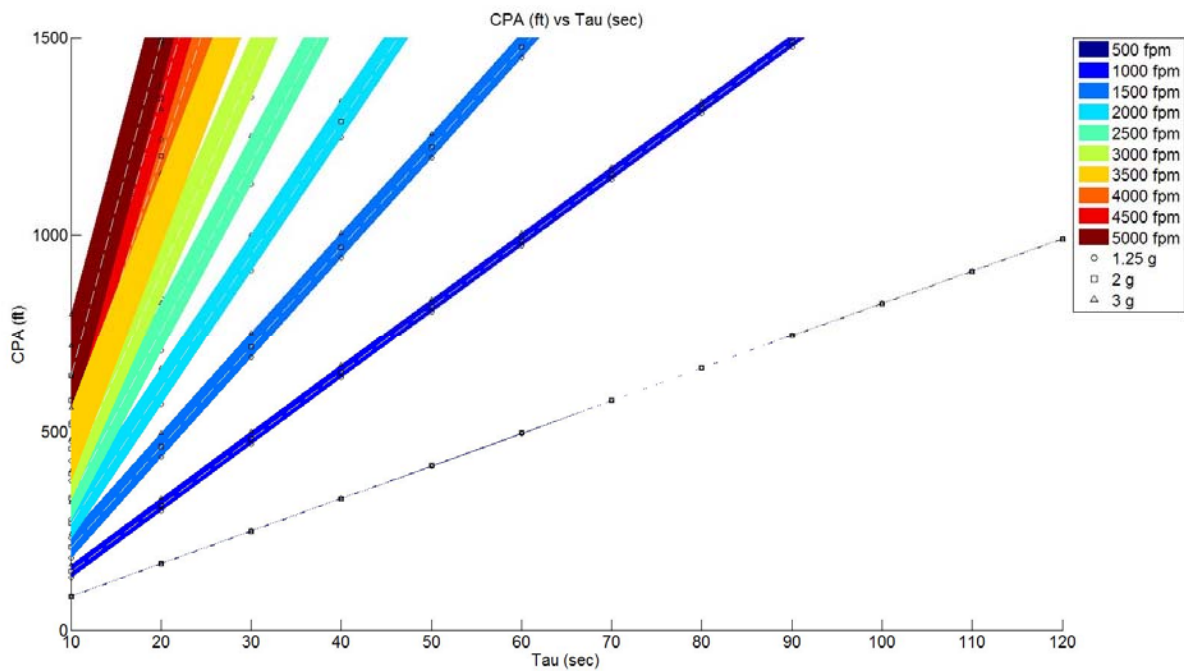

Figure 27: Application of SPD Group Parametric Equation; CPA vs τ; Commanded Climb Rate Shown by Color.

The results shown in this section provide a useful relationship between CPA and three key parameters: τ, commanded climb rate, and g_{limit}. These results are valid for any UAS and encounter in the study as long as the UAS/encounter combination is in the SPD group. Thus, a UAS that can sustain a commanded climb rate in Figure 26 or Figure 27 from its current flight condition can use the predictive equation to determine when it must initiate the climb to achieve a particular CPA. The caveat is that results are for a precise and immediate maneuver initiation and execution. Also key is that many UAS will not be in the SPD group if the $\dot{h}_{command}$ is very large. Even many single-engine general aviation aircraft cannot sustain climb rates above 500 ft/min without sacrificing significant speed. This brings us to the next and much more difficult performance group.

3.2.4   Insufficient Power Differential Group

The airplanes that occupy this performance group attempt to climb at the commanded rate, but are forced to sacrifice forward velocity to do so. These airplanes may be required to adjust their climb rate to V_{BA} at some time during the encounter. Depending on the specific airplane, initial condition, and encounter, they may continue to lose speed throughout the encounter without reaching V_{BA}. The performance of individual airplanes within this group is very difficult to predict without running the time history. A goal of this study was to model them using multi-dimensional modeling techniques based on numerous results from the 2PAIRS simulation and to gain insight on relationships between various airplanes in this group and SAA system requirements. It was known that this was a very difficult task and no suitable response surface model has been developed to date. However, a technique for narrowing down the minimum requirements and understanding the details of the parameter relationships within this group has been developed and is presented.

Figure 28 shows all of the CPA responses for the IPD group as a function of specific excess power with the result color coded by commanded climb rate. Note that commanded does not equal achieved or sustained rate for this group like it did in the previous group. Analysis of this
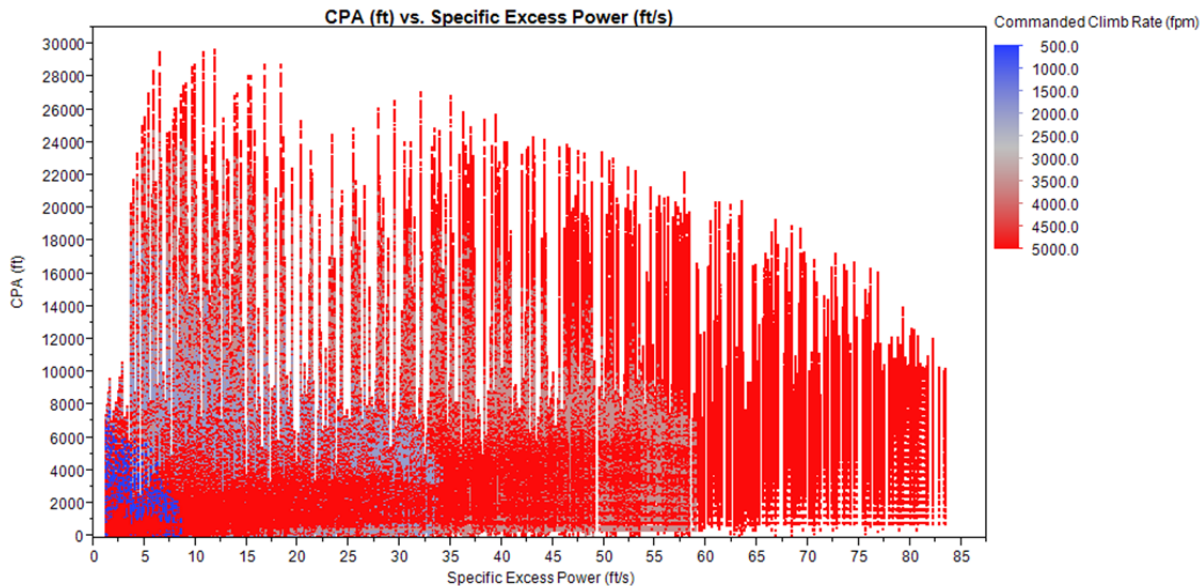

Figure 28: Design Space with only IPD Group; Commanded Climb Rate Shown by Color.

performance group focuses on encounters which result in CPA values below 2000 ft. Figure 29 shows the CPA responses for the IPD group limited to 2000 ft. As P_{S_i} increases, the performance of the aircraft approaches that of the SPD group, which results in the horizontal clusters of points. Figure 30 shows the same design space segregated by τ. It is difficult to glean conclusive information from either of these plots. The sections that follow dig deeper to gain insight and draw some conclusions.
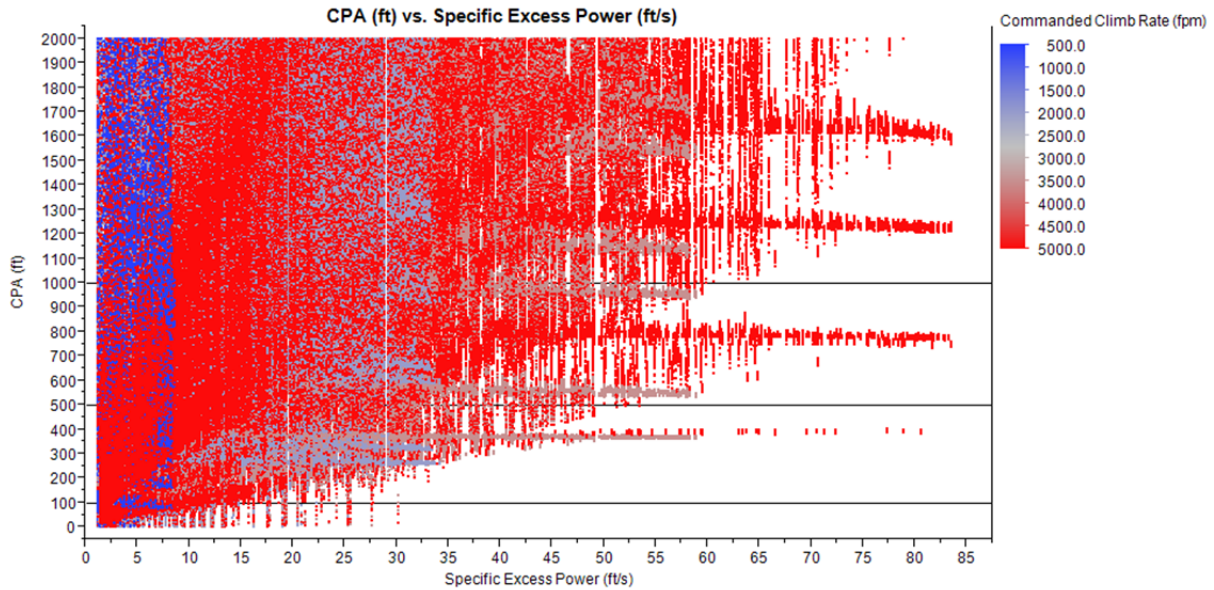

Figure 29: Design Space with CPA Range with only IPD Group; Commanded Climb Rate Shown by Color.
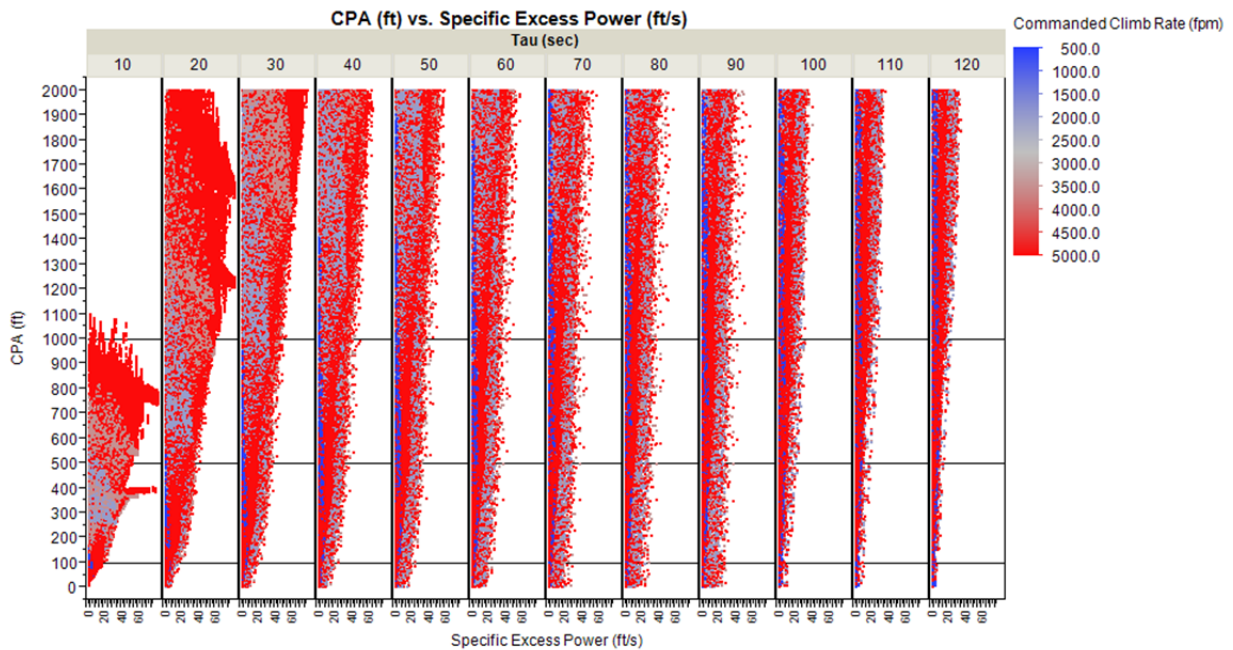

Figure 30: Design Space with CPA Range with only IPD Group; Segregated by Time-to-go; Commanded Climb Rate Shown by Color.

3.2.4.1 Analysis of Parameter Effects on Climb Maneuver for IPD Performance Group

The IPD group is characterized by airplanes that are unable to maintain the commanded climb rate without sacrificing speed. Within this group a hierarchy of parameter effects on CPA exists. The most influential parameters are discussed in this section. Many parameter effects for this performance group are very similar to the effects on the SPD group, as described earlier.

3.2.4.1.1 Effect of Intruder Vertical Rate

Unlike the SPD group, some intruder elevation angles can cause large variations in the achieved CPA. Figure 31 shows the Insufficient Power Group design space segregated by intruder vertical rate with τ shown by color. Figure 31 reveals an area of high τ values with near-zero CPA for encounters with an intruder climbing at a high rate. These intruders are climbing toward the UAS altitude when the simulation starts and will reach it at the predicted τ. Once the simulation starts, both aircraft are climbing and the intruder may be climbing faster than the UAS. Additionally, in this performance group, the UAS is slowing down. Thus, with the right combination of intruder vertical rate, time-to-go, and ownship performance limitations, the two airplanes may collide during the maneuver.

Figure 31: Design Space with CPA Range with only IPD Group; Time-to-go shown by Color; Segregated by Intruder Vertical Rate.

As an example of a collision caused by this effect, Figure 32 shows the trajectory of the UAS and intruder during such an encounter. In the example, the UAS is initially flying at 176 KTAS and given a 5000-ft/min commanded climb rate. The intruder is flying at 250 KCAS and climbing at 5000 ft/min. The UAS begins the simulation at 6666.7 ft MSL with 80 seconds until collision. If either airplane were given a different commanded climb rate, the collision would not happen. Obviously, a different avoidance maneuver would be more appropriate for this encounter. Note that predicting the collision would likely require a trajectory generator currently. However, use of results from this data may be useful in producing guidelines for predicting the bad outcome with

less computational expense given the current flight state, performance information for the UAS, and the intruder's trajectory.
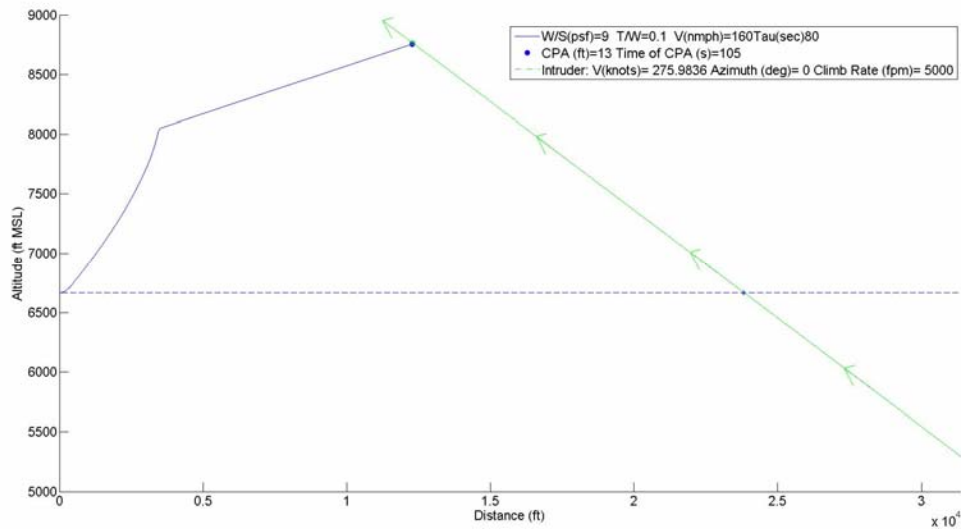

Figure 32: Example GUI Output Showing Example of Collision after Maneuver.

3.2.4.1.2 Effect of g_{limit}

Figure 31 depicts cluster pairs of maximum achievable CPA values for each τ. Figure 33 reveals the cause of these cluster pairs is common g_{limit} values in the data. Figure 34 is a closer look showing only cases with τ = 10 seconds with g_{limit} shown by color. It is important to
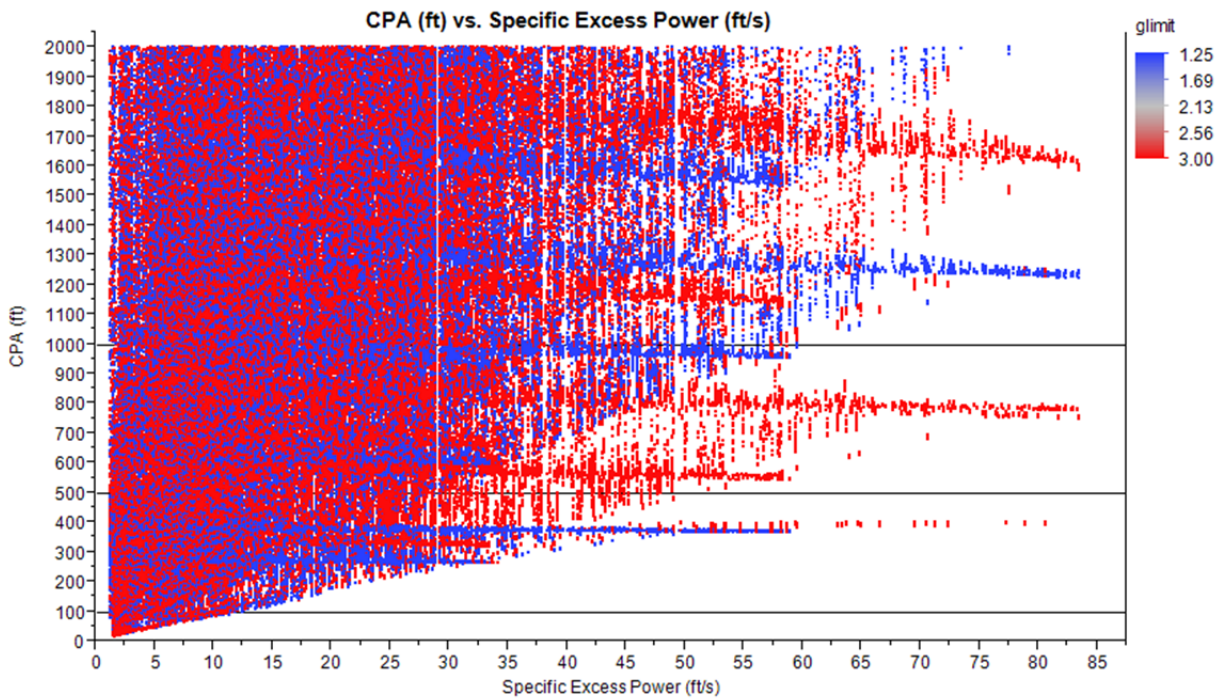

Figure 33: Design Space with CPA Range with only IPD Group; g_{limit} Shown by Color.

note that the resulting analysis of τ = 10 seconds extrapolates to the larger τ values. Since only two values were used to span the g_{limit} range of interest, there are only two colors in Figure 34. From the figure, there are several airplanes with high values of g_{limit} (i.e., red in the figure) that seem to follow the trend of lower g_{limit} airplanes (i.e., blue in the figure).
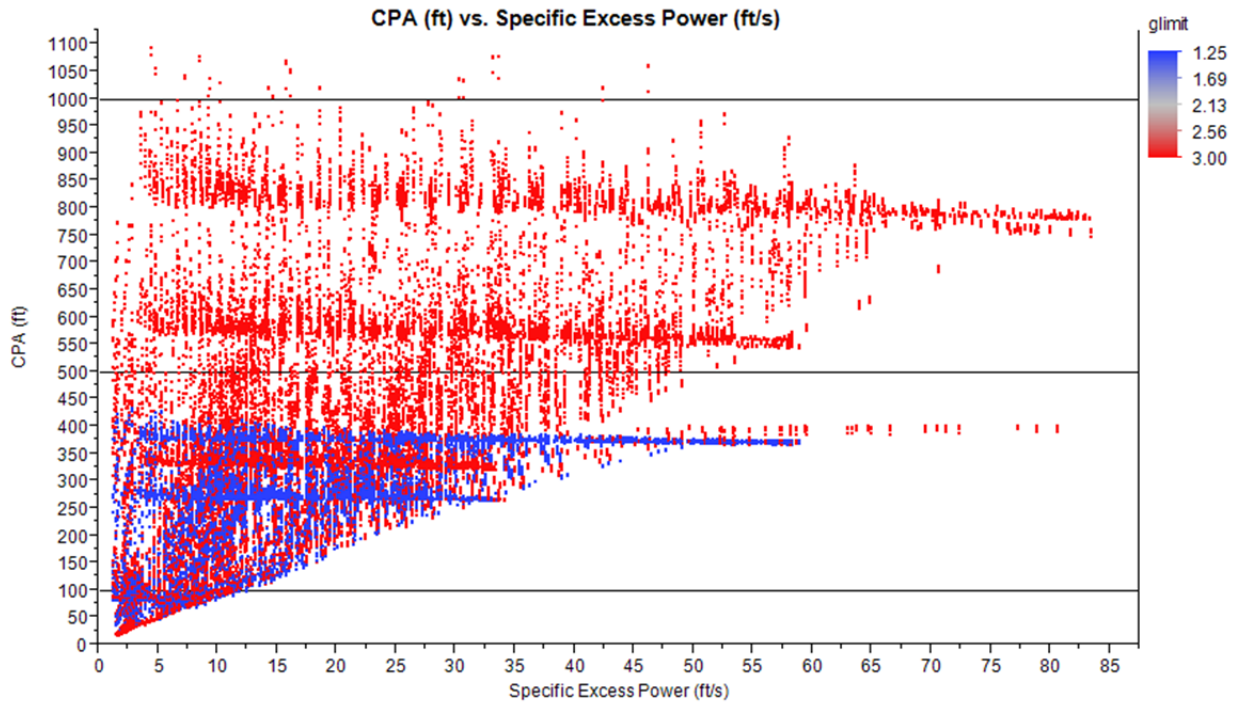

Figure 34: Design Space of τ = 10 seconds; with CPA Range with only IPD Group; g_{limit}
Shown by Color.

To address this, Figure 35 shows the same plot with the color legend now showing the aerodynamic g_{limit} the airplanes can achieve rather than the commanded g_{limit}, as described in Section 2.2.7. This created a third value of g_{limit} equal to 2.2727 g's. The total of only three values of g_{limit} attainable is due to the coarseness of the current design space. Due to the multi-dimensionality of the design, most parameters were limited to only 3-5 step changes within their respective ranges, as shown in Table 2. Thus, there were only 3 steps of % $C_{L_{max}}$, which dictates the initial velocity and flight condition, for all airplane configurations. The values used were 8%, 44% and 80%. The lowest value was an assumed value for cruise condition, the highest for loiter, and 44% is the midpoint. From Equation 6, these % $C_{L_{max}}$ values correspond to g_{limit} values of 12.5, 2.27, and 1.25, respectively. The maximum g_{limit} commanded in the test matrix is 3 g's, and therefore, the maximum limit is well below the achievable 12.5 g's for some configurations. However, when the 3-g command cannot be achieved the aircraft will be aerodynamically limited to either 1.25 or 2.27 g.

Even with the separation of attainable g_{limit} values at a single τ, there still exist multiple groups of each g_{limit}. This is due to the commanded climb rate and is discussed further in the following section.
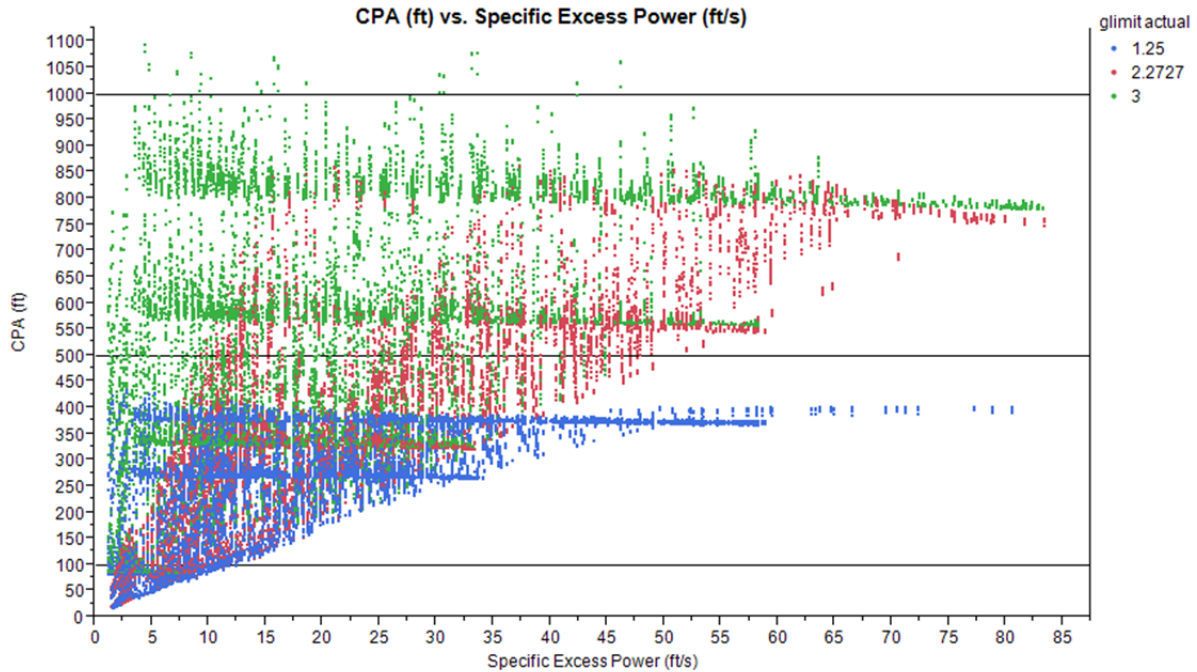
Figure 35: Design Space of τ = 10 seconds; with CPA Range with only IPD Group; g_{limit} Actual Shown by Color.

3.2.4.1.3 Effect of Commanded Climb Rate

As previously mentioned, there are multiple clusters of points in Figure 35 for a single attainable g_{limit} and τ combination. These clusters can be shown, as in Figure 36, to be due to various commanded climb rate values. With the commanded climb rates separated, there is only a single cluster for each attainable g_{limit} and τ combination.

Figure 36 clearly shows the quantity of runs for each commanded climb rate. An artifact of the performance group, there are fewer airplanes with a 500-ft/min climb rate because more airplanes are able to sustain the low climb rate, which places those configurations in the SPD group.
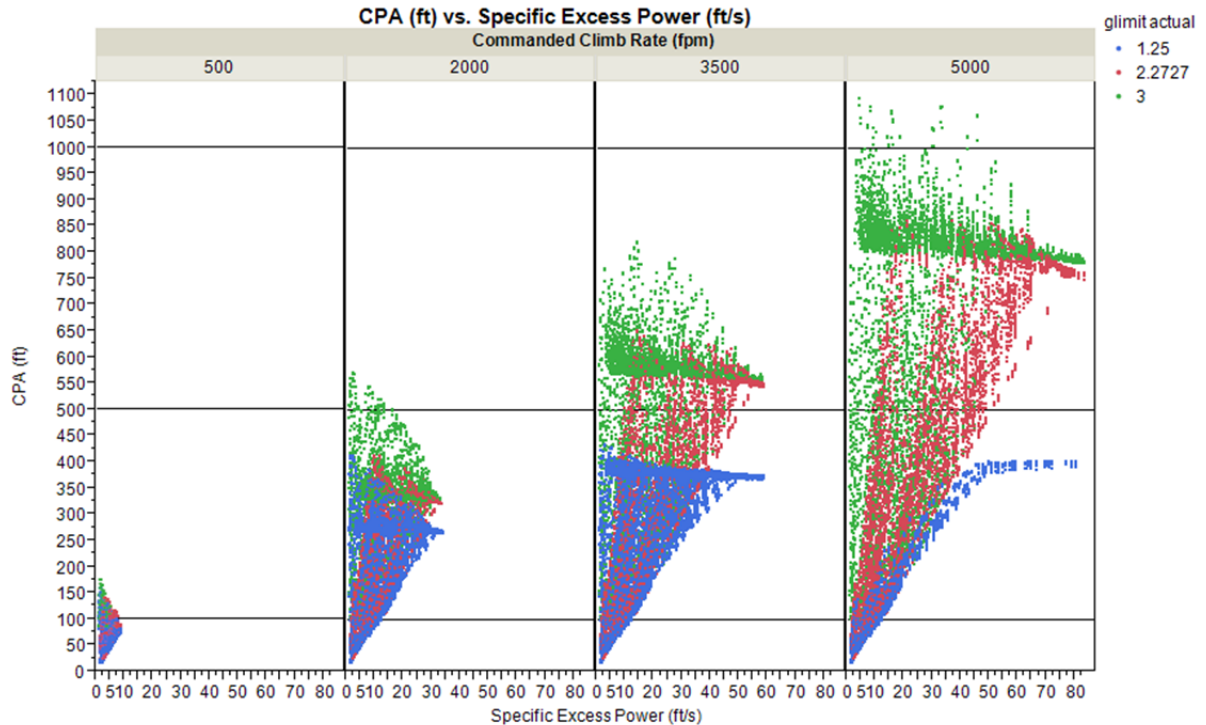
Figure 36: Design Space of τ = 10 seconds; with CPA Range with only IPD Group; g_{limit} Actual Shown by Color; Segregated by Commanded Climb Rate.

3.2.4.1.4 Effect of ΔV and P_{S_i}

As previously mentioned, a key indicator of climb performance is P_{S_i}. Figure 37 shows clear minimum values of P_{S_i} that will assure a minimum CPA value for each τ. Essentially the large number of points form a lower right boundary with all larger P_{S_i} values yielding a minimum CPA value or better. Values of P_{S_i} lower than a selected value will yield some CPAs larger and others smaller. Thus, a minimum P_{S_i} is an indicator that can assure a minimum separation or be used to determine a minimum τ to initiate a maneuver for a desired separation. For instance, with τ = 30 seconds, assuring a CPA greater than VFR-IFR separation of 500 ft is accomplished with P_{S_i} values of 28 ft/sec or greater without regard to other parameters. Thus, if the airplane has a larger value of P_{S_i}, the airplane will be able to achieve the separation of 500 ft for $\tau \geq 30$ seconds. Some airplanes with lower P_{S_i} can also generate CPA $\geq$ 500 ft, but it is not assured. This single parameter is too limiting on the design space because other combinations of parameters can also meet the same requirement. One thing the aircraft with lower P_{S_i} values have in common is speed available (ΔV) to sacrifice for altitude. The interaction between P_{S_i} and ΔV was the apparent area to explore.

The P_{S_i} value necessary to achieve a 500-ft separation is shown to be applicable to airplanes with very little velocity to sacrifice, meaning the initial velocity is near the limiting velocity, V_{BA}. If an airplane has a high ΔV, a smaller P_{S_i} is required to achieve the same CPA. This is shown graphically in Figure 37 as red and grey points above and to the left of the blue line.

As the value of ΔV increases, the CPA response increases. This relationship indicates that the amount of speed an airplane is able to sacrifice directly affects the achievable CPA. Figure 38 shows a subset of the previous plot, focusing on P_{S_i} less than 30 ft/sec, τ = 30 seconds and

segregates the data by $\dot{h}_{command}$. From this figure, there exists a P_{S_i} value that can guarantee a specified separation for a commanded climb rate. For instance, if an airplane attempts a 2000 ft/min climb, a $P_{S_i} \geq 26$ ft/s will guarantee 500 ft of separation from the intruder. Further, there are different P_{S_i} values for various intruder azimuths, as shown in Figure 39. This figure shows airplanes given a 2000 ft/min commanded climb rate segregated by intruder azimuth. From the figure, the ownship requires roughly 26 ft/sec, 18 ft/sec and 18 ft/sec for intruder azimuths of 0º, 45º, and 90º, respectively. There is a large deviation in required P_{S_i} between encounters of 0º and 45º, while there is little to no deviation between encounters of 45º to 90º. Thus, future work should address additional increments between 0º and 45º.
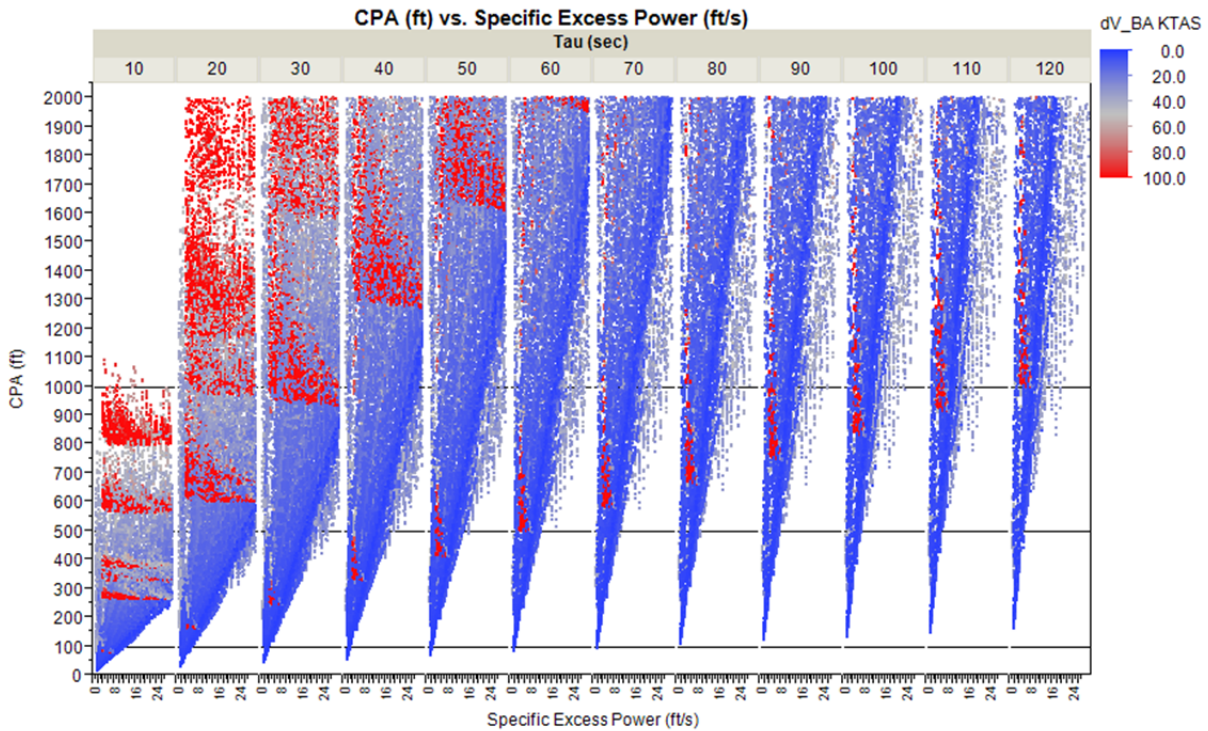
Figure 37: Design Space with CPA Range with only IPD Group; ΔV Shown by Color; Segregated by τ; Limited to $P_S \leq 30$ ft/sec.

Figure 38: Design Space with CPA Range with only IPD Group; ΔV Shown by Color; $\tau = 30$ seconds; Limited to $P_S \leq 30$ ft/sec; Segregated by $\dot{h}$.

Figure 39: Design Space with CPA Range with only IPD Group; ΔV Shown by Color; $\tau = 30$ seconds; Limited to $P_S \leq 30$ ft/sec; Commanded Climb Rate = 2000 fpm; Segregated by Intruder Azimuth.

Focusing on the head-on encounter from Figure 39, a $P_{S_i} \geq 26$ ft/sec will guarantee a separation of 500 ft; however, there exist airplanes with lower P_{S_i} values that are able to achieve more than 500 ft of separation. To examine this further, Figure 40 shows the airplanes with $P_{S_{i\,max}}$ less than 26 ft/sec. The figure relates CPA to the amount of forward speed the airplanes have to sacrifice for vertical speed. From the figure, if the airplane has P_{S_i} less than 26 ft/sec, a 500-ft separation can be achieved if the airplane has more than 55 KTAS to sacrifice, or 55 KTAS between initial speed and V_{BA}.
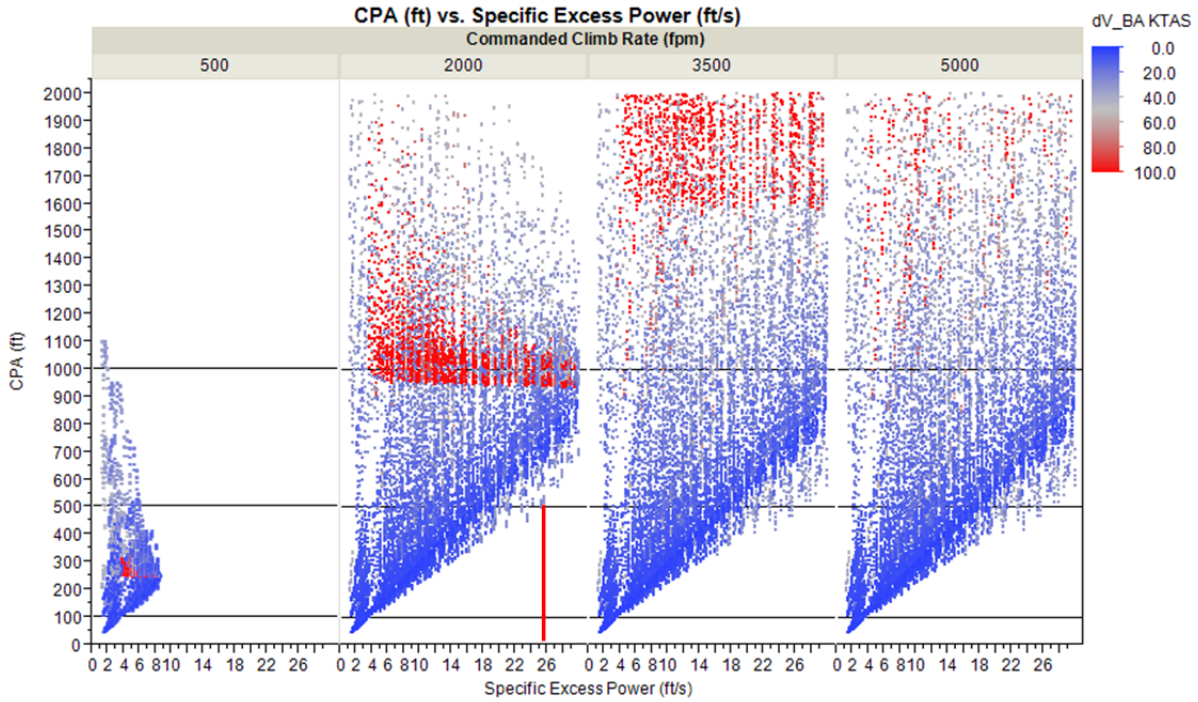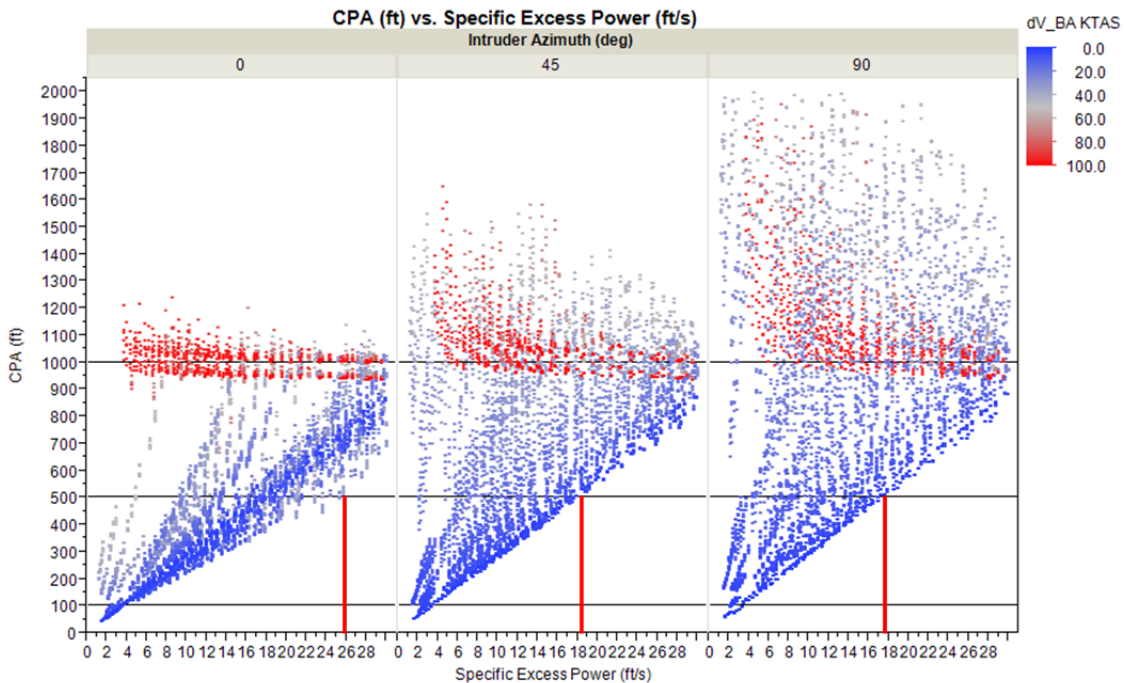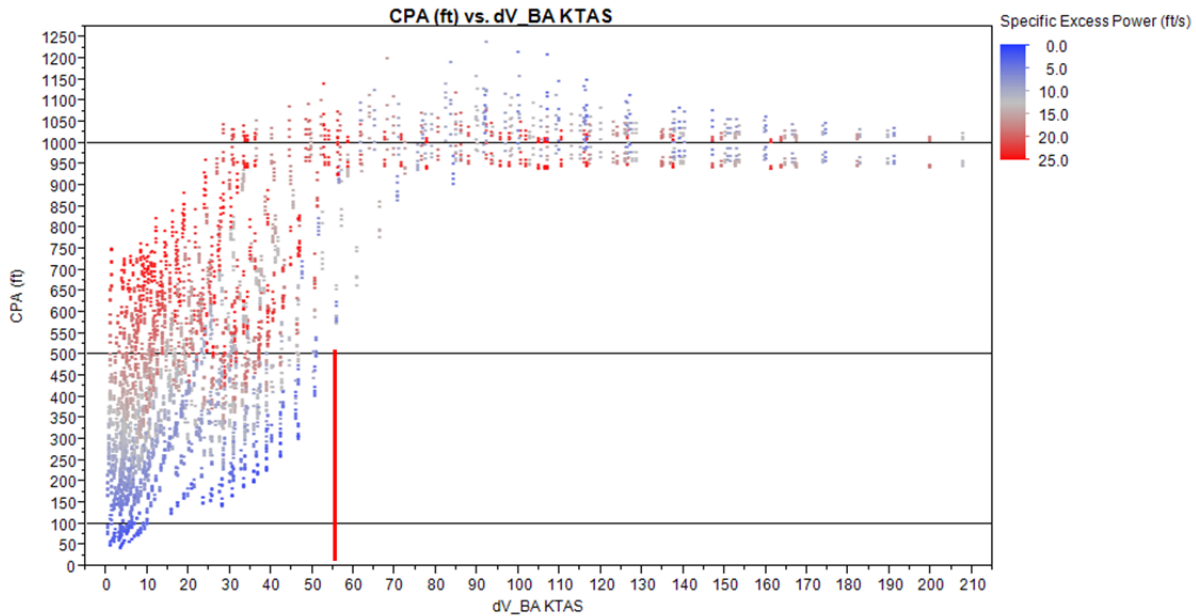

Figure 40: Design Space with CPA Range with only IPD Group; ΔV Shown by Color; τ = 30 seconds; Limited to $P_S \leq 26$ ft/sec; Commanded Climb Rate = 2000 fpm; Head-on Encounter.

The described performance parameters are capable of providing insight into the CPA a specified airplane configuration can achieve during a climb avoidance maneuver without sufficient power differential to maintain the commanded rate. Provided enough time, excess power or the ability to sacrifice forward speed for vertical, an airplane can predict an achievable separation that assures safe separation from an intruder on a collision course.

4 Results and Analysis of Descent Maneuver

This section presents the data from the vertical descent maneuvers along with analysis of the results. For reference, Table 4 shows the design space overview for descent maneuvers. Descriptions of key influential performance parameters are included as they are presented.

Table 4:   Simulation Parameters Relevant to Descent Maneuver.

Parameter	Parameter Symbol	Values
Wing loading (lbs/ft^2)	$\dfrac{W}{S}$	1, 9, 17, 25
Thrust-to-weight ratio	$\dfrac{T}{W}$	0.1, 0.2, 0.3, 0.4
Aspect ratio	AR	5, 16.67, 28.3, 40
Maximum coefficient of lift	$C_{L_{max}}$	0.6, 1.3, 2
Initial percent of maximum coefficient of lift	$\%C_{L_{max}}$	8, 44, 80
Maximum lift-to-drag ratio	$\dfrac{L}{D}_{max}$	5, 20, 35, 50
Load factor Limit	g_{limit}	1.25, 3
Altitude (ft MSL)	h	1000, 6666.7, 12333, 18000
Commanded climb rate (ft/min)	$\dot{h}_{command}$	500, 2000, 3500, 5000
Intruder velocity (KCAS)	V_{intr}	50, 150, 250
Intruder vertical rate	$\dot{h}_{intr}$	-5000, -2750, -500, 0, 500, 2750, 5000
Intruder azimuth (deg)	β	0, 45, 90
Time-to-go (seconds)	τ	10, 20, 30, … 120
Velocity Not to Exceed	V_{NE}	1.15 * V_{cruise}

4.1   Descent Maneuver Performance Parameters

The descent maneuver shares some performance parameters with the climb maneuver though they are generally associated with opposite signs. It has some additional considerations as well. The most significant difference is obviously that the airplane tends to speed up when descending vs. tending to lose speed in a climb. This section describes key performance parameters that limit descent maneuvers.

4.1.1   Specific Excess Power (P_S)

The primary performance parameter for the climb maneuver was $P_{S_{i\,max}}$, as defined in Equation 25. This equation defines the airplane's specific excess power as a function of the maximum thrust available. The power parameter of interest for the vertical descent maneuver is associated with minimum thrust:

$$P_{S_{i\,min}} = \left(\frac{T}{W}_{min} - \frac{D}{W_i}\right) * V_i. \qquad \text{Equation 33}$$

For this study, the minimum thrust of all airplane configurations is zero. Consequently, Equation 33 becomes:

$$P_{S_i \, min} = \left(-\frac{D}{W_i}\right) * V_i. \qquad\qquad \text{Equation 34}$$

In the climb maneuver this parameter determined how fast the aircraft could climb without losing speed. Here the parameter determines how fast the aircraft can descend without gaining speed as well as how rapidly and how much speed it will gain if constant speed is not possible. Akin to the climb maneuver, there is a maximum velocity an aircraft cannot exceed, V_{NE}, which is discussed in more detail below. For the discussion of vertical descent performance, all references to P_{S_i} refer to the $P_{S_i \, min}$ as calculated in Equation 34.

4.1.2 Potential Change in Velocity (ΔV)

An aircraft can have a number of maximum speeds; maximum turbulence penetration speed, maximum flap extend speed, and velocity to never exceed (V_{NE}) are key ones. V_{NE} is the only one of interest to this effort. It is related primarily to structural limitations normally, but when it is a maximum Mach number it may be related to stability and control. Either way, it can limit the ability to descend at high rates or at high rates for extended periods of time. Like the potential change in velocity for the climb, the descent maneuver has the same parameter but it is related to V_{NE}. The amount of speed the airplane can gain affects the achievable separation. This parameter is a measure of the speed a given airplane can gain before reaching the V_{NE}. The equation for this parameter is:

$$\Delta V = V_{NE} - V_i. \qquad\qquad \text{Equation 35}$$

This parameter in association with $P_{S_i \, min}$ is directly related to the rate and duration of descent an airplane can maintain to generate separation from an intruder.

4.1.3 Difference between Commanded Descent Rate and Accelerating Descent Rate ($\Delta \dot{h}_{Accelerate}$)

For a given airplane configuration there is a maximum descent angle and rate above which the airplane cannot avoid accelerating from its initial speed even at idle power. If the airplane is commanded to descend at a smaller angle, the airplane will be able to descend without increasing velocity. The difference between the commanded descent rate and this sustainable rate will provide insight into the rate of acceleration the airplane configuration will experience during the maneuver. This performance parameter can be expressed mathematically as:

$$\Delta \dot{h}_{accelerate} = \dot{h}_{command} - \dot{h}_{accelerate} = \dot{h}_{command} - P_{S_i \, min}. \qquad \text{Equation 36}$$

This parameter is similar to, and has a similar impact as the $\Delta \dot{h}_{Sustainable}$ parameter discussed in the vertical climb maneuver section.

4.2 Performance Grouping of Descent Maneuver Data

Initial analysis revealed multiple performance groups independent of the airplane design parameters. Several different ways of grouping the descent maneuver data were considered. Initial response surface models were fit to preliminary data and residual analysis was done. These groups were revealed to be negatively affecting the accuracy of the model fit. Using JMP® data exploration tools and 2PAIRS GUI functionality, individual airplane configurations within each group were analyzed.

Three predictable performance groups presenting three different characteristic flight performances during the commanded maneuver were created. The process for discovering and segregating the three performance groups was similar to the process outlined in Section 3.2,

and the resulting groups are analogous to three of the groups identified for the climb maneuver: a Sufficient Power Differential (SPD) group, an Insufficient Power Differential (IPD) group, and an Insufficient Time to Pitch (ITP) group. The three performance groups are detailed in the following subsections.

Like the climb maneuvers, an airplane configuration alone does not set the performance group. The combination of airplane design parameters, commanded maneuver rate, initial flight condition, and encounter parameters are all required to determine performance group association as it relates to the SAA system requirements. Additionally, small deviations within an airplane's design parameters or the commanded maneuver may result in that configuration changing performance group. Association with each of the performance groups is predictable prior to the initiation of the 2PAIRS simulation runs using the aircraft design, encounter, and maneuver parameters.

4.2.1 Insufficient Time to Pitch Group

Similar to the ITP climb maneuver performance group, the airplane configurations that fall within this grouping are unable to reach the commanded descent rate during the given encounters. This grouping is dominated by fast-moving airplanes with low g_{limit} involved in encounters with short τ, generally 10 seconds in the data evaluated to date. These same airplane configurations are found in the other performance groups with higher τ values.

4.2.2 Insufficient Power Differential Group

For the cases in this group, the airplane configurations attempt to fly at the given commanded descent rate and gain speed during the maneuver because the commanded descent rate is greater than their $\dot{h}_{accelerate}$. Due to the acceleration, these airplanes may be required to adjust their descent rate to a sustainable rate if V_{NE} is reached. Given a separation threshold of interest, an analysis approach analogous to the IPD group done in the climb avoidance maneuver analysis can be used for airplanes within this group. Thus, once a specified separation threshold is established, analysis can be completed similar to that outlined in Section 3.2.4.

Within this performance group, there exist several characteristic maneuver scenarios. Given adequate time, the airplanes will either: 1) reach terminal velocity for the commanded descent rate and maintain the commanded descent rate throughout the simulation, or 2) reach their specified V_{NE} and be forced to adjust to a sustainable descent rate. Which of these maneuver scenarios occurs is highly dependent on the airplane's drag configuration and the commanded descent rate. Without adequate time, the airplane will continue to accelerate throughout the simulation run reaching CPA before it reaches V_{NE}. Currently, it is difficult to predict which of these scenarios will occur as it is highly dependent on the airplane configuration, commanded maneuver, and τ value of the encounter.

4.2.3 Sufficient Power Differential Group

For the cases that occupy this performance group, the airplane configurations do not accelerate during the commanded descent maneuver because they are given a commanded descent rate that is less than their $\dot{h}_{accelerate}$. Therefore, the $\Delta \dot{h}_{accelerate}$ value for cases within this performance group is positive. This group is directly analogous to the climb SPD group described in Section 3.2.3.

The commanded descent rate is very influential on when airplane configurations fall within this group. The higher the commanded descent rate, the greater the influence of the gravitation force on the acceleration of the aircraft. Thus, there exist more airplane configurations with a

500-ft/min commanded descent rate than those with a 5000-ft/min descent rate within this performance group.

The lack of acceleration results in highly predictable separation performance for these airplane configurations. Using JMP® software, a parametric equation was developed to predict CPA as a function of τ, commanded descent rate, and g_{limit}. The equation is:

$$CPA = -1170.71 + 17.62 * \tau + 1.06 * \dot{h} + 19.08 * g_{limit} + (\dot{h} - 1058.3) * [.0167 * (\tau - 65) + .0365 * (g_{limit} - 1.96)]. \qquad \text{Equation 37}$$

Figure 41 and Figure 42 show the application of the parametric equation to a matrix of the three parameters. The use of these figures enables quick prediction of achievable separation. Figure 41 shows CPA versus the commanded descent rate, while Figure 42 shows CPA versus τ. The g_{limit} effect on these figures is similar to that described for the climb SPD Group described in Section 3.2.3.3

From Figure 41, if an aircraft is able to detect the intruder with τ = 20 seconds, with the knowledge that it can perform a 3000-ft/min descent without accelerating, the airplane can achieve between roughly 800 and 1000 ft of separation depending on the g_{limit}. If further separation is required, the airplane must either have a longer detect time to CPA or have an increased sustainable descent rate. A similar application can be used for Figure 42.
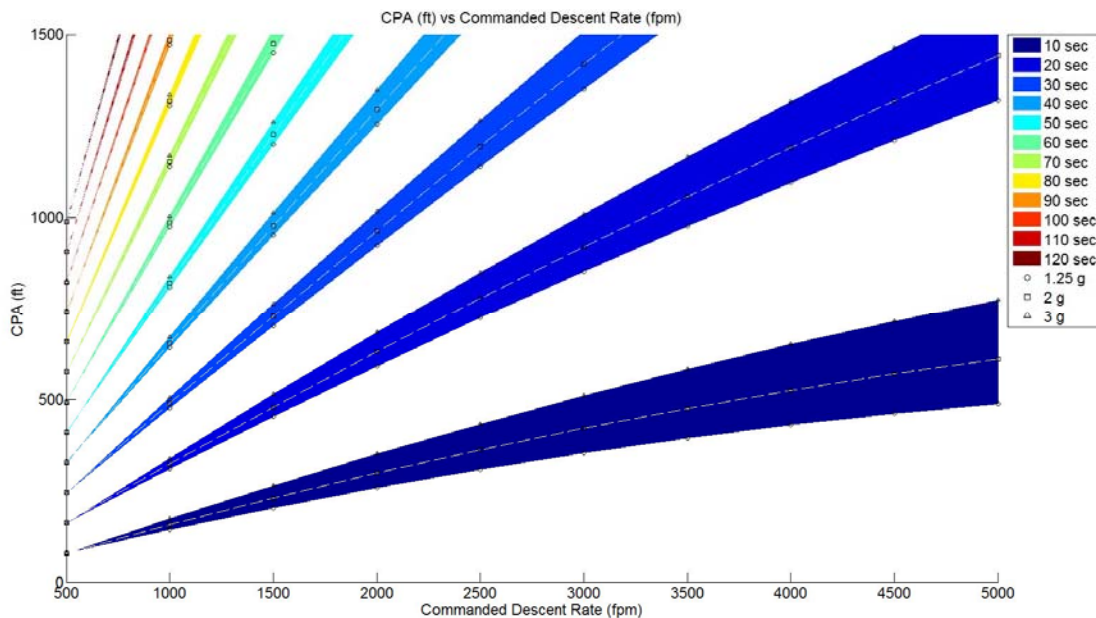

Figure 41: Application of SPD Group Parametric Equation; CPA vs Commanded Descent Rate; τ Shown by Color.
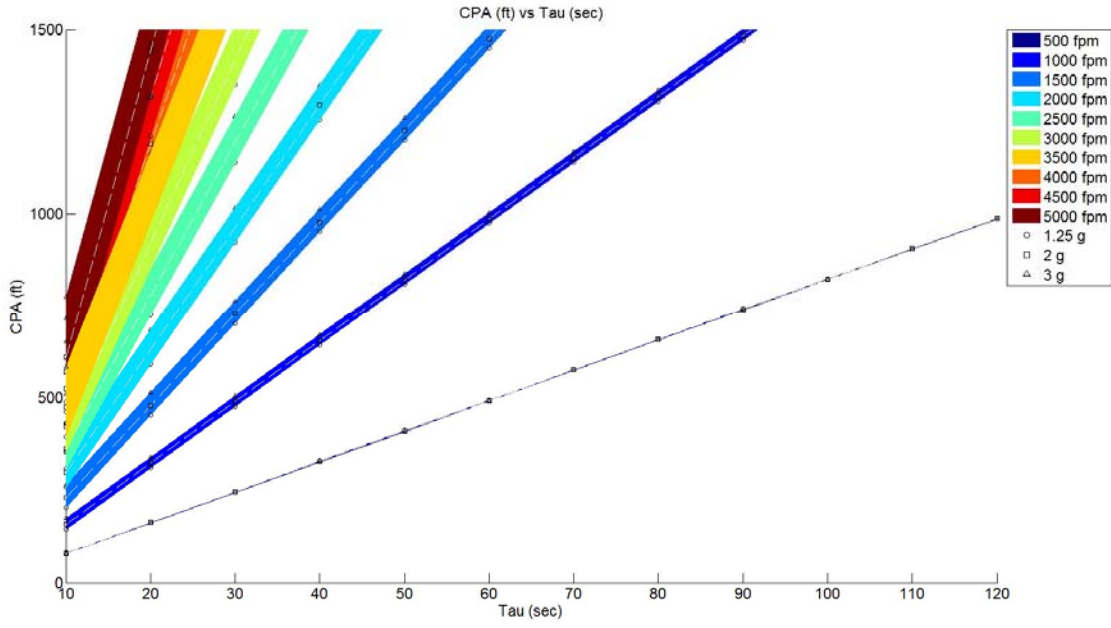
Figure 42: Application of SPD Group Parametric Equation; CPA vs τ; Commanded Descent Rate Shown by Color.

5 Results and Analysis of Level Turn Maneuver

This section presents the data from simulation runs of the level turn maneuver along with analysis of the results including exploration of various parameter effects on CPA. For reference during the following discussions, the design and encounter parameters relevant to the descent maneuver simulations are listed in Table 5 showing the discrete values simulated. These parameters were described above in Sections 0 and 0.

Table 5: Simulation Parameters Relevant to Level Turn Maneuver

Parameter	Parameter Symbol	Values
Wing loading (lbs/ft^2)	$\dfrac{W}{S}$	1, 9, 17, 25
Thrust-to-weight ratio	$\dfrac{T}{W}$	0.1, 0.2, 0.3, 0.4
Aspect ratio	AR	5, 16.67, 28.3, 40
Maximum coefficient of lift	$C_{L_{max}}$	0.6, 1.3, 2
Initial percent of maximum coefficient of lift	$\%C_{L_{max}}$	8, 44, 80
Maximum lift-to-drag ratio	$\dfrac{L}{D}_{max}$	5, 25, 35, 50
Load factor Limit	g_{limit}	1.5
Altitude (ft MSL)	h	1000, 6666.7, 12333, 18000
Commanded climb rate (ft/min)	$\dot{h}_{command}$	500, 2000, 3500, 5000
Intruder velocity (KCAS)	V_{intr}	50, 150, 250
Intruder vertical rate	$\dot{h}_{intr}$	-5000, -500, 0, 500, 5000
Intruder azimuth (deg)	β	-90, -45, 0, 45, 90
Time-to-go (seconds)	τ	10, 20, 30, … 120
Turn Rate Command (deg/sec)	$\dot{\psi}_{command}$	1, 3, 5, 10
Roll Rate (deg/sec)	$\dot{\phi}$	30
Heading Change (deg)	$\Delta\psi$	90

Attempts to develop a response surface model have not resulted in adequately accurate representations to date. Results from the large number of runs made are presented and discussed. Useful conclusions are drawn for the segment of airplanes evaluated. Analysis only includes airplanes doing maneuvers that are not limited by their g_{limit} and are able to perform the commanded maneuver without changing speed. This approach eliminates artificial limits that impact evaluation of trends. The g_{limit} enforced for the results presented is 1.5 g, which is equivalent to a 48º bank-angle limit. The encounter scenarios and aircraft configurations are not exhaustive, but are representative of the key behaviors of interest.

The level turn avoidance maneuver is the only maneuver studied that is not used by TCAS to prevent collisions. It is commonly used by pilots to remain well clear of other aircraft. Also, small deviations are generally less disruptive to the NAS. Thus, although it is less likely to be the better choice for collision avoidance than a vertical maneuver, it is usually the first choice for remaining well clear.

As detailed in Section 2.5, the acceptable horizontal separation is difficult to discern from current separation standards. The section concludes that the range of interest for horizontal CPA results encompasses 500 ft and 3 nm of horizontal separation.

5.1 Parameter Effects on Level Turn Maneuver

There are several possible limitations to the turn performance of an airplane. For a given airplane configuration, the turn rate can be expressed as:

$$\dot{\psi} = \frac{g}{V} * \sqrt{n_z^2 - 1} = g * \sqrt{\frac{\frac{1}{2} * \rho * C_L}{\frac{W}{S}}} * \sqrt{\frac{n_z^2 - 1}{n_z}}. \qquad \text{Equation 38}$$

As the equation shows, for a fixed g_{limit}, $\frac{W}{S}$, and ρ, there is a fixed V and C_L combination that must be met for the flight condition to be valid.

Similarly, the turn radius can be expressed as:

$$R = \frac{\left(2 * \frac{W}{S}\right)}{\rho * g * C_L} * \left(\frac{n_z}{\sqrt{n_z^2 - 1}}\right) = \frac{V}{\dot{\psi}}. \qquad \text{Equation 39}$$

From Equation 38, the airplane configuration with fixed $\frac{W}{S}$ and g_{limit}, large C_L and low altitude (high ρ) lead to higher turn rates. The encounter scenario, which includes the intruder parameters, altitude, and τ, also impacts the separation performance for a given scenario. Examples of these effects are shown in the sub-sections below.

5.1.1 Effect of Altitude

Equation 39 shows the relationship between the turn rate, turn radius, and velocity. As altitude increases, the true airspeed (KTAS) of the UAS increases for a constant calibrated airspeed (KCAS). Thus, for a constant turn rate, as the altitude increases, the radius of the turn increases. Figure 43 shows this effect on the CPA. The ownship and intruder have the same KCAS for both results. The UAS is given a constant commanded turn rate for both encounters, but the altitude varies from 1000 ft MSL (blue line) to 18,000 ft MSL (red line). The lower-altitude UAS makes a tighter turn and initially generates a larger CPA. However, the faster aircraft may ultimately generate a larger CPA over longer τ. Note that aerodynamic performance limitations
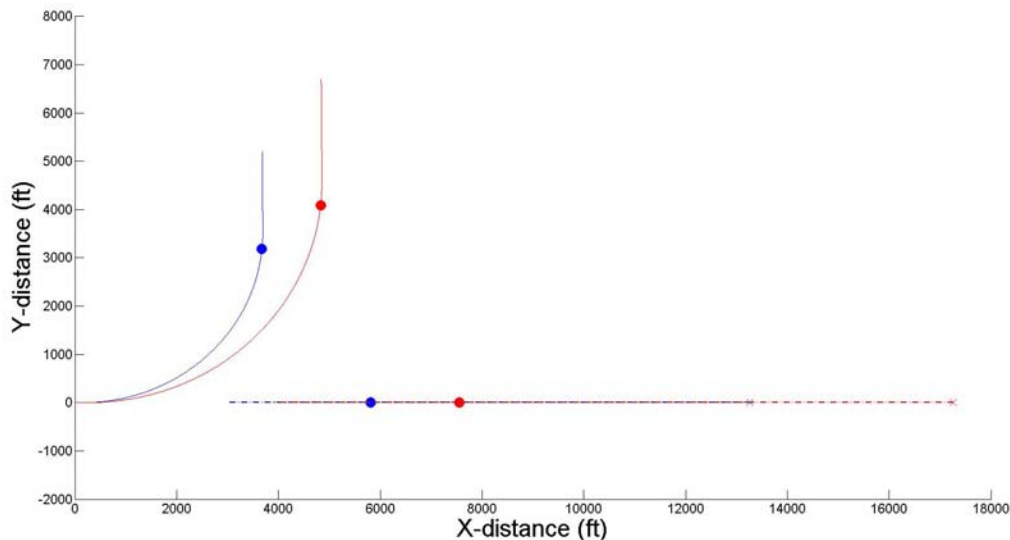

Figure 43: Level Turn Maneuver; Altitude Effect on Response.

that drive turn rate are associated with KCAS while this demonstrates that the resulting turn performance (radius) is linked to KTAS.

5.1.2 Effect of Intruder Azimuth

The intruder's azimuth intuitively was expected to have a large effect on the achievable separation. For the level turn maneuvers in this study, the intruder may approach perpendicular to the ownship's trajectory from either side. With the ownship only turning right, if the intruder is initially right of the ownship's trajectory, the UAS may turn directly into the intruder's constant flight path. Trivially, this may create a smaller CPA value than if the ownship were to turn directly away from the intruder. The only encounter scenario where this may be a recommended avoidance maneuver is if the ownship can turn and fly parallel to the intruder with a separation greater than the required threshold.

Conversely, if the ownship turns away from an intruder that is approaching at a 90° azimuth, the UAS may gain separation from the intruder depending on the relationship between the ownship's speed and the intruder's speed. For example: if the UAS is flying faster than the intruder, it will turn to the commanded 90° heading change and will create further separation from the intruder.

Figure 44 shows a single UAS configuration involved in an encounter with intruders approaching from an array of azimuths. Each intruder is slower than the UAS and all have the same speed. Thus, intruder azimuth is the only parameter that varies between the cases shown in the figure. The intruders' trajectories are represented by the colored dashed lines with the initial positions marked by a star. The CPA for both the UAS and intruder is represented as a colored dot. If no avoidance maneuver were performed, a direct collision (CPA = 0 ft) would occur where the intruder trajectories intersect.
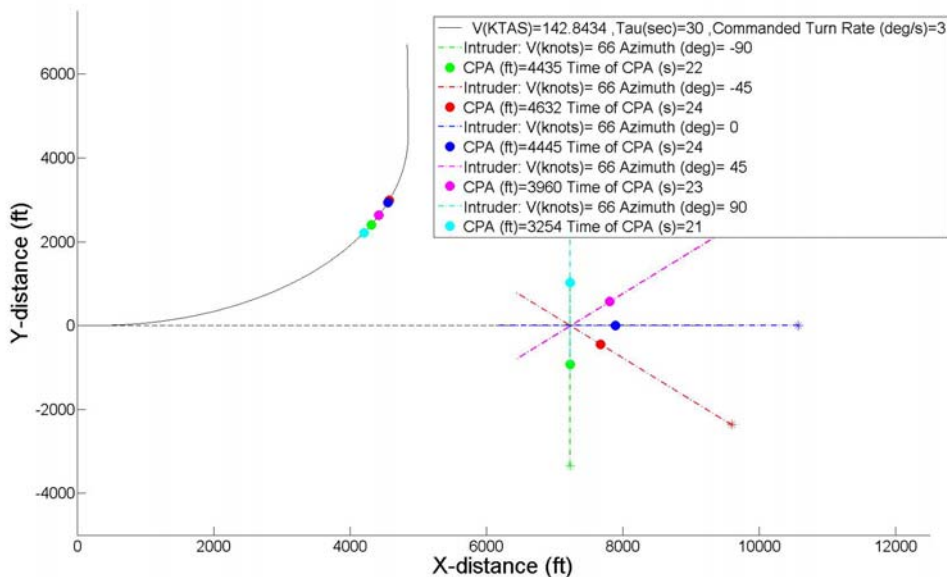

Figure 44: Level Turn Maneuver; Intruder Azimuth Effect.

The UAS is able to achieve a separation of greater than 0.5 nm regardless of the angle from which the intruder approaches, for the given encounter parameters. Although the CPA occurs before the initial τ value, a greater amount of separation occurs and a direct collision is avoided. This shows that intruder azimuth does not have a large effect when the intruder is significantly

slower than the UAS. The next section discusses other effects of the speed ratio between the UAS and intruder.

5.1.3 Effect of Intruder Speed

The magnitude of the intruder's speed effectively changes the closure rate between the ownship and intruder for a given UAS configuration. This effect is especially influential if the ownship is turning away from the intruder. Figure 45 shows the same encounter as Figure 44, but the intruder's speed is increased to 198 KTAS, significantly faster than the UAS. Comparing Figure 44 and Figure 45, one significant difference is the time of CPA for the intruders approaching from the right (-90 and -45º). For the -90º intruder, once the UAS reaches a 90º heading change, the two aircraft are flying parallel to each other. If CPA has not yet occurred, the CPA will occur when the intruder catches the UAS. This is a result of the systematic way the maneuvers are being flown with a heading change of 90º. A maneuver algorithm or UAS pilot would make a more effective avoidance maneuver based on the applicable mission profile. Intruder azimuth had a less consistent effect on the difference between predicted and actual τ with the faster intruder than the slower intruder. The increase in intruder speed resulted in actual τ being larger than predicted τ for the -90º and -45º azimuth intruders. The remaining azimuths resulted in actual τ being smaller than predicted τ but with very little difference for the head-on (0º) case. Thus, turning away from the intruder gives the UAS and its operator more time to consider options if the intruder is faster than the UAS. However, depending on τ and the turn radius, the CPA could become very small.
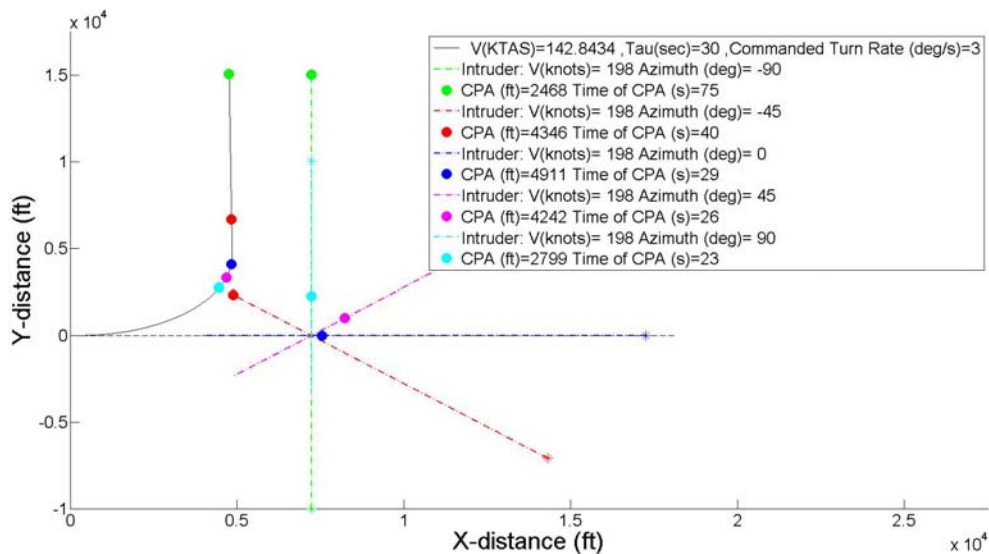

Figure 45: Level Turn Maneuver; Intruder's Speed Effect on Various Azimuths.

5.1.4 Effect of Turn Rate

Figure 46 throughFigure 49 are contour plots showing achievable CPA for several velocity and τ combinations. The contour lines in each depict CPAs of 500 ft, 1 nm, 2 nm and 3 nm. For this study, a g_{limit} of 1.5 was used in the turning maneuver for all airplane configurations. The airplanes represented in these contour plots did not reach this limit so they were following the commanded turn rate. From Equation 38, the g_{limit} would be a factor at or above 234 KTAS for

a 5-deg/sec turn and 120 KTAS for 10-deg/sec turn. The contour plots are not valid for speeds above these limiting values and are, thus, shaded out.
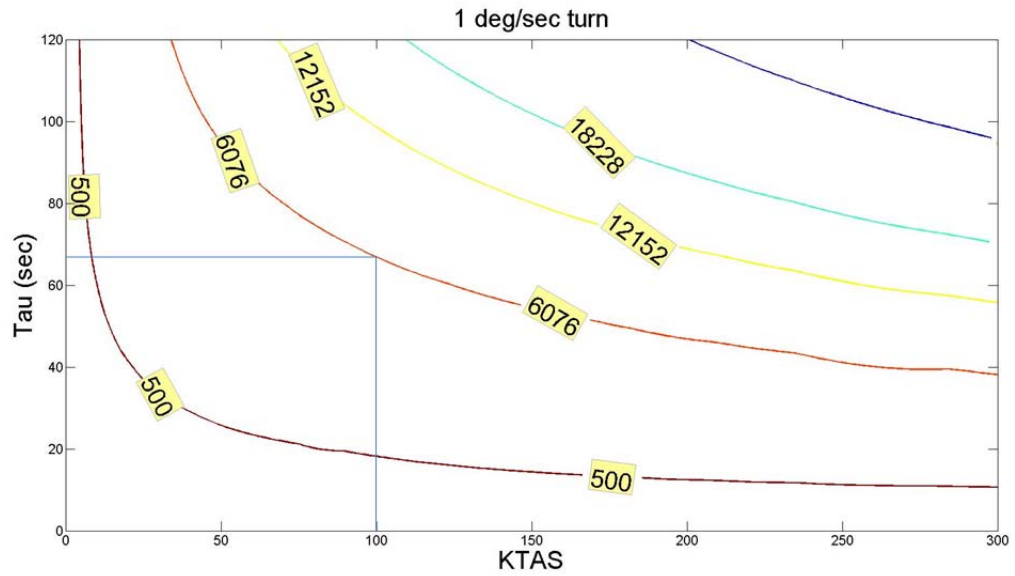

Figure 46: Level Turn Maneuver; Head-On Encounter; g_{limit} < 1.5; h = 18,000 ft MSL; V_{intr} = 50 KTAS; Contour Showing Achievable CPA for 1-deg/sec Turn.

Figure 47: Level Turn Maneuver: Head-On Encounter; g_{limit} < 1.5; h = 18,000 ft MSL; V_{intr} = 50 KTAS; Contour Showing Achievable CPA for 3-deg/sec Turn.

Figure 48: Level Turn Maneuver; Head-On Encounter; g_{limit} < 1.5; h = 18,000 ft MSL; V_{intr} = 50 KTAS; Contour Showing Achievable CPA for 5-deg/sec Turn.

Figure 49: Level Turn Maneuver; Head-On Encounter; g_{limit} < 1.5; h = 18,000 ft MSL; V_{intr} = 50 KTAS; Contour Showing Achievable CPA for 10-deg/sec Turn.
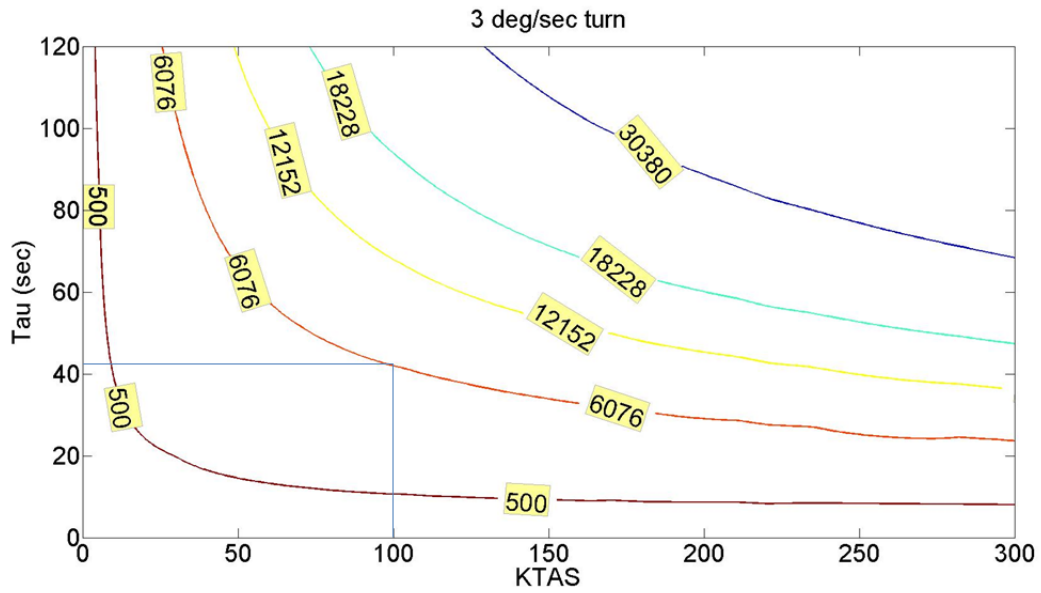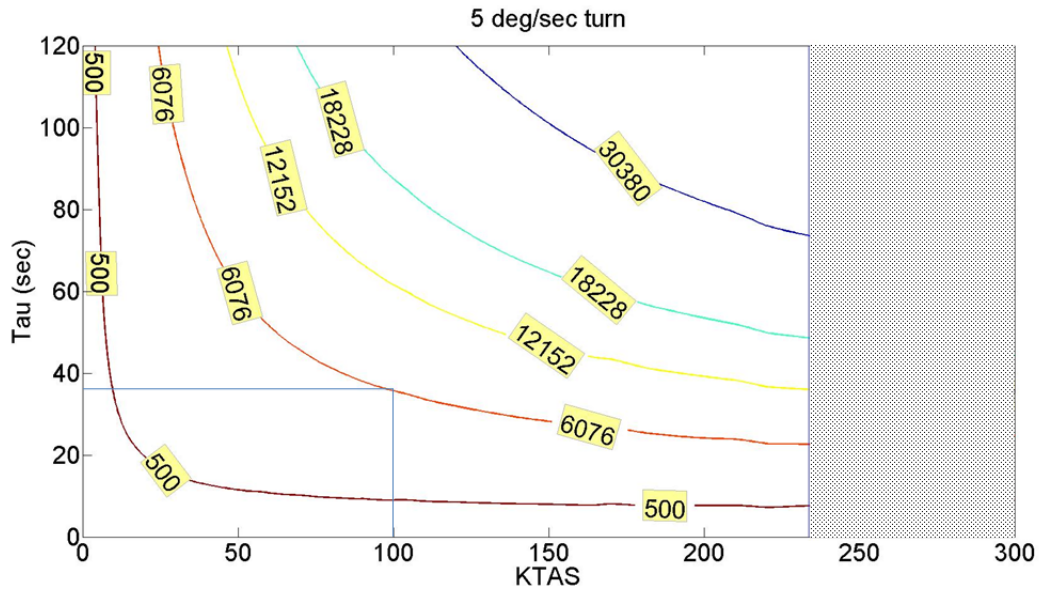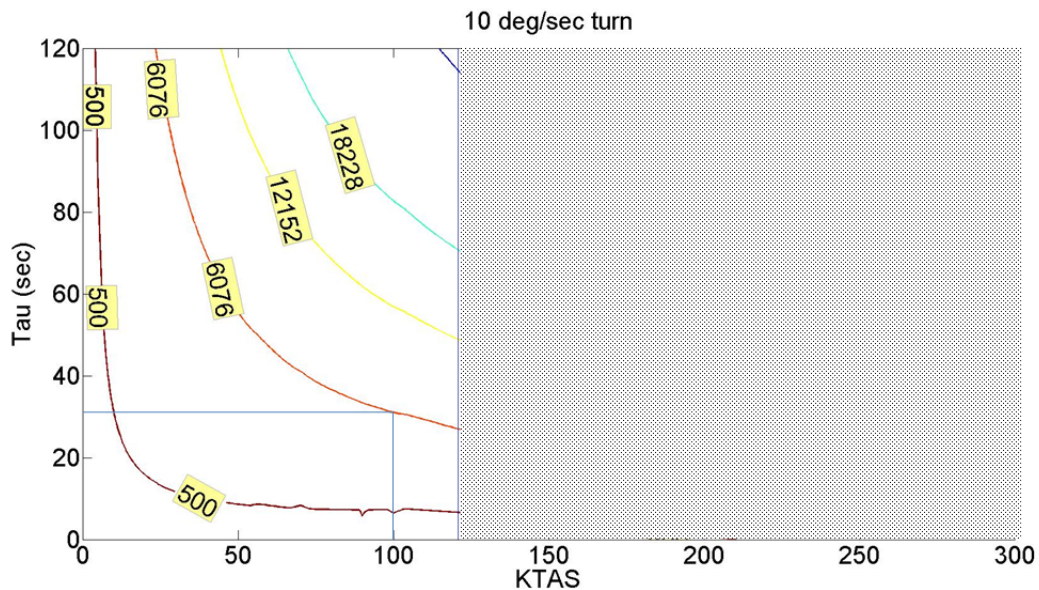
As an example of how these plots can be used, the dark blue lines added to each graph point out the τ required for a UAS flying at 100 KTAS to achieve a CPA of 1 nm. Each figure provides results from a different commanded turn rate for a head-on (β = 0°) encounter with a 50-knot level intruder flying co-altitude at 18,000 ft MSL. Table 6 shows the required τ for each commanded turn rate and the results are plotted in Figure 50. As expected, as the turn rate increases, less time is required to achieve the 1-nm separation, although the relationship between turn rate and time required is non-linear. Due to the variation in τ required between a 1-deg/sec and 5-deg/sec turn rate, further data should be analyzed between these values to

determine the knee in the curve. This figure may be used to determine a required turn rate ability for a set τ, or vice versa. For instance, given a τ of 40 seconds, the 100 KTAS airplane must be able to sustain a turn rate greater than 3-deg/sec for a 1-nm CPA.

Table 6: Time Required to Achieve Horizontal Separation of 1 nm for 100 KTAS UAS at Various Commanded Turn

Turn Rate (deg/sec)	$\tau_{required}$
1	67
3	42
5	36
10	31

These contour plots are valid for all airplane configurations that sustain the turn through a 90° heading change without losing speed and do not reach the 1.5 g_{limit} flying at 18,000 ft MSL with a 50-knot intruder approaching head-on. Varying these constant parameters would result in a series of contours applicable to many encounter scenarios. The series of contours in Figures 46 through 49 can be used to make Figure 50 into a 3-D plot of turn rate, CPA, and τ. Additionally, contours for other conditions can expand the applicable results.
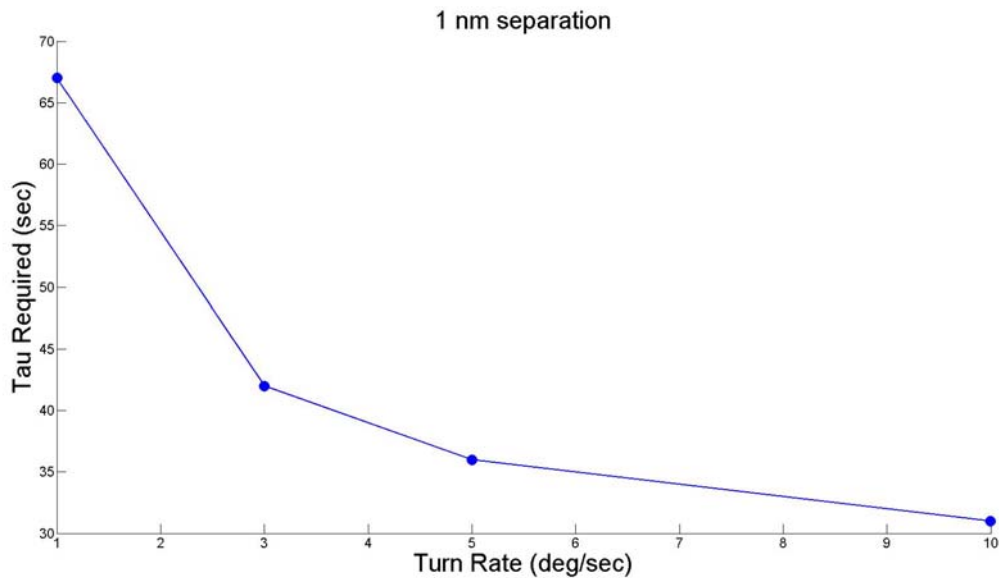

Figure 50: Level Turn Maneuver; Head-On Encounter; g_{limit} < 1.5; h = 18,000 ft MSL; V = 100 KTAS; V_{intr} = 50 KTAS; Required τ vs Turn Rate to Achieve 1 nm of Separation.

6   Concluding Remarks

This study of the trade space between UAS maneuver performance and SAA system performance provides informative results, analysis, and methodologies to help regulators and UAS designers develop regulations and capabilities for safe and efficient integration of UAS into the NAS. Simulators for assessing the trade space across a broad range of UAS maneuver performance capability and encounters were developed for climb, descent, and level turn maneuvers. The UAS maneuver performance modeling approach used in developing the simulators was described. The simulator has both batch and GUI interfaces supporting: 1) evaluations of macro results from large numbers of UAS performance models and encounter geometries; and 2) more detailed time history analysis of model/encounter combinations, respectively.

Test matrix parameter ranges for UAS aerodynamic and propulsive parameters, encounter model parameters, and intruder states were established based on existing airplanes and near-term NAS integration plans as described by RTCA SC-228's Terms of Reference and Work Plan [4,5]. The test matrix and reasoning behind it were discussed.

Discussion of expected closest-point-of-approach ranges of interest was presented and used in analyzing results. Results and methodology for analyzing the large volume of data was presented for the three maneuvers. Early evaluation made it clear that successful analysis would require compartmentalizing UAS performance capabilities into groups. The performance capabilities are grouped by UAS aerodynamic/propulsive performance, initial flight condition, commanded maneuver rate, and the encounter time to go. An airplane performance model alone cannot determine the performance group in which the airplane belongs, because it is also dependent on the encounter scenario and commanded maneuver. The Insufficient Power Differential (IPD) group, which consists of cases where the UAS has insufficient performance to sustain the commanded climb, descent, or turn rate at the initial speed were considered to be of most interest for this work. They are also significantly more difficult to analyze as a group than the Sufficient Performance Group, where the UAS is able to sustain the commanded maneuver. The latter amounts to a geometry problem of lines and curves. Two groups were not analyzed in detail because they were deemed unlikely to occur, especially in flight conditions for transit from an airport area to Class A or Special Use Airspace. The transit condition is the focus of SC-228 [4].

A limited evaluation was shown using approximate aerodynamic/propulsive performance of an existing manned aircraft. This data served as verification and validation of the simulation tool and to provide insight on the impact of initial conditions and aerodynamic/propulsive parameters on CPA.

A detailed discussion of the impact of UAS performance on achievable CPA was presented for the vertical climb maneuver and to a lesser extent the vertical descent and level turn maneuvers. Results demonstrated that specific excess power, P_S, of a given aircraft is a key parameter in predicting achievable CPA for the vertical maneuvers. Results also show that while a minimum P_S value can assure a minimum CPA for a given time-to-go, the same or greater CPA may be achievable with a lower P_S if the aircraft has sufficient speed to trade for altitude (kinetic energy to trade for potential energy). The level turn maneuver is much less likely to encounter specific excess power limitations for the load factors allowable for most aircraft. Thus, level turn analysis focused on aircraft speed and turn rates limited to a 1.5-g load factor, which equates to a maximum of 48º of bank. Future work will attempt to better quantify the relationships for the overall test matrix and is expected to be conducted in conjunction with SC-228 Work Group 1 - Detect and Avoid.

7 Future Work

The simulators, results, and methodologies presented in this paper attempted to establish a basis and framework for determining a minimum UAS performance that can be associated with performance of a given sense and avoid system. This was accomplished for climb, descent, and level turn maneuvers. However, some of the specific analysis necessarily made assumptions about CPA ranges of interest as well as the overall design space. Going forward the authors will work with RTCA SC-228 to target analysis and results to the group's needs. In particular, SC-228's Work Group 1, Detect and Avoid, has sub-groups established to develop system requirements. The authors are working with the UAS Performance group and will continue to use the tools and methods presented here in the work.

Additionally, the simplified maneuvers and perfect sensors used in this study yield idealized results. Future studies will expand on the lessons learned from this work to study their more real-world implications associated with sensor noise and maneuver algorithms.

8 References

[1]   General Operating and Flight Rules. 14 CFR Part 91, 2013.

[2]   FAA Sponsored 'Sense & Avoid' Workshop, "Sense and Avoid (SAA) for Unmanned Aircraft Systems (UAS) – Second Caucus Workshop Report," January 18, 2013.

[3]   US Department of Transportation Federal Aviation Administration, Introduction to TCAS II, version 7, November 2000.

[4]   "Terms of Reference, RTCA Special Committee 228, Minimum Performance Standards for Unmanned Aircraft Systems," RTCA Paper No. 109-13, May 20, 2013.

[5]   "Detect and Avoid (DAA) White Paper", RTCA Special Committee 228, Minimum Performance Standards for Unmanned Aircraft Systems, RTCA Paper No. SC228-WG1-WP01-01, November 1, 2013.

[6]   Jack, D. P., Hoffler, K. D., and Johnson, S. C., "Exploration of the Trade Space Between Unmanned Aircraft Systems Descent Maneuver Performance and Sense-and-Avoid System Performance Requirements," AIAA Aviation Technology, Integration and Operations Conference, Atlanta, GA, June 2014 (submitted for publication).

[7]   Airworthiness Standards: Normal, Utility, Acrobatic, and Commuter Category Airplanes. 14 CFR Part 23, 2013.

[8]   Anderson, John D., Jr., *Introduction to Flight*, 4th ed., The McGraw-Hill Companies, Inc., Boston, 2000.

[9]   Shaw, Robert L., *Fighter Combat: Tactics and Maneuvering*, United States Naval Institute, Annapolis, Maryland, 1985.

[10] Euteneuer, Eric, "Encounter Parameters and 'Geometric Encounter' Generation," RTCA SC-203, draft March 22, 2013.

[11] SAS Institute Inc. JMP® 10 Discovering JMP. SAS Institute Inc., Cary, NC: 2012.

REPORT DOCUMENTATION PAGE

Form Approved
OMB No. 0704-0188

The public reporting burden for this collection of information is estimated to average 1 hour per response, including the time for reviewing instructions, searching existing data sources, gathering and maintaining the data needed, and completing and reviewing the collection of information. Send comments regarding this burden estimate or any other aspect of this collection of information, including suggestions for reducing this burden, to Department of Defense, Washington Headquarters Services, Directorate for Information Operations and Reports (0704-0188), 1215 Jefferson Davis Highway, Suite 1204, Arlington, VA 22202-4302. Respondents should be aware that notwithstanding any other provision of law, no person shall be subject to any penalty for failing to comply with a collection of information if it does not display a currently valid OMB control number.
PLEASE DO NOT RETURN YOUR FORM TO THE ABOVE ADDRESS.

1. REPORT DATE *(DD-MM-YYYY)*	2. REPORT TYPE	3. DATES COVERED *(From - To)*
01-05-2014	Contractor Report	

4. TITLE AND SUBTITLE

Exploration of the Trade Space Between UAS Maneuver Performance and SAA System Performance Requirements

5a. CONTRACT NUMBER

NNL10AA14B

5b. GRANT NUMBER

5c. PROGRAM ELEMENT NUMBER

6. AUTHOR(S)

Jack, Devin P.; Hoffler, Keith D.; Johnson, Sally C.

5d. PROJECT NUMBER

5e. TASK NUMBER

A089.001

5f. WORK UNIT NUMBER

425425.04.01.07.02

7. PERFORMING ORGANIZATION NAME(S) AND ADDRESS(ES)

NASA Langley Research Center
Hampton, Virginia 23681

8. PERFORMING ORGANIZATION REPORT NUMBER

9. SPONSORING/MONITORING AGENCY NAME(S) AND ADDRESS(ES)

National Aeronautics and Space Administration
Washington, DC 20546-0001

10. SPONSOR/MONITOR'S ACRONYM(S)

NASA

11. SPONSOR/MONITOR'S REPORT NUMBER(S)

NASA/CR-2014-218264

12. DISTRIBUTION/AVAILABILITY STATEMENT

Unclassified - Unlimited
Subject Category 03
Availability: NASA CASI (443) 757-5802

13. SUPPLEMENTARY NOTES

Work was performed by Adaptive Aerospace Group, Inc., for Stringer Ghaffarian Technologies (SGT) under NASA Contract NNL10AA14B, Task, A089.001
Langley Technical Monitor: William L. Fehlman

14. ABSTRACT

Replacing manned aircraft's see-and-avoid capability in the absence of an onboard pilot is one of the key challenges associated with safely integrating Unmanned Aircraft Systems (UAS) into the National Airspace System. The work described in this paper is aimed at understanding the trade space between UAS maneuver performance and SAA system performance requirements. A simulator was developed with sufficient fidelity to assess SAA system performance requirements across a range of UAS for a wide range of encounters. Results using approximate performance data from a well-known manned aircraft is presented as verification and validation of the simulator. Results and methodology for developing UAS maneuver performance requirements are presented for climb, descent, and level turn maneuvers. Results for the vertical maneuver indicate that a minimum specific excess power value can assure a minimum CPA for a given time-to-go prediction. However, smaller values of specific excess power may achieve or exceed the same CPA if the UAS has sufficient speed to trade for altitude. Level turn results are less impacted by specific excess power and are presented as a function of turn rate. Future studies will lead to better quantification of the preliminary results and cover the remainder of the proposed test matrix.

15. SUBJECT TERMS

Avoid; Avoidance maneuver; Closet point of approach; Detect; Performance requirements; Sense; Separation assurance; Unmanned aircraft systems

16. SECURITY CLASSIFICATION OF:			17. LIMITATION OF ABSTRACT	18. NUMBER OF PAGES	19a. NAME OF RESPONSIBLE PERSON
a. REPORT	b. ABSTRACT	c. THIS PAGE			STI Help Desk (email: help@sti.nasa.gov)
U	U	U	UU	72	19b. TELEPHONE NUMBER *(Include area code)* (443) 757-5802

Standard Form 298 (Rev. 8-98)
Prescribed by ANSI Std. Z39.18